สหสัมพันธ์ของปริมาณรังสียังผลที่ผู้ป่วยได้รับจากการตรวจเอกซเรย์คอมพิวเตอร์ส่วนช่องท้องโดยวิธีการคำนวณและการวัดปริมาณรังสีที่ผิวหนังด้วยเครื่องวัดชนิดโซลิดสเตท

เรืออากาศโทหญิง เพียงตะวัน กาญจนะ

วิทยานิพนธ์นี้เป็นส่วนหนึ่งของการศึกษาตามหลักสูตรปริญญาวิทยาศาสตรมหาบัณฑิต
สาขาวิชาฉายาเวชศาสตร์ ภาควิชารังสีวิทยา
คณะแพทยศาสตร์ จุฬาลงกรณ์มหาวิทยาลัย
ปีการศึกษา 2552

THE CORRELATION OF EFFECTIVE DOSE FROM CALCULATION METHOD AND THE PATIENT SKIN DOSE MEASUREMENT USING SOLID STATE DETECTOR FOR ABDOMINAL COMPUTED TOMOGRAPHY EXAMINATION

Flying Officer Piangtawan Kanjana

A Thesis Submitted in Partial Fulfillment of the Requirements
for the Degree of Master of Science Program in Medical Imaging
Department of Radiology
Faculty of Medicine
Chulalongkorn University
Academic Year 2009

Thesis Title	THE CORRELATION OF EFFECTIVE DOSE FROM CALCULATION METHOD AND THE PATIENT SKIN DOSE MEASUREMENT USING SOLID STATE DETECTOR FOR ABDOMINAL COMPUTED TOMOGRAPHY EXAMINATION
By	Flying Officer Piangtawan Kanjana
Field of Study	Medical Imaging
Thesis Advisor	Associate Professor Anchali Krisnachinda, Ph.D.

Accepted by the Faculty of Medicine, Chulalongkorn University in Partial Fulfillment of the Requirements for the Master's Degree

.....Dean of the Faculty of Medicine

(Professor Adisorn Patradul, M.D.)

THESIS COMMITTEE

.....Chairman

(Associate Professor Somjai Wangsuphachart, M.D.)

.....Thesis Advisor

(Associate Professor Anchali Krisanachinda, Ph.D.)

.....Examiner

(Assistant Professor Panruethai Trinavarat, M.D.)

.....External Examiner

(Professor Franco Milano, Ph.D.)

เพียงตะวัน กาญจนะ : สหสัมพันธ์ของปริมาณรังสียังผลที่ผู้ป่วยได้รับจากการตรวจเอกซเรย์คอมพิวเตอร์ส่วนช่องท้องโดยวิธีการคำนวณและการวัดปริมาณรังสีที่ผิวหนังด้วยเครื่องวัดชนิดโซลิดสเตท. (THE CORRELATION OF EFFECTIVE DOSE FROM CALCULATION METHOD AND THE PATIENT SKIN DOSE MEASUREMENT USING SOLID STATE DETECTOR FOR ABDOMINAL COMPUTED TOMOGRAPHY EXAMINATION) อ.ที่ปรึกษาวิทยานิพนธ์หลัก: รศ.ดร.อัญชลี กฤษณจินดา. 95 หน้า.

เอกซเรย์คอมพิวเตอร์(ซีที) เป็นการตรวจวินิจฉัยซึ่งให้ปริมาณรังสีแก่ผู้ป่วยสูงกว่าการตรวจทางรังสีอื่นๆ เนื่องจากมีการตรวจด้วยซีทีเพิ่มขึ้นอย่างรวดเร็วทำให้มีรายงานเกี่ยวกับปริมาณรังสีที่ผู้ป่วยได้รับ แต่การวัดปริมาณรังสีที่ผู้ป่วยได้รับจากการตรวจซีทีโดยตรงเป็นสิ่งที่ทำได้ยาก ในปัจจุบันได้มีการพัฒนาเครื่องวัดปริมาณรังสีที่ผิวหนังโดยบริษัท Unfors เพื่อวัดปริมาณรังสีที่ผู้ป่วยได้รับโดยตรง วัตถุประสงค์ของการศึกษานี้เพื่อกำหนดสหสัมพันธ์ของปริมาณรังสียังผลที่ผู้ป่วยได้รับจากการตรวจเอกซเรย์คอมพิวเตอร์ส่วนช่องท้องโดยวิธีการคำนวณและการวัดปริมาณรังสีที่ผิวหนังด้วยเครื่องวัดชนิดโซลิดเสตท ทำการศึกษาในผู้ป่วย 58 คน สำหรับการตรวจเอกซเรย์คอมพิวเตอร์ช่องท้องส่วนบน และ 86 คนในการตรวจเอกซเรย์คอมพิวเตอร์ส่วนช่องท้องทั้งหมด ทำการเก็บข้อมูลในเรื่องของอายุ, เพศ, น้ำหนัก, ความสูง, ความหนาของช่องท้อง, ความต่างศักย์ของหลอดเอกซเรย์, กระแสหลอด-วินาที,ความหนาของสไลซ์, จำนวนชุดการตรวจ, $CTDI_{vol}$ และ DLP จากเครื่องซีที 16 สไลซ์ ผลิตภัณฑ์ซีเม็นส์ ณ โรงพยาบาลจุฬาลงกรณ์ สภากาชาดไทย การคำนวณปริมาณรังสียังผลทำโดยการใช้ conversion factor สำหรับช่องท้องส่วนบนและช่องท้องทั้งหมดซึ่งแยกตามเพศและค่า scanner factor ตามชนิดของเครื่องกับค่า DLP การศึกษานี้ทำการเก็บข้อมูลปริมาณรังสีที่ผิวหนังโดยการติดเครื่องวัดรังสีที่ผิวหนังใกล้กับอวัยวะสืบพันธุ์ (เพศหญิงติดเหนือรังไข่ซ้าย เพศชายติดบริเวณอัณฑะซ้าย) ผลการศึกษา: ค่าเฉลี่ยของปริมาณรังสีที่ผิวหนัง, $CTDI_{vol}$, DLP และปริมาณรังสียังผลต่อการตรวจสำหรับเอกซเรย์คอมพิวเตอร์ช่องท้องส่วนบน คือ 0.27 ± 0.22 มิลลิเกรย์, 11.77 ± 1.02 มิลลิเกรย์, 352.26 ± 44.35 มิลลิเกรย์เซนติเมตร และ 5.24 ± 0.69 มิลลิซีเวิร์ต ตามลำดับ และสำหรับการตรวจเอกซเรย์คอมพิวเตอร์ส่วนช่องท้องทั้งหมด คือ 7.64 ± 3.56 มิลลิเกรย์, 11.41 ± 0.94 มิลลิเกรย์, 485.59 ± 66.80 มิลลิเกรย์เซนติเมตร และ 7.02 ± 1.40 มิลลิซีเวิร์ต ตามลำดับ ระดับปริมาณรังสีอ้างอิง (ดีอาร์แอล) สำหรับการตรวจเอกซเรย์คอมพิวเตอร์ส่วนช่องท้องต่อครั้ง ค่า $CTDI_w$ คือ 35 มิลลิเกรย์ ค่า DLP 800 มิลลิเกรย์เซนติเมตร และค่าปริมาณรังสียังผลคือ12.0 มิลลิซีเวิร์ต ค่าเฉลี่ยปริมาณรังสีที่ผิวหนัง, $CTDI_{vol}$, DLP และ ปริมาณรังสียังผลรวมทั้งการตรวจสำหรับการตรวจเอกซเรย์คอมพิวเตอร์ช่องท้องส่วนบน คือ 1.10 ± 1.01 มิลลิเกรย์, 42.12 ± 10.18 มิลลิเกรย์, 1260 ± 337.67 มิลลิเกรย์เซนติเมตร และ 18.71 ± 5.02 มิลลิซีเวิร์ต ตามลำดับ และ 31.50 ± 14.69 มิลลิเกรย์, 42.26 ± 11.74 มิลลิเกรย์, 1763.19 ± 410.74 มิลลิเกรย์เซนติเมตร และ 25.46 ± 6.63 มิลลิซีเวิร์ตสำหรับการตรวจเอกซเรย์คอมพิวเตอร์ช่องท้องซึ่งเป็นปริมาณรังสีที่สูงมากเพราะต้องทำการตรวจ 3-5 ชุดการตรวจ สรุปผล: ปริมาณรังสียังผลสามารถหาได้จากความสัมพันธ์ระหว่างปริมาณรังสียังผลและปริมาณรังสีที่ผิวหนังซึ่งมีค่าเท่ากับ 17.82 มิลลิซีเวิร์ตต่อมิลลิเกรย์ และ 0.92 มิลลิซีเวิร์ตต่อมิลลิเกรย์ สำหรับการตรวจเอกซเรย์คอมพิวเตอร์ช่องท้องส่วนบนและช่องท้องทั้งหมด ตามลำดับ

ภาควิชา :	รังสีวิทยา	ลายมือชื่อนิสิต	
สาขาวิชา :	ฉายาเวชศาสตร์	ลายมือชื่ออ.ที่ปรึกษาวิทยานิพนธ์หลัก	
ปีการศึกษา :	2552		

5174802730: MAJOR MEDICAL IMAGING
KEYWORDS : EFFECTIVE DOSE/ SOLID STATE DOSEMETER/ ABDOMINAL COMPUTED TOMOGRAPHY EXAMINATION

PIANGTAWAN KANJANA: THE CORRELATION OF EFFECTIVE DOSE FROM CALCULATION METHOD AND THE PATIENT SKIN DOSE MEASUREMENT USING SOLID STATE DETECTOR FOR ABDOMINAL COMPUTED TOMOGRAPHY EXAMINATION. THESIS ADVISOR: ASSOC.PROF.ANCHALI KRISANACHINDA, Ph.D., 95 pp.

Computed Tomography (CT) is a diagnostic imaging modality resulting in higher patient dose than other radiological procedures. As the rapid growing of CT, the patient dose from CT examination is questioned and needed to know. As the direct measurement of patient dose is not practical, the patient skin dosemeter (PSD) has been developed by Unfors to measure dose directly. The aim of this study is to determine the patient dose from abdominal CT using PSD and correlate to the calculated methods. Fifty-eight patients in CT upper abdomen and eighty-six in CT whole abdomen were prospectively included in the study. The collected data were patient age, gender, height, weight, body thickness, kVp, effective mAs, slice thickness, number of series, $CTDI_{vol}$ and DLP from CT scanner, Siemens SOMATOM Sensation 16 at King Chulalongkorn Memorial Hospital. The effective dose was determined by applying the conversion factor for different regions of the body and patient groups and scanner factor. In this study, the PSD was attached to the patient skin close to the gonad (over left ovary position for female and over left testis position for male) to measure the skin dose. **Result**: The average patient skin dose, $CTDI_{vol}$, DLP and effective dose per scan series for CT upper abdomen were 0.27 ± 0.22 mGy, 11.77 ± 1.02 mGy, 352.26 ± 44.35 mGy·cm and 5.24 ± 0.69 mSv respectively. For CT whole abdomen, the results per scan series were 7.64 ± 3.56 mGy, 11.41 ± 0.94 mGy, 485.59 ± 66.80 mGy·cm and 7.02 ± 1.40 mSv, respectively. The diagnostic reference levels (DRLs) for CT abdomen is 35 mGy for $CTDI_w$, 800 mGy.cm for DLP and 12.0 mSv for effective dose. The average patient skin dose, $CTDI_{vol}$, DLP and effective dose for all series were 1.10 ± 1.01 mGy, 42.12 ± 10.18 mGy, 1260 ± 337.67 mGy·cm and 18.71 ± 5.02 mSv, respectively for upper abdomen and 31.50 ± 14.69 mGy, 42.26 ± 11.74 mGy, 1763.19 ± 410.74 mGy·cm and 25.46 ± 6.63 mSv for whole abdomen which were very high as the protocol for CT abdomen requires 3-5 series. **Conclusions:** The effective dose could be determined by using the correlation between the average effective dose and the skin dose of the value 17.82 $mSv.mGy^{-1}$ and 0.92 $mSv.mGy^{-1}$ for upper and whole abdomen, respectively.

Department : Radiology Student's Signature Piangtawan Kanjana

Field of Study: Medical Imaging Advisor's Signature Anchali Kri

Academic Year : 2009

ACKNOWLEDGEMENTS

I would like to express gratitude and deepest appreciation to Associate Professor Anchali Krisanachinda, Ph.D., Division of Nuclear Medicine, Department of Radiology, Faculty of Medicine, Chulalongkorn University, my advisor for her guidance, helpful suggestion, supervision, constructive comments and polishing of the thesis writing to improve the readability and English expression.

I would like to extremely grateful Associate Professor Sivalee Suriyapee, Chief of Physicist at Division of Radiation Oncology, Department of Radiology, Faculty of Medicine, Chulalongkorn University, my teacher for her invaluable advices, constructive comments, encouragement and providing the required equipments to perform this research.

I would like to deeply thank Associate Professor Somjai Wangsuphachart, M.D. and Assoc. Prof. Kiat Arjhansiri, M.D., Head, Department of Radiology, Faculty of Medicine, Chulalongkorn University, for their helpful suggestions, constructive comments in this research.

I would like to thank Mr. Wallop Makmool, M.Sc. Ms. Petcharleeya Suwanpradit, M.Sc., technologists, technicians and medical staff at the Section of Computed Tomography, Department of Radiology, King Chulalongkorn Memorial Hospital, Thai Red Cross Society for their instruction of using the machine, facilitate in providing the required instrument, useful advices and encouragement.

I would like to thank Mr. Taweap Sanghangthum, Mr. Sonjarod Oonsiri and staff at Division of Radiation Oncology, Department of Radiology, King Chulalongkorn Memorial Hospital, Thai Red Cross Society for their kindness in providing suggestions.

I am extremely grateful Associate Professor Katsumi Tsujioka, Faculty of Radiological Technology, School of Health Sciences, Fujita Health University, Japan for his teaching of much knowledge in Computed Tomography and kindness in sharing useful experiences of my thesis.

I would like to thank Professor Franco Milano from University of Florence Italy, who is the external examiner of the thesis defense for his helpful recommendations, constructive comments and teaching of knowledge in Medical Imaging.

I am thankful for all teachers, lecturers and staff at Master of Science Program in Medical Imaging, Faculty of Medicine, Chulalongkorn University for their helps, suggestions and unlimited teaching knowledge during the course of Medical Imaging. My grateful is forwarded to the Graduate Studies, Faculty of Medicine Chulalongkorn University for the financial support as a tutor, Medical Imaging Program.

In particular, I am most grateful to Unfors Co. ltd., Sweden for support patient skin dosemeter for the research purpose.

Finally, I am extremely grateful to my family for their financial support, invaluable encouragement, entirely care and understanding during the entire course of study.

CONTENTS

Page

Page

LIST OF TABLES

LIST OF FIGURES

Figure Page

LIST OF ABBREVIATIONS

Abbreviation	Terms
+ve	Positive
-ve	Negative
2D	Two dimensions
3D	Three dimensions
AAPM	American Association of Physicist in Medicine
CV	Coefficient of Variation
cm	Centimeter
cm^2	Centimeter square
CNR	Contrast to Noise Ratio
CT	Computed Tomography
CTDI	Computed Tomography Dose Index
$CTDI_{vol}$	Volume Computed Tomography Dose Index
$CTDI_w$	Weighted Computed Tomography Dose Index
DFOV	Displayed Field of Views
DLP	Dose Length Product
DRLs	Diagnostic reference levels
E	Effective dose
eff.mAs	Effective milli-ampere second
FDA	Food and Drug Administration
FWHM	Full width at half-maximum
HU	Hounsfield unit
IEC	International Electrotechnical Commission
ImPACT	Imaging Performance Assessment of Computed Tomography
kg	Kilogram
kV	Kilo voltage
kVp	Kilo voltage peak

Abbreviation	Terms
LED	Light emitting diode
LDPE	Low density polyethylene
lp/mm	Line pairs per millimeter
mA	Milliampere
mAs	Milliampere-second
MDCT	Multi-detector computed tomography
mGy	Milligray
mGy.cm	Milligray-centimeter
mm	Millimeter
MSAD	Multiple Scan Average Dose
mSv	Millisievert
NRPB	The National Radiological Protection Board
PMMA	Polymethyl methacrylate
PMP	Polymethylpentene
PSD	Patient Skin Dose
QA	Quality assurance
QC	Quality control
ROI	Region of interest
SD	Standard deviation
sec	second
SFOV	Scan field of view
SNR	Signal to noise ratio
V	voltage

CHAPTER I

INTRODUCTION

1.1 Background and rationale

Computed Tomography is a specialized x-ray imaging technique which cross-sectional image of body has been obtained since its introduction into diagnostic radiology in early 1970s. CT is a diagnostic imaging modality resulting in higher patient dose in comparison with other radiological procedures. Spiral CT was developed in 1989 and multi slice spiral CT in the early 1990s. As the rapid growing of the CT, the patient dose during CT examination was observed. Nevertheless the direct measurement of patient dose during CT examination is complicated [1-5].

During the scan, the x-ray beam enters the patient from all directions at some area. It is not clear where, on surface or inside the patient, the maximum dose occurs, or the calculation of the dose at any point in or on the patient straightforward [6]. Patient dose in CT is usually expressed in terms of volume dose and dose-length product (DLP) leading to the calculation of the effective dose. The main dosimetric quantities are the Computed Tomography Dose Index (CTDI) and DLP [7]. CTDI is a good measure of CT scanner output for applications where the table is incremented during the scan. However, it has limitations, as CTDI is measured by using a standardized, homogeneous, cylindrical phantom; it questionably represents the dose for objects of substantially different size, shape, or attenuation, like the human body. Methods exist to estimate organ doses for a variety of human or humanoid volumes; these typically require use of Monte Carlo simulations. The 14-cm length of the body CTDI phantom does not provide a sufficiently long scatter path relative to the typical length of a human torso; hence, patient dose may be underestimated with CTDI values. In addition, while the current 100-mm integration length is sufficient for measurement of the dose tails for nominal beam widths of several centimeters, it is not sufficient for beam widths greater than 10 cm, such as the 12-cm nominal beam width for the prototype Toshiba 256-section system or C-arm-based cone-beam CT systems. Finally, CTDI does not indicate the dose to a specific point in the scan volume when the patient table remains stationary for multiple scans, such as for interventional or perfusion CT [8].

Nowadays, the patient skin dosemeter (PSD) has been developed by Unfors manufacturer, Sweden, to measure patient entrance skin dose. PSD is a solid state, silicon detector of small size which can monitor patient dose in real-time during CT examination and fluoroscopy procedure for radiation protection to excessive dose usage and consequential patient lesions. An audio-visual warning system indicates to the user when specific dose levels are reached.

1.2 Hypothesis

1.2.1 Null Hypothesis (H_0): There is no correlation between the measured and calculated effective doses at gonad from abdominal CT examination.

1.2.2 Alternative Hypothesis (H_a): There is correlation between the measured and calculated effective doses at gonad from abdominal CT examination.

1.3 Objectives

1.3.1 To determine the effective dose at gonads from abdominal CT examination in patients.

1.3.2 To estimate the correlation of effective dose at gonads between the measurement using patient skin dosemeter and calculated method.

1.4 Definition

Computed Tomography Dose Index (CTDI)	The equivalent of the dose value inside the irradiated slice that would result if the absorbed radiation dose profile were entirely concentrated to rectangular profile of width equal to the nominal slice thickness. Accordingly, all dose contributions from outside the nominal slice width, i.e. the areas under the tails of the dose profile, are added to the area inside the slice.
Multiple Scan Average Dose (MSAD)	The measurement of average absorbed dose (mGy) to the irradiated area from a series of slices. It is a consequence of the fact that the dose profile of each CT scan is not perfect (square), but is bell-shaped. The need of MSAD manifests itself when a sequence of adjacent CT scans is made. For cases where the couch increment is equal or less than the nominal slice width the bell shaped edges of the dose profiles of each CT scan overlap, and result in the average (summed) dose being higher than the dose in a single CT scan. Obviously the higher is the spread of the bell shape of the dose profile, the higher is the MSAD.
Effective dose (E)	The organ doses from a partial irradiation of the body are converted into an equivalent uniform dose to the entire body.

CHAPTER II

REVIEW OF RELATED LITERATURES

2.1 Theory

2.1.1 The introduction of Computed Tomography (CT) [9]

At the Annual Congress of the British Institute of Radiology, in April of 1972, G.N. Hounsfield, a senior research scientist at EMI Limited in Middlesex, England, announced the invention of a revolutionary new imaging technique, which he called "computerized axial transverse scanning". The basic concept was quite simple: a thin cross-section of the head, a tomographic slice, was examined from multiple angles with a pencil-like x-ray beam. The transmitted radiation was counted by a scintillation detector, fed into a computer for analysis by a mathematical algorithm, and reconstructed as a tomographic image. The image had a remarkable characteristic, one never seen before in an x-ray image. It demonstrated a radiographic difference in the various soft tissue; blood clots, gray matter, white matter, cerebrospinal fluid, tumors, and cerebral edema all appeared as separate entities. The soft tissues could no longer be assigned the physical characteristics of water. The computer had changed that concept.

Like most great discoveries, CT was the end product of years of work by numerous investigators. As Austrian mathematician, J. Radon, working with gravitational theory, proved in 1917 that a two- or three-dimensional object could be reproduced from an infinite set of all its projections. Thus, the mathematical concept was established 55 years before the production of a commercial CT scanner. Workers in several unrelated fields (i.e., electron microscopy, astronomy, optics) were all struggling with a similar problem. In 1956, Bracewell, working in radioastronomy, constructed a solar map from ray projections. Oldendorf in 1961 and Cormack in 1963 understood the concept of computed tomography and built laboratory models. Kuhl and Edwards in 1968 built a successful mechanical scanner for nuclear imaging, but did not extend their work into diagnostic radiology. It remained for Hounsfield to put a CT system together and demonstrate its remarkable ability.

As with all fields in radiology, CT units are being continuously changed and upgraded by manufacturers. The physical principles are probably most easily explained in terms of rotation and translation motion because radiation attenuation information may be collected by a pencil x-ray beam and a single detector.

2.1.2 Basic principle of Computed Tomography (CT) [9]

The basic principle behind CT is that the internal structure of an object can be reconstructed from multiple projections of the object. The principle is illustrated in

Figure 2.1. The object is made up of multiple square blocks, five of which have been removed to form a central cross (Figure 2-1A). Projections could be obtained by passing an x-ray beam through the blocks and measuring the transmitted radiation. The ray projections that represent attenuated radiation, by the number of blocks in each row are presented. The horizontal sums (called "ray projections") are shown on the right; the vertical ray sums are shown below the object. All the horizontal and vertical ray sums are added, like the two shown in Figure 2.1B, to produce a numerical reconstruction of the object (Figure 2.1C). The numbers included in the reconstruction are 4, 6, 7, 8, 9, and 10. A gray scale value is then assigned to numbers to produce an image like the one shown in Figure 2-1D. The image can be manipulated to highlight certain areas; that is, contrast can be adjusted. For example, the gray scale can be narrowed to include only black and white, and applied at any point along the numerical sequence. In Figure 2.1E, the scale is centered at the 9-10 level. Blocks with the number 10 are white and all other blocks are black. A perfect reproduction is achieved in Figure 2.1F by centering the black-white scale at the 6-7 level. This simple method of reconstructing an object may illustrate the basic idea, but unfortunately will not work in practice.

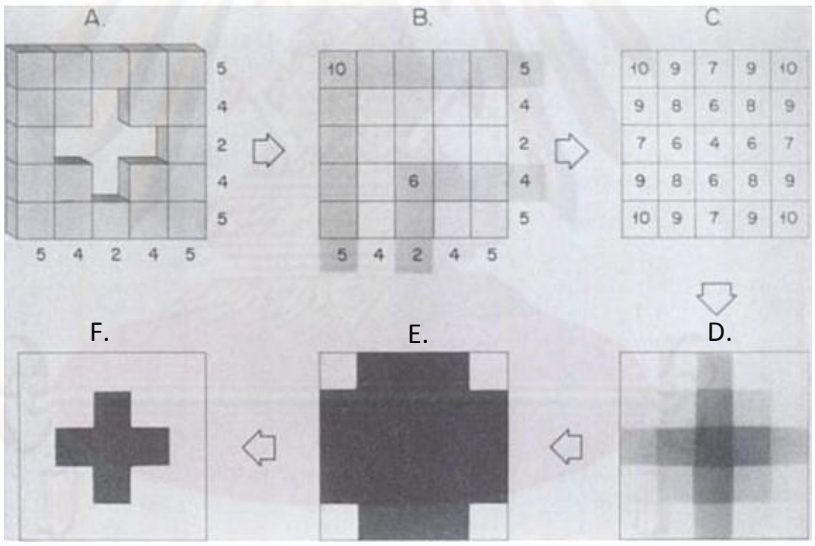

Figure 2.1 The basic principle of computed tomography. (Curry S Thomas, Dowdey E James and Murry C Robert, Christensen's Physics of Diagnostic Radiology, Lippincott Williams & Wilkins, 1990)

2.1.3 Tomographic acquisition [10]

A single transmission measurement through the patient made by a single detector at a given moment in time is called a *ray*. A series of rays that pass through the patient at the same orientation is called *projection or view*. There are two projection geometries that have been used in CT imaging (Figure 2.2). The more basic type is *parallel beam*

geometry, in which all of the rays in a projection are parallel to each other. In *fan beam geometry*, the rays at a given projection angle diverge and have the appearance of a fan. All modern CT scanners incorporate fan beam geometry in the acquisition and reconstruction process. The purpose of the CT scanner hardware is to acquire a large number of transmission measurements through the patient at different positions. The acquisition of a single axial CT image may involve approximately 800,000 transmission measurements. Before the axial acquisition of the next slice, the table that the patient is lying on is moved slightly in the cranio-caudal direction (the "z-axis" of the scanner), which positions a different slice of tissue in the path of the x-ray beam for the acquisition of the next image.

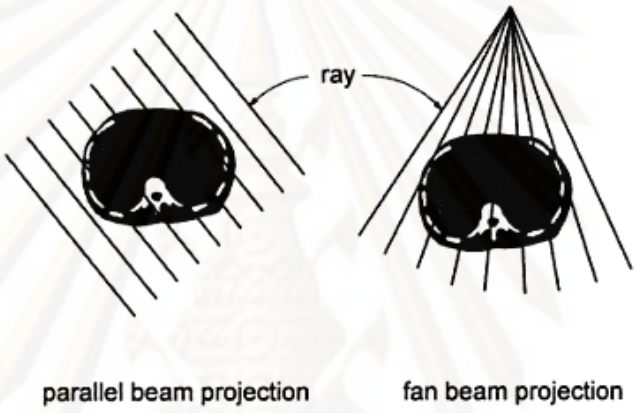

Figure 2.2 Two different geometries have been used in CT, parallel beam projection and fan beam projection. (Bushberg J T, Seibert J A, Leiholdt EM and Boone J M, The essential physics of medical imaging, Lippincott Williams & Wilkins, 2002)

2.1.4 Tomographic reconstruction [10]

Each ray that is acquired in CT is a transmission measurement through the patient along a line, where the detector measures an x-ray intensity, I_t. The unattenuated intensity of the x-ray beam is also measured during the scan by a reference detector, and this detects an x-ray intensity I_0. The relationship between I_t and I_0 is given by the following equation:

$$I_t = I_0 e^{-\mu t} \qquad (2.1)$$

Where t is the thickness of the patient along the ray and μ is the average linear attenuation coefficient along the ray. Notice that I_t and I_0 are machine-dependent values, but the product μt is an important parameter relating to the anatomy of the patient along a given ray. When the equation is rearranged, the measured values I_t and I_0 can be used to calculate the parameter of interest:

$$\ln\left(\frac{I_0}{I_t}\right) = \mu t \qquad (2.2)$$

Where *ln* is the natural logarithm (to base *e*, *e* =2.78…), *t* ultimately cancels out, and the value μ for each ray is used in the CT reconstruction algorithm. This computation, which is a preprocessing step performed before image reconstruction, reduces the dependency of the CT image on the machine-dependent parameters, resulting in an image that depends primarily on the patient's anatomic characteristics. This is very much a desirable aspect of imaging in general, and high clinical utility of CT results, in part, from this feature. By comparison, if a screen-film radiograph is underexposed (I_0 is too low) it appear too white, and if it is overexposed (I_0 is too high) it appear too dark. The density of CT images is independent of I_0, although the noise in the image is affected.

After preprocessing of the raw data, a CT *reconstruction algorithm* is used to produce the CT images. There are numerous reconstruction strategies; however, *filter back-projection* reconstruction is most widely used in clinical CT scanners. The back-projection method builds up the CT image in the computer by essentially reversing the acquisition steps. In Figure 2.3, the data acquisition in CT scanner involves making transmission measurements through the object at numerous angles around the object (left) and the process of computing the CT image from the acquisition data essentially reverses the acquisition geometry mathematically (right). During acquisition, attenuation information along a known path of the narrow x-ray beam is integrated by a detector. During back-projection reconstruction, the μ value for each ray is smeared along this same path in the image of the patient. As the data from a large number of rays are back-projected onto the image matrix, areas of high attenuation tend to reinforce each other, and areas of flow attenuation also reinforce, building up the image in the computer.

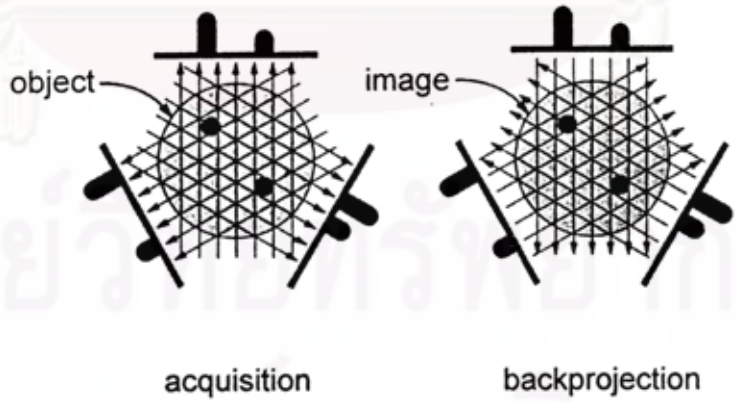

Figure 2.3 Data acquisition in CT scanner around the object and the process of computing the CT image. (Bushberg J T, Seibert J A, Leiholdt EM and Boone J M, The essential physics of medical imaging, Lippincott Williams & Wilkins, 2002)

2.1.5 Detectors and Detector Arrays [10]

A) Xenon detectors

Xenon detectors use high-pressure (about 25 atm) nonradioactive xenon gas, in long thin cells between two metal plates (Figure 2.4). Although a gaseous detector does not have the same detection efficiency as a solid one, the detector can be made very thick (e.g., 6 cm) to compensate in part for its relatively low density. The metal septa that separate the individual xenon detectors can also be made quite thin, and this improves the geometric efficiency by reducing dead space between detectors. The geometric efficiency is the fraction of primary x-rays exciting the patient that strike active detector elements.

The long, thin ionization plates of a xenon detector are highly directional. For this reason, xenon detectors must be positioned in a fixed orientation with respect to the x-ray source. Therefore, xenon detectors cannot be used for fourth-generation scanners, because those detectors have to record x-rays as the source moves over a very wide angle. Xenon detectors can be used only for third-generation systems.

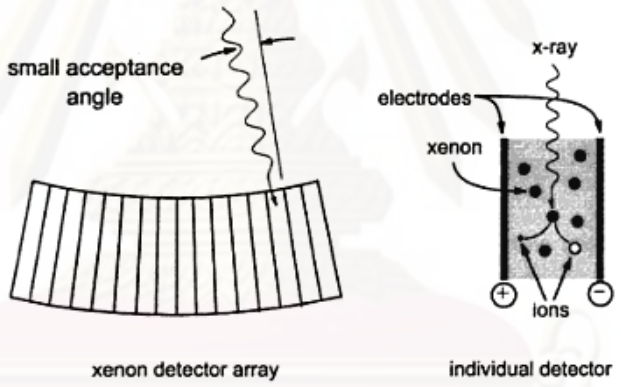

Figure 2.4 Xenon detector arrays. (Bushberg J T, Seibert J A, Leiholdt EM and Boone J M, The essential physics of medical imaging, Lippincott Williams & Wilkins, 2002)

Xenon detectors for CT are ionization detectors—a gaseous volume is surrounded by two metal electrodes, with a voltage applied across the two electrodes. As x-rays interact with the xenon atoms and cause ionization (positive atoms and negative electrons), the electric field (volts per centimeter) between the plates causes the ions to move the electrodes, where the electronic charge is collected. The electronic signal is amplified and then digitized, and its numerical value is directly proportional to the x-ray intensity striking the detectors, and its use is now relegated to inexpensive CT scanners.

B) Solid-State Detectors

A solid-state CT detector is composed of a scintillator couple tightly to a photodetector. The scintillator emits visible light when it is struck by x-rays, just as in an x-ray intensifying screen. The light emitted by the scintillator reaches the photodetector, typically a photodiode, which is an electrode device that converts light intensity into an electrical signal proportional to the light intensity. This scintillator-photodiode design of a solid-state CT detector is very similar in concept to many digital radiographic x-ray detector systems; however, the performance requirements of CT are slightly different. The detector size in CT is measured in millimeters (typically 1.0 × 15 mm or 1.0 × 1.5 mm for multiple detector array scanners), whereas detector elements in digital radiography systems are typically 0.10 to 0.20 mm on each side. CT requires a very high-fidelity, low-noise signal, typically digitized to 20 or more bits.

The scintillator used in solid-state CT detectors varies among manufacturers, with $CdWO_4$ yttrium and gadolinium ceramics, and other materials. Because the density and effective atomic number of scintillators are substantially higher than the pressurized xenon gas, solid-state detectors typically have better x-ray absorption efficiency. However, to reduce crosstalk between adjacent detector elements, a small gap between detector elements is necessary, and this reduces the geometric efficiency.

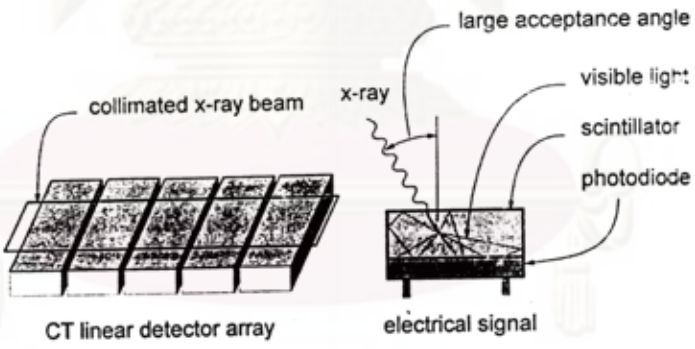

Figure 2.5 Solid-state detectors comprise a scintillator coupled to a photodiode. (Bushberg J T, Seibert J A, Leiholdt EM and Boone J M, The essential physics of medical imaging, Lippincott Williams & Wilkins, 2002)

The top surface of a solid-state CT detector is essentially flat and therefore is capable of x-ray detection over a wide range of angles, unlike the xenon detector. Solid-state detectors are required for fourth-generation CT scanners, and they are used in most high-tier third-generation scanners as well.

C) Multiple Detector Arrays

Multiple detector arrays are a set of several linear detector arrays, tightly abutted (Figure 2.6). The multiple detector array is an assembly of a multiple solid-state detector array modules. With a traditional single detector array CT system, the detectors are quite wide (e.g., 15 mm) and the adjustable collimator determines slice thickness, typically between 1 and 13 mm. with these systems, the spacing between the collimator blades is adjusted by small motors under computer control. With multiple detector arrays, slice width is determined by the detectors, not by the collimator (although a collimator does limit the beam to the total slice thickness). To allow the slice width to be adjustable, the detector width must be adjustable. It is not feasible, however, to physically change the width of the detector arrays per se. therefore, with multislice systems, the slice width is determined by grouping one or more detector units together. For one manufacturer, the individual detector elements are 1.25 mm wide, and there are 16 contiguous detectors across the module. The detector dimensions are referenced to the scanner's *isocenter*, the point at the center of gantry rotation. The electronics are available for four detect array channels, and one, two, three or four detectors on the detector module can be combined to achieve slices of 4 × 1.25 mm, 4 × 2.50 mm, 4 × 3.75 mm, or 4 × 5.00 mm. to combine the signal from several detectors, the detectors are essentially wired together using computer-controlled switches. Other manufacturers use the same general approach but with different detector spacings.

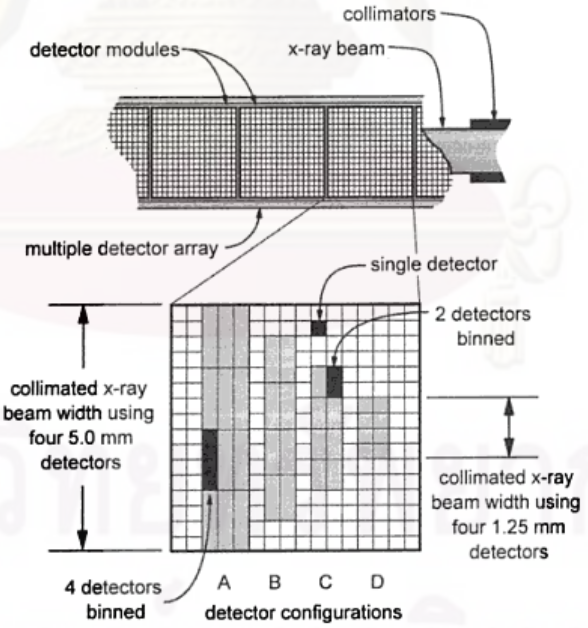

Figure 2.6 A multiple detector array composed of multiple detector modules (top) and four different detector configurations each allowing the detection of four simultaneous slices but at different slice widths determined by number of detectors binned together (bottom). (Bushberg J T, Seibert J A, Leiholdt EM and Boone J M, The essential physics of medical imaging, Lippincott Williams & Wilkins, 2002)

Multiple detector array CT scanners make use of solid-state detectors. For a third-generation multiple detector array with 16 detectors in the slice thickness dimension and 750 detectors along each array, 12,000 individual detector elements are used. The fan angle commonly used in third-generation CT scanners is about 60 degrees, so fourth-generation scanners (which have detectors placed around 360 degrees) require roughly six times as many detectors as third-generation systems. Consequently, all currently planned multiple detector array scanners make use of third-generation geometry.

2.1.6 Details of Acquisition [10]

A) Slice thickness: multiple detector array scanners

The slice thickness of multiple detector array CT scanners is determined not by the collimation, but rather by the width of the detectors in the slice thickness dimension. The width of the detectors is changed by *binning* different numbers of individual detector elements together—that is, the electronic signals generated by adjacent detector elements are electronically summed. Multiple detector arrays can be used both in conventional axial scanning and in helical scanning protocols. In axial scanning (i.e., with no table movement) where, for example, four detector arrays are used, the width of the two center detector arrays almost completely dictates the thickness of the slices. For the two slices at the edges of the scan (detector arrays 1 and 4 of the four active detector arrays), the inner side of the slice is determined by the edge of the detector, but the outer edge is determined either by the collimator penumbra or the outer edge of the detector, depending on collimator adjustment. With a multiple detector array scanner in helical mode, each detector array contributes to every reconstructed image, and therefore the slice sensitivity profile for each detector array needs to be similar to reduce artifacts. To accommodate this condition, it is typical to adjust the collimation so that the focal spot-collimator blade penumbra falls outside the edge detectors. This causes the radiation dose to be a bit higher (especially for small slice widths) in multislice scanners, but it reduces artifacts by equalizing the slice sensitivity profiles between the detector arrays.

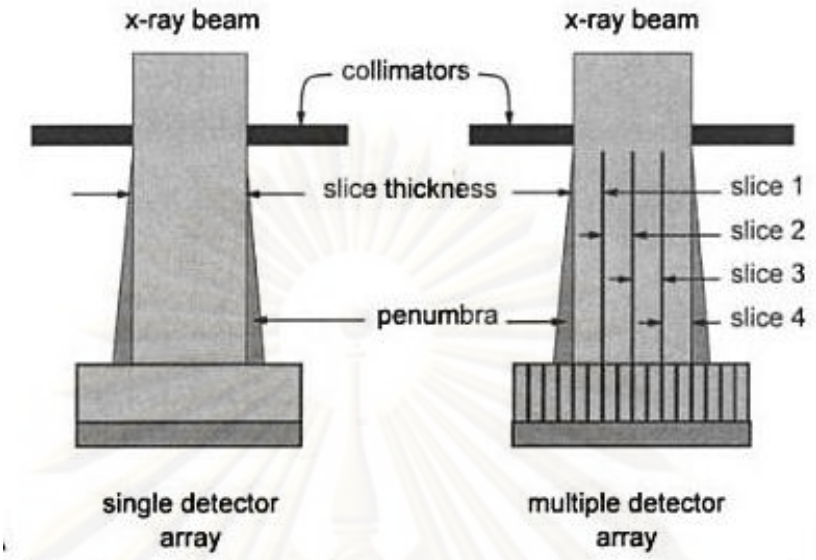

Figure 2.7 Slice thickness of single detector array and multiple detector arrays scanners. (Bushberg J T, Seibert J A, Leiholdt EM and Boone J M, The essential physics of medical imaging, Lippincott Williams & Wilkins, 2002)

B) Detector pitch and collimator pitch

Pitch is a parameter that comes to play when helical scan protocols are used. In a helical CT scanner with one detector array, the pitch is determined by the collimator (collimator pitch) and is defined as:

$$Collimator\ pitch\ = \frac{table\ \ movement\ \ (mm)per\ 360\ degree\ \ rotation\ \ of\ \ gantry}{collimator\ \ \ width\ (mm)at\ \ isocenter} \qquad (2.5)$$

It is customary in CT to measure the collimator and detector widths at the isocenter of the system. The collimator pitch represents the traditional notion of *pitch*, before introduction of multiple detector array CT scanners. Pitch is an important component of the scan protocol, and it fundamentally influences radiation dose to the patient, image quality, and scan time. For single detector array scanners, a pitch of 1.0 implies that the number of CT view acquired, when averaged over the long axis of the patient, is comparable to the number acquired with contiguous axial CT. A pitch of less than 1.0 involves overscanning, which may result in some slight improvement in image quality and a higher radiation dose to patient. CT manufacturers have spent a great deal of developmental effort in optimizing scan protocols for pitches greater than 1.0, and pitches up to 1.5 are commonly used. Pitches with values greater than 1.0 imply some degree of partial scanning along the long axis of the patient. The benefit is faster scan time, less patient motion, and, in circumstances, use of a smaller volume of contrast agent. Although CT acquisitions around 360 degrees are typical for images of the highest fidelity, the minimum requirement to produce an adequate CT image is a scan of 180

degrees plus the fan angle. With fan angles commonly at about 60 degrees, this means that, at a minimum, (180 + 60)/360, or 0.66, of the full circle is required.

This implies that the upper limit on pitch should be about 1/0.66, or 1.5, because 66% of the data in a 1.5-pitch scan remains contiguous.

Scanners that have multiple detector arrays require a different definition of pitch. The collimator pitch defined previously is still valid, and collimator pitches range between 0.75 and 1.5, as with single detector array scanners. The *detector pitch* is also a useful concept for multiple detector array scanners, and it is defined as:

$$Detector\ pitch = \frac{table\ movement\ (mm)per\ 360\ degree\ rotation\ of\ gantry}{detector\ width\ (mm)} \quad (2.6)$$

The need to define detector pitch and collimator pitch arises because beam utilization between single and multiple detector array scanners is different. For a multiple detector array scanner with N detector arrays, the collimator pitch is as follows:

$$Collimator\ pitch = \frac{Detector\ pitch}{N} \quad (2.7)$$

For scanners with four detector arrays, detector pitches running from 3 to 6 are used. A detector pitch of 3 for a four-detector array scanner is equivalent to a collimator pitch of 0.75 (3/4), and a detector pitch of 6 corresponds to a collimator pitch of 1.5 (6/4).

2.1.7 Tomographic Reconstruction [10]

A) Rays and views: the sinogram

The data acquired for one CT slice can be displayed before reconstruction. This type of display is called a *sinogram*. Sinograms are not used for clinical purposes, but the concepts that they embody are interesting and relevant to understanding principles. The horizontal axis of the sinogram corresponds to the different rays in each projection. For a third-generation scanner, for example, the horizontal axis of the sinogram corresponds to the data acquired at one instant in time along the length of the detector array. A bad detector in a third-generation scanner would show up as a vertical line on the sinogram. The vertical axis in the sinogram represents each projection angle. A state-of-the-art CT scanner may acquire approximately 1,000 views with 800 rays per view, resulting in a sinogram that is 1,000 pixels tall and 800 pixels wide, corresponding to 800,000 data points. The number of data points (rays/view × views) acquired by the CT scanner has some impact on the final image quality. For example, first- and second-generation scanners used 28,800 and 324,000 data points, respectively. A modern 512 × 512 circular CT image contain about 205,000 image pixels, and therefore the ratio between raw data points and image pixels is in the range of about 3.2 to 3.9 (800,000/205,000 = 3.9).

The number of rays used to reconstruct a CT image has a profound influence on the radial component of spatial resolution, and the number of views affects the circumferential component of the resolution. CT images of a simulated object reconstructed with differing numbers of rays show that reducing the ray sampling results in low-resolution, blurred images. CT images of the simulated object reconstructed with differing numbers of views show the effect of aliasing in using too few angular views. The sharp edges (high spatial frequencies) of the bar patterns produce radiating artifacts that become more apparent near the periphery of the image. The view aliasing is mild with 240 views and becomes pronounced with 60 views. The presence of high-frequency objects (sharp edges) in the image exacerbates the impact of view aliasing. In Figure 2.8, the reconstruction with 960 views in each image is shown, but with the number of rays differing as indicated. As the number of rays is reduced, the detector aperture was made wider to compensate. With only 32 rays, the detector aperture becomes quite large and the image is substantially blurred as a result. In Figure 2.9 three images which were reconstructed using 512 rays but differing numbers of views are shown. In going from 960 to 240 views, a slight degree of view aliasing is seen (center image). When only 60 views are used (right image), the view aliasing is significant. The presence of the aliasing is exacerbated by objects with sharp edges, such as the line pair phantom in the image.

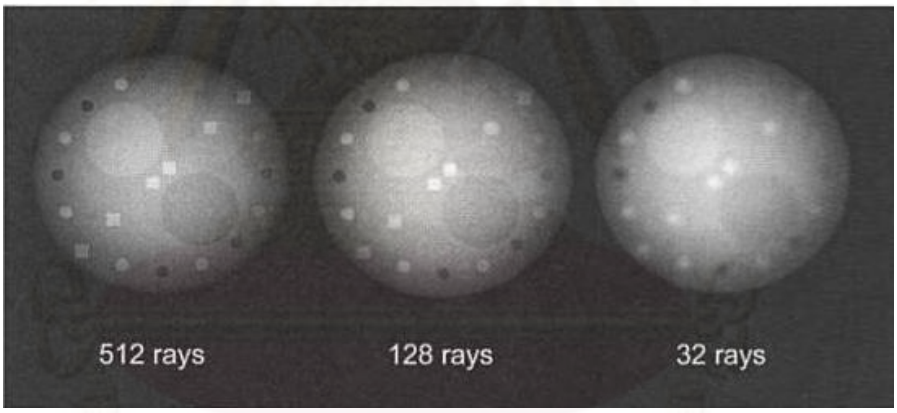

Figure 2.8 An image of a test object, reconstructed with 960 views in each image, but with the number of rays are 512 rays, 128 rays and 32 rays resulting in different image quality from shape to blurred images. (Bushberg J T, Seibert J A, Leiholdt EM and Boone J M, The essential physics of medical imaging, Lippincott Williams & Wilkins, 2002)

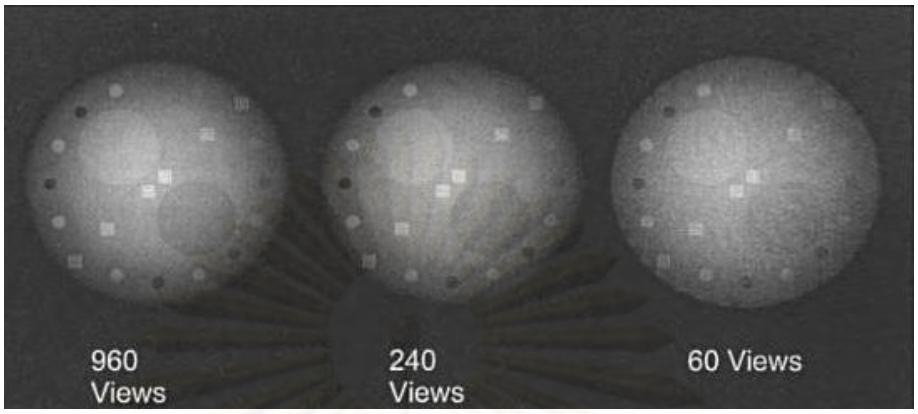

Figure 2.9 Each of three images was reconstructed using 512 rays but the number of views of 960, 240 and 60 showing different degree of alising. (Bushberg J T, Seibert J A, Leiholdt EM and Boone J M, The essential physics of medical imaging, Lippincott Williams & Wilkins, 2002)

B) Processing the data

The raw data acquired by a CT scanner is preprocessed before reconstruction. Numerous preprocessing steps are performed. Electronic detector systems produce a digitized data set that is easily processed by the computer. Calibration data determined from air scans provide correction data that are used to adjust the electronic gain of each detector in the array. Variation in geometric efficiencies caused by imperfect detectors alignments is also corrected. For example, in fourth-generation scanners, the x-ray source rotates in an arc around each of the detectors in the array. As the angle and the distance between the detector and the x-ray tube change over this arc, the geometric efficiency of x-ray detection changes. (Similarly, the intensity of sunlight shining on one palm changes as the wrist is rotated.) These geometric efficiencies are measured during calibration scans and stored in the computer; they are corrected in the preprocessing steps.

After the digital data are calibrated, the logarithm of the signal is computed by the following equation:

$$\ln I_0/I_t = \mu t \qquad (2.8)$$

Where I_0 is the reference data, I_t is the data corresponding to each ray in each view, t is the patient's overall thickness (in centimeters) for that ray, and μ is the linear attenuation coefficient (in cm^{-1}). Note that the data used to calculate the images is linear with respect to the linear attenuation coefficient, μ. The linear attenuation coefficient is determined by the composition and density of the tissue inside each voxel in the patient. Whereas μ is the total attenuation coefficient for each ray, it can be broken down into its components in each small path length Δt

$$\mu t = \mu_1 \Delta t + \mu_2 \Delta t + \mu_3 \Delta t + \ldots + \mu_n \Delta t = \Delta t[\mu_1 + \mu_2 + \mu_3 + \ldots + \mu_n] \quad (2.9)$$

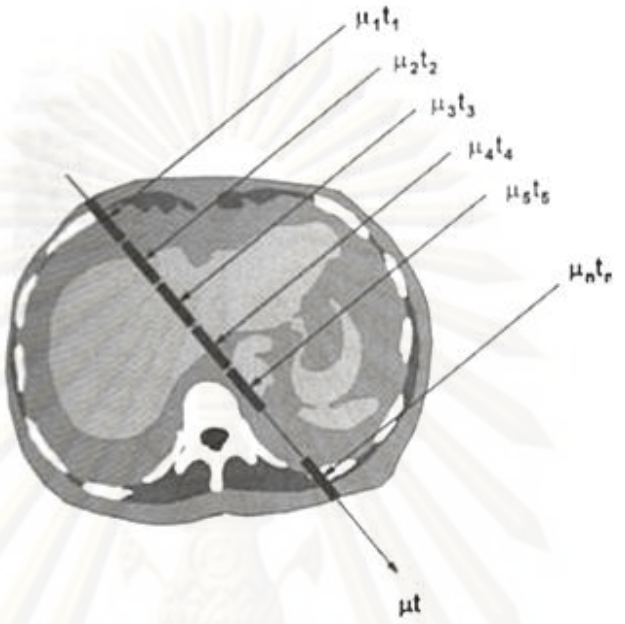

Figure 2.10 The measured value of a single ray is equivalent to the attenuation path (t) times the linear attenuation coefficient (μ). The single measurement of μt can be broken up into a series of measurements $\mu_1 t_1, \mu_2 t_2, \ldots, \mu_n t_n$ as shown. (Bushberg J T, Seibert J A, Leiholdt EM and Boone J M, The essential physics of medical imaging, Lippincott Williams & Wilkins, 2002)

The constant Δt factors outs, resulting in the following:

$$\mu = \mu_1 + \mu_2 + \mu_3 + \ldots + \mu_n \quad (2.10)$$

Therefore, the reconstructed value in each pixel is the linear attenuation coefficient for the corresponding voxel.

C) Interpolation (Helical)

Helical CT scanning produces a data set in which the x-ray source has traveled in a helical trajectory around the patient. Present-day CT reconstruction algorithms assume that the x-ray source has negotiated a circular, not a helical, path around the patient. To compensate for these differences in the acquisition geometry, before the actual CT reconstruction the helical data set is interpolated into a series of planar image data sets, as illustrated in Figure 2.11. Although this interpolation represents an additional step in the computation, it also enables an important feature. With conventional axial scanning, the standard is to acquire contiguous images, which abut one another along the cranio-caudal

axis of the patient. With helical scanning, however, CT images can be reconstructed at any position along the length of the scan to within $(1/2)$ (pitch) (slice thickness) of each edge of the scanned volume. During helical acquisition, the data are acquired in a helical path around the patient. Before reconstruction, the helical data are interpolated to the reconstruction plane of interest. Interpolation is essentially a weighted average of the data from either side of the reconstruction plane, with slightly different weighting factors used for each projection angle. Helical scanning allows the production of additional overlapping images with *no additional dose* to patient. The added clinical importance of using interleaved images. The sensitivity of the CT image to objects not centered in the voxel is reduced (as quantified by the slice sensitivity profile), and therefore subtle lesions, which lay between two contiguous images, may be missed. With helical CT scanning, interleaved reconstruction allows the placement of additional images along the patient, so that the clinical examination is almost uniformly sensitive to subtle abnormalities. Interleaved reconstruction adds no additional radiation dose to the patient, but additional time is required to reconstruct the images. Although an increase in the image count would increase the interpretation time for traditional side-by-side image presentation, this concern will ameliorate as more CT studies are read by radiologists at computer workstations.

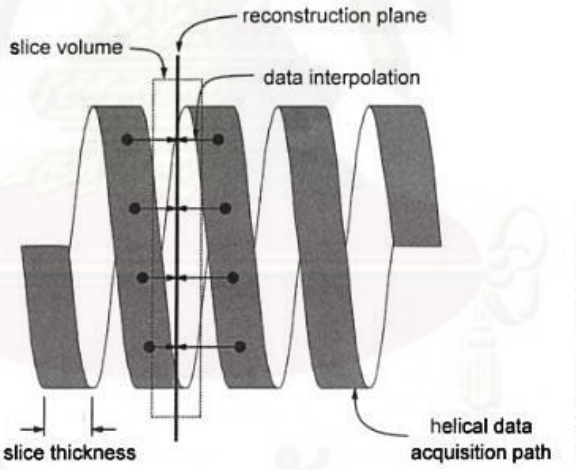

Figure 2.11 During helical acquisition, the data are acquired in a helical path around the patient. (Bushberg J T, Seibert J A, Leiholdt EM and Boone J M, The essential physics of medical imaging, Lippincott Williams & Wilkins, 2002)

It is important not to confuse the ability to reconstruct CT images at short intervals along the helical data set with axial resolution itself. The slice thickness (governed by collimation with single detector array scanners and by the detector width in

multislice scanners) dictates the actual spatial resolution along the long axis of the patient. For example, images with 5-mm slice thickness can be reconstructed every 1-mm, but this does not mean that 1-mm spatial resolution is achieved. It simply means that the images are sampled at 1-mm intervals. To put the example in technical terms, the *sampling pitch* is 1 mm but the *sampling aperture* is 5 mm. In practice, the use of interleaved reconstruction much beyond a 2:1 interleaved yields diminishing returns, except for multiplanar reconstruction (MPR) or 3D rendering applications.

D) Simple back-project reconstruction

Once the image raw data have been preprocessed, the final step is to use the planar projection data sets (i.e., the preprocessed sinogram) to reconstruct the individual tomographic images. *Iterative reconstruction techniques* are discussed here because they are not used in clinical x-ray CT. As a basic introduction to the reconstruct process, consider Figure 2.12. Assume that a very simple 2 × 2 "image" is known only by the projection values. Using algebra ("N equations in M unknowns"), one can solve or the image values in the simple case of a 4-pixel image. A modern CT image contains approximately 205,000 pixels (the circle within a 512 × 512 matrix) or "unknowns," and each of the 800,000 projections represent an individual equation. Solving this kind of a problem is beyond simple algebra, and back-projection is the method of choice.

Simple back-projection is a mathematical process, based on trigonometry, which is designed to emulate the acquisition process in reverse. Each ray in each view represents an individual measurement of μ. In addition to the value of μ for each ray, the reconstruction algorithm also "knows" the acquisition angle and position in the detector array corresponding to each ray. Simple back-projection starts with an empty image matrix (an image with all pixels set to zero), and the μ value from each ray in all views is smeared or back-projected onto the image matrix. In other words, the value of μ is added to each pixel in a line through the image corresponding to the ray's path.

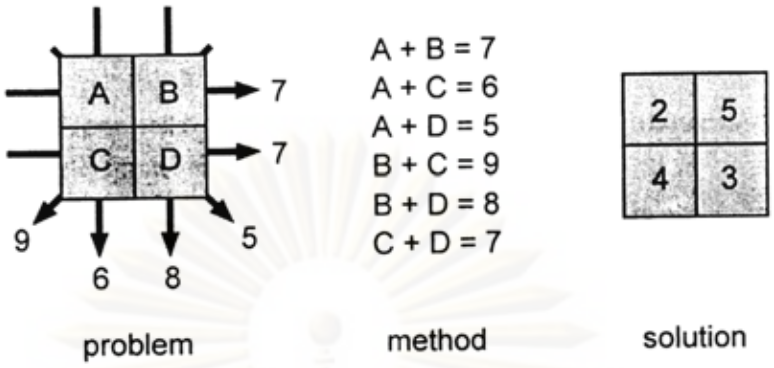

Figure 2.12 The mathematical problem posed by CT reconstruction is to calculate image data (the pixel values—A, B, C, and D) from the projection values (arrows). (Bushberg J T, Seibert J A, Leiholdt EM and Boone J M, The essential physics of medical imaging, Lippincott Williams & Wilkins, 2002)

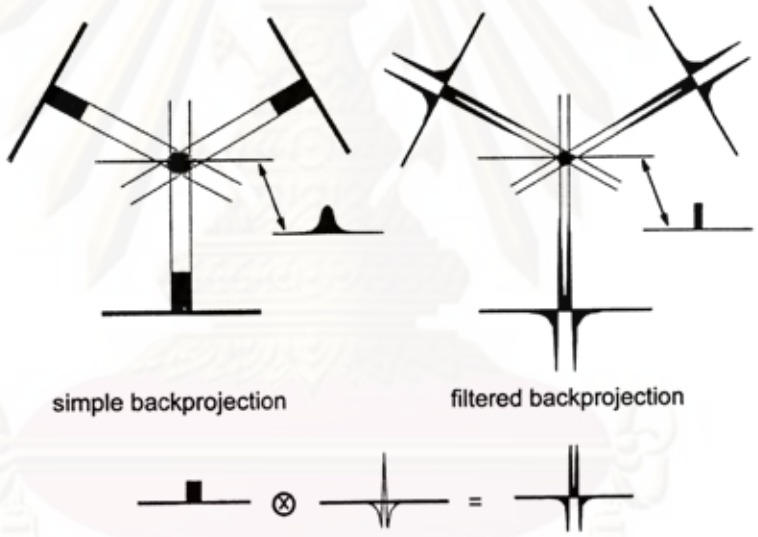

Figure 2.13 Simple back-projection and filtering back-projection methods of reconstruction. (Bushberg J T, Seibert J A, Leiholdt EM and Boone J M, The essential physics of medical imaging, Lippincott Williams & Wilkins, 2002)

Simple back-projection comes very close to reconstructing the CT image as desired. However, a characteristic 1/r blurring is a byproduct of simple back-projection. Imagine that a thin wire is imaged by a CT scanner perpendicular to the image plane; this should ideally result in a small point on the image. Rays not running through the wire will contribute little to the image ($\mu = 0$). The back-projected rays, which do run through the wire, will converge at the position of the wire in the image plane, but these projections run from one edge of the reconstruction circle to the other. These projections (i.e., lines) will therefore “radiate” geometrically in all directions away from a point

input. If the image gray scale is measured as a function of distance away from the center of the wire, it will gradually diminish with a 1/r dependency, where r is the distance away from the point. This phenomenon results in a blurred image of the actual object when simple back-projection is used. A filtering step is therefore added to correct this blurring, in a process known as *filtered back-projection.*

E) Filtering back-projection reconstruction

In filtered back-projection, the raw view data are mathematically filtered before being back-projected onto the image matrix. The filtering step mathematically reverses the image blurring, restoring the image to an accurate representation of the object that was scanned. The mathematical filtering step involves *convolving* the projection data with a convolution *kernel*. Many convolution kernels exist, and different kernels are used for varying clinical applications such as soft tissue imaging or bone imaging. The kernel refers to the shape of the filter function in the spatial domain, whereas it is common to perform the filtering step in frequency domain. Much of the nomenclature concerning filtered back-projection involves an understanding of the frequency domain. The Fourier transform (FT) is used to convert a function expressed in the spatial domain (millimeters) into the spatial frequency domain (cycles per millimeter, sometimes expressed as mm^{-1}); the inverse Fourier transform (FT^{-1}) is used to convert back. Convolution is an integral calculus operation and is represented by the symbol$\otimes$. Let p (x) represent projection data (in the spatial domain) at a given angle (p(x) is just one horizontal line from a sinogram), and let k(x) represent the spatial domain kernel as shown in equation 2.11. The filtered data in the spatial domain, p´(x), is computed as in equation 2.11:

$$p'(x) = p(x) \otimes k(x) \tag{2.11}$$

The difference between filtered back-projection and simple back-projection is the mathematical filtering operation (convolution) shown in equation 2.11. In filtered back-projection, p´(x) is back-projected onto the image matrix, whereas in simple back-projection, p(x) is back-projected. The equation can also be performed, quite exactly, in the frequency domain:

$$p'(x) = FT^{-1}\{FT[p(x)] \times K(f)\} \tag{2.12}$$

Where K(f) = FT[k(x)], the kernel in the frequency domain. This equation shows that the convolution operation can be performed by Fourier transforming the projection data, *multiplying* by the frequency domain kernel (K(f)), and then applying the inverse Fourier transform on that product to get the filtered data, ready to be back-projected.

F) CT numbers or Hounsfield units [10]

After CT reconstruction, each pixel in the image is represented by a high-precision floating point number that is useful for computation but less useful for display. Most computer display hardware makes use of integer images. Consequently, after CT reconstruction, but before storing and displaying, CT images are normalized and truncated to integer values. The number *CT(x,y)* in each pixel, *(x,y)*, of the image is converted using the following expression:

$$CT(x,y) = 1{,}000\frac{\mu(x,y)-\mu_{water}}{\mu_{wat\ er}} \tag{2.13}$$

where $\mu(x,y)$ is the floating point number of the (x,y) pixel before conversion, μ_{water} is the attenuation coefficient of water, and CT(x,y) is the CT number (or Hounsfield unit) that ends up in the final clinical CT image. The value of μ_{water} is about 0.195 for the x-ray beam energies typically used in CT scanning. This normalization results in CT numbers ranging from about -1,000 to +3,000, where -1,000 corresponds to air, soft tissue range from -300 to -100, water is 0, and dense bone and areas filled with contrast agent range up to +3,000.

CT numbers corresponds to physically in the patient as the following details. CT images are produced with a highly filtered, high-kV x-ray beam, with an average energy of about 75 keV. At this energy in muscle tissue, about 91% of x-ray interactions are Compton scatter. For fat and bone, Compton scattering interactions are 94% and 74% respectively. Therefore, CT numbers and hence CT images derive their contrast mainly from the physical properties of tissue that influence Compton scatter. Density, g/cm^3, is a very important discriminating property of tissue (especially in lung tissue, bone and fat), and the linear attenuation coefficient, μ tracks linearly with density. Other than physical density, the Compton scatter cross section depends on the electron density (ρ_e) in tissue: $\rho_e = NZ/A$, where N is Avogadro's number (6.023×10^{23}), Z is the atomic number, and A is the atomic mass of the tissue. The main constituents of soft tissue are hydrogen (Z = 1, A = 1), carbon (Z = 6, A = 12), nitrogen (Z = 7, A = 14), and oxygen (Z = 8, A = 16). Carbon, nitrogen, and oxygen all have the same Z/A ratio of 0.5, so their electron densities are the same. Because the Z/A ratio for hydrogen is 1.0, the relative abundance of hydrogen in a tissue has some influence on CT number. Hydrogenous tissue such as fat is well visualized on CT. Nevertheless, density plays the dominant role in forming contrast in medical CT.

CT numbers are *quantitative*, and this property leads to more accurate diagnosis in some clinical settings. For example, pulmonary nodules that are calcified are typically benign, and the amount of calcification can be determined from the CT image based on the mean CT number of the nodule. Measuring the CT number of a single pulmonary nodule is therefore common practice, and it is an important part of the diagnostic work-

up. CT scanners measure bone density with good accuracy, and when phantoms are placed in the scan field along with the patient, quantitative CT techniques can be used to estimate bone density, which is useful in assessing fracture risk. CT is also quantitative in terms of linear dimensions, and therefore it can be used to accurately assess tumor volume or lesion diameter.

2.1.8 Radiation Dose [10]

Different x-ray modalities address radiation dose in different ways. For example, in chest radiography it is the entrance *exposure* (not the *dose*) that is the commonly quoted comparison figure. In mammography, the *average glandular dose* is the standard measure of dose. The distribution of radiation dose in CT is markedly different than in radiography, because of the unique way in which radiation dose is deposited. There are three aspects of radiation dose in CT that are unique in comparison to x-ray projection imaging. First, because a single CT image is acquired in a highly collimated manner, the volume of tissue that is irradiated by the primary x-ray beam is substantially smaller compared with, for example, the average chest radiograph. Second, the volume of tissue that is irradiated in CT exposed to the x-ray beam from almost all angles during the rotational acquisition, and this more evenly distributes the radiation dose to the tissues in the beam. In radiography, the tissue irradiated by the entrance beam experiences exponentially more dose than the tissue near the exit surface of the patient. Finally, CT acquisition requires a high SNR to achieve high contrast resolution, and therefore the radiation dose to the slice volume is higher because the techniques used (kV and mAs) are higher. As a rough comparison, a typical PA chest radiograph may be acquired with the use of 120 kV and 5 mAs, whereas a thoracic CT image is typically acquired at 120 kV and 200 mAs.

A) Dose measurement [10]

Compton scattering is the principal interaction mechanism in CT, so the radiation dose attributable to scattered radiation is considerable, and it can be higher than the radiation dose from the primary beam. Scattered radiation is not confined to the collimated beam profile as primary x-rays are, and therefore the acquisition of a CT slice delivers a considerable dose from scatter to adjacent tissues, outside the primary beam. Furthermore, most CT protocols call for the acquisition of a series of near-contiguous CT slices over the tissue volume under examination. Take, for example, a protocol in which ten 10-mm CT slices are acquired in the abdomen. The tissue in slice 5 will receive both primary and scattered radiation from slices 4 and 6, and to a lesser extent from slices 3 and 7.

Patient dose in CT is usually expressed in terms of organ dose and effective dose. This is the calculation method of effective dose. The main dosimetric quantity used in CT

is the Computed Tomography Dose Index (CTDI). CTDI is defined as the integral of the dose profile along a line parallel to the axis of rotation for a single scan, divided by the nominal slice thickness [7].

$$CTDI = \frac{1}{NT}\int_{-\infty}^{\infty} D(z)dz \quad (2.14)$$

Where *D(z)* is the dose as a function of position z along the axis of rotation of scanner. *N* is the number of tomographic sections imaged in a single axial scan. This is equal to the number of data channels used in a particular scan. The value of N may be less than or equal to the maximum number of data channels available on the system, and *T* is the width of the tomographic section along the z-axis imaged by one data channel. In multiple-detector-row (multi-slice) CT scanners, several detector elements may be grouped together to form one data channel. In single-detector-row (single-slice) CT, the z-axis collimation (T) is the nominal scan width [11].

CTDI represents the average absorbed dose, along the z-axis, from a series of contiguous irradiations. It is measured from one axial CT scan (one rotation of the x-ray tube), and is calculated by dividing the integrated absorbed dose by the nominal beam collimation. The CTDI is always measured in the axial scan mode for single rotation of the x-ray source, and theoretically estimates the average dose within the central region of a scan volume consisting of multiple, contiguous CT scans [Multiple Scan Average Dose (MSAD)] for the case where the scan length is sufficient for the central dose to approach its asymptotic upper limit. The MSAD represents the average dose over small interval (-I/2 , I/2) about the center of scan length (z=0) for a scan interval I, but nominally equivalent method of estimating this value, and required only a single-scan acquisition, which in the early days of CT, saved a considerable amount of time [12].

The CTDI varies across the field of view (FOV). For example, for body CT imaging, the CTDI is typically a factor or two higher at the surface than at the center of the FOV. The average CTDI across the FOV is estimated by the Weighted CTDI ($CTDI_w$) , where

$$CTDI_w = \frac{1}{3}\,CTDI_{100,center} + \frac{2}{3}\,CTDI_{100\,,perip\,hery} \quad (2.15)$$

The values of 1/3 and 2/3 approximate the relative areas represented by the center and periphery. $CTDI_w$ is useful indicator of scanner radiation output for a specific kVp and mAs. According to IEC 60601-2-44, $CTDI_w$ must use $CTDI_{100}$ as described above and f-factor for air (0.87 rad/R or 1.0 mGy/mGy)

To represent dose for a specific scan protocol, which almost always involves a series of scans, it is essential to take into account any gaps or overlaps between the x-ray

beams from consecutive rotations of the x-ray source. This is accomplished with use of a dose descriptor known as the Volume $CTDI_w$ ($CTDI_{vol}$), where

$$CTDI_{vol} = \frac{NT}{I} \times CTDI_w \quad (2.16)$$

And I = the table increment per axial scan (mm).

Since pitch is defined as the ratio of the table travel per rotation (I) to the total nominal beam width (NT),

$$Pitch = \frac{I}{N \times T} \quad (2.17)$$

Thus, Volume CTDI can be expressed as

$$CTDI_{vol} = \frac{1}{pitch} \times CTDI_w \quad (2.18)$$

Whereas $CTDI_w$ represents the average absorbed radiation dose over the x and y directions at the center of the scan from a series of axial scans where the scatter tails are negligible beyond the 100-mm integration limit, $CTDI_{vol}$ represents the average absorbed radiation dose over the x, y, and z directions. It is conceptually similar to the MSAD, but is standardized with respect to the integration limits (± 50 mm) and the f-factor used to convert the exposure or air kirma measurement into dose to air.

The $CTDI_{vol}$ provides a single CT dose parameter, based on a directly and easily measured quantity, which represents the average dose within the scan volume for a standardized (CTDI) phantom. The SI unit is milligray (mGy). $CTDI_{vol}$ is a useful indicator of the dose to a standardized phantom for a specific exam protocol, because it takes into account protocol-specific information such as pitch. Its value may be displayed prospectively on the console of newer CT scanners, although it may be mislabeled on some systems as $CTDI_w$. The IEC consensus agreement on these definitions is used on most modern scanners.

While $CTDI_{vol}$ estimates the average radiation dose within the irradiated volume for and object of similar attenuation to the CTDI phantom, it does not represent the average dose for objects of substantially different size, shape, or attenuation or when the 100-mm integration limits omit a considerable fraction of scatter tails. Further, it does not indicate the total energy deposited into the scan volume because it is independent of the length of the scan. That is, its value remains unchanged whether the scan coverage is 10 or 100 cm. It estimates the dose for a 100-mm scan length only, even though the actual volume-averaged dose will increase with scan length up to the limiting equilibrium dose value.

To better represent the overall energy delivered by a given scan protocol, the absorbed dose can be integrated along the scan length to compute the Dose Length Product (DLP), where

$$DLP(mGy \cdot cm) = CTDI_{vol}(mGy) \times scan\ length(cm) \quad (2.19)$$

The DLP reflects the total energy absorbed (and thus the potential biological effect) attributable to the complete scan acquisition. Thus, an abdomen-only CT exam might have the same $CTDI_{vol}$ as an abdomen/pelvis CT exam, but the latter exam would have a greater DLP, proportional to the greater z-extent of the scan volume.

In helical CT, data interpolation between two points must be performed for all projection angles. Thus, the images at the very beginning and end of a helical scan require data from z-axis projections beyond the defined "scan" boundaries (i.e., the beginning and end of the anatomic range over which images are desired). This increase in DLP due to the additional rotation(s) required for the helical interpolation algorithm is often referred to as "overranging". For MDCT scanners, the number of additional rotations is strongly pitch dependent, with a typical increase in irradiation length of 1.5 times the total nominal beam width.

The implications of overranging with regard to the DLP depend on the length of imaged body region. For helical scans that are short relative to the total beam width, the dose efficiency (with regard to overranging) will decrease. For the same anatomy coverage, it is generally more dose efficient to use a single helical scan than multiple helical scans.

It is important to recognize that the potential biological effects from radiation depend not only on the radiation dose to a tissue or organ, but also on the biological sensitivity of the tissue or organ irradiated. Effective dose, E, is a dose descriptor that reflects this difference in biological sensitivity. It is a single dose parameter that reflects the risk of non-uniform exposure in terms of an equivalent whole-body exposure. The units of effective dose are millisieverts (mSv) used in diagnostic radiology [11].

The concept of effective dose was designed for radiation protection of occupationally exposed personnel. It reflects radiation detriment averaged over gender and age, and its application has limitation when applied to medical populations. However, it does facilitate the comparison of biologic effect between diagnostic exams of different types. The use of effective dose facilitates communication with patients regarding the potential harm of a medical exam that use ionizing radiation. The effective dose describes the relative "whole-body" dose for a particular exam and scanner, but is not the dose for any one individual. Effective dose calculation use many assumptions, including a mathematical model of a "standard" human body that does not accurately reflects any one individual (it is androgynous and of an age representative of a radiation

worker). Effective dose is best used to optimize exams and to compare risks between proposed exams. It is a board measure of risk, and as such, should not be quoted with more than one or two significant digits [11].

The most direct way of estimating doses to patients undergoing CT examinations is to measure organ doses in patient-like phantoms. Another way of obtaining the pattern of energy deposition in patients undergoing CT examinations is by calculation. Computations that use Monte Carlo methods follow the paths of a large number of x-rays as they interact with a virtual phantom and estimate the probability of the dominant interaction processes (i.e., Compton scatter and photoelectric absorption). This type of calculation assumes that the patient resembles the phantom used for measurements or Monte Carlo simulation. When patients differ in size and composition, appropriate corrections might need to be used. The resultant information is the absorbed dose to specified tissue, which may be used to predict the biological consequences to that (single) tissue. CT examinations, however, irradiate multiple tissues having different radiation sensitivities. The effective dose takes into account how much radiation is received by an individual tissue, as well as the tissue's relative radiation sensitivity [11].

Specific values of effective dose can be calculated using several different software packages, which are based on the use of data from one of two sources, the National Radiological Protection Board (NRPB) in the United Kingdom or Institute of Radiation Protection (GSF) in Germany. A free Excel spreadsheet can be downloaded from *www.impactscan.org* to perform organ dose and effective dose estimates using the NRPB organ dose coefficients. Other packages are available for purchase [11].

To minimize controversy over differences in effective dose values that are purely the result of calculation methodology and data sources, a generic estimation method was proposed by the European Working Group for Guidelines on Quality Criteria in Computed Tomography. Effective dose values calculated from the NRPB Monte Carlo organ coefficients were compared to DLP values for the corresponding clinical exams to determine a set of coefficients k, where the values of k are dependent only on the region of the body being scanned (head, neck, thorax, abdomen, or pelvis) shown in Table 2.1. Using this methodology, E can be estimated from the DLP, which is reported on most CT systems:

$$E(mSv) \approx k \times DLP \tag{2.20}$$

The values of E predicted by DLP and the values of E estimated using more rigorous calculations methods are remarkably consistent, with a maximum deviation from the mean of approximately 10% to 15%. Hence, the use of DLP to estimate E appears to be a reasonably robust method for estimating effective dose. Similarly, Huda has compared effective dose, as calculated from the NRPB data, to estimates of energy

imparted in order to develop conversion coefficients by which to later estimate effective dose from energy imparted [11].

Table 2.1 Normalized effective dose per dose length product (DLP) for adults (standard physique) and pediatric patients of various ages over various body regions.

Region of body	k (mSv/mGy·cm)				
	0 year old	1 year old	5 year old	10 year old	Adult
Head and neck	0.013	0.085	0.0057	0.0042	0.0031
Head	0.011	0.067	0.0040	0.0032	0.0021
Neck	0.017	0.012	0.011	0.0079	0.0059
Chest	0.039	0.026	0.018	0.013	0.014
Abdomen≈&pelvis	0.049	0.030	0.020	0.015	0.015
Trunk	0.044	0.028	0.019	0.014	0.015

On the other hand, the effective dose can also be deduced in a simplified manner as [13]:

$$E(mSv) = DLP_{air} \times f_{mean} \times k_{CT} \tag{2.21}$$

With f_{mean} being the average value of the conversion factors f(z) for each region of the body and patient group. These data are listed in Table 2.1. The results obtained by using equation 2.20 are certainly less accurate than those found by taking into account the conversion factors f(z) for each individual slice. Nevertheless, the method is much more precise than the very approximate. Since there are many uncertainties involved in the assessment of effective dose, the accuracy thus achieved is more than sufficient for most purposes.

The conversion factors given in Table 2.1 require as the input parameter the axial dose free-in-air. Therefore, the dose-length product used in this context must also be calculated with $CTDI_{air}$. This is inconvenient in so far as dose recommendations (and dose display on the operator's console of some newer scanners) are given in terms of $CTDI_w$. The problem arises from a lack of conversion coefficients with $CTDI_w$ as the input parameter. Therefore the displayed DLP_w must be converted with the aid of the phantom factors.

In this way, a DLP based on $CTDI_w$ can now be related to $CTDI_{air}$ and so used for those purposes where $CTDI_{air}$ is required, such as equation 2.21 and Table 2.2.

The scanner-specific correction is made by application of a scanner factor k_{CT}. Values of k_{CT} for 6 different categories of scanner type (0-V) are tabulated in Table 2.3,

based on data given in Shrimpton98. The scanner factors appropriate for a range of different models can be derived from the information on scanner category. These factors relate to the most commonly used tube potentials. The assignment of individual scanner models to a particular category (0-V) (‘scanner matching’) follows the recommendations given in Shrimpton98 and ImPACT02. The scanner-related error in the present method for the determination of effective dose can thus be reduced to approximately ± 10% [13].

Scanner category refers to the classification of the particular scanner for the purposes of assigning the scanner-specific correction factors k_{CT} listed in Table 2.3. In most cases, the classification was made according to the recommendations given in Shrimpton98 and ImPACT02. In a few, less well-defined cases, classification was made by using the matching formalism developed by ImPACT [13].

The scanner factors k_{CT} are arranged in steps of approximately 10% for the head/neck region and 20% for the trunk region. Scanners with relatively hard beam qualities (higher tube potentials and/or larger filtration) are usually classified in scanner categories I or II; those with softer beam qualities (lower tube potentials and/or smaller filtration) in scanner categories IV and V. Moreover, geometrical effects (focus-axis distance, beam shaper) are also taken into account by this classification [13]. For this study used Siemens SOMATOM Sensation 16 category II had been used in this study.

If the calculations of effective dose have been made for a tube potential U, which the basic dose data (normalized dose free in air ($_nCTDI_{air}$), k_{CT}) for a specific scanner model refer, then a two-step correction is required. The first step takes into account the change in tube output, in terms of $CTDI_{air}$, with tube potential. This varies approximately with the second power of the tube voltage. The corresponding correction factor $k_{U,1}$ is obtained from

$$k_{U,1} = \left(\frac{U}{U_{ref}}\right)^2 \tag{2.21}$$

In the second step, a correction is made for the influence of tube potential on the conversion coefficients used to calculate organ doses (and effective dose). This implicitly means that the scanner factor k_{CT} also changes, with a rate of change of roughly 5% per 10 kV. The second correction factor $k_{U,2}$ therefore is obtained from equation 2.22.

$$k_{U,2} = \left(\frac{U}{U_{ref}}\right)^{0.5} \tag{2.22}$$

Overall, the effective dose thus varies with changes in tube voltage according to the power of 2.5, provided the tube current-time product is kept constant. The same holds true for all phantom-related CTDI quantities.

Table 2.2 Average values f_{mean} of conversion factor (in mSv/mGy·cm) to convert from dose free-in-air on the axis of rotation into effective dose for different regions of the body and patient groups (beam quality: 125 kV, 9 mm Al-equivalent); demarcation of the body regions was made according to Hidajat96/2.

Body region	Adults		Children (7 year-old)		Babies (8 week-old)	
	Female	Male	Female	Male	Female	Male
Head	0.0022	0.0020	0.0028	0.0028	0.0075	0.0074
Neck	0.0051	0.0047	0.0056	0.0055	0.018	0.017
Chest	0.0090	0.0068	0.018	0.015	0.032	0.027
Upper abdomen	0.010	0.0091	0.020	0.016	0.036	0.034
Pelvis*	0.011	0.0062	0.018	0.011	0.045	0.025
Entire abdomen*	0.010	0.0072	0.019	0.014	0.041	0.031

*without direct irradiation of gonads of male patients

Table 2.3 Scanner factors to correct for scanner-specific influences when assessing effective dose.

Scanner category	Scanner factor k_{CT}	
	Head/Neck/Children	Trunk (adults)
0	1.10	1.25
I	1.00	1.00
II	0.90	0.80
III	0.80	0.65
IV	0.70	0.50
V	0.60	0.40

Table 2.4 Summary of the principle for the assessment of the effective dose; U_{ref} is the tube potential to which the basic dose data ($_nCTDI_{air}$, k_{CT}) of the scanner refer. The example given here applies to an examination of the upper abdomen of a female adult of average size and weight.

Step	Influencing factor	Calculation	Provisional result	Example	Reference
1	Tube current	I		120 mA	Protocol setting (PS)
2	Exposure time	·t		· 1.5 s	PS
		= Q	mAs-product (dose)	= 180 mAs	
3	Normalized dose free in air	$\cdot_nCTDI_{air}$	Dose free in air	·0.20 mGy/mAs	Basic dose specifications for CT scanners
4	1st voltage correction	$\cdot k_{U,1}$		$\cdot (140/120)^2$	PS
		$= CTDI_{air}$		= 49 mGy	
5	Slice thickness	· h		· 0.7 cm	PS
6	Number of slices	· n		· 30	PS
		$= DLP_{air}$	Dose-length product	= 1029 mGy·cm	
7	Conversion factor	$\cdot f_{mean}$		· 0.01 mSv/mGy·cm	Table 2.1
8	Scanner factor	$\cdot k_{CT}$		· 0.8	Table 2.2
9	2nd voltage	$\cdot k_{U,2}$		$\cdot (140/120)^{0.5}$	PS
		= E	**Effective dose**	**= 8.9 mSv**	

B) Dose Considerations in Helical Scanning

Helical scanning with a collimator pitch of 1.0 is physically similar to performing a conventional (nonhelical) axial scan with contiguous slices. For CT scanners with multiple detector arrays, the collimator pitch (not the detector pitch) should be used for dose calculations. The dose in helical CT is calculated in exactly the same manner as it is with axial CT, using the CTDI; however a correction factor is needed when the pitch is not 1.0:

$$Dose\ (helical) = Dose\ (axial) \times \frac{1}{Collimator\ \ pitch} \qquad (2.23)$$

For example, with a collimator pitch of 1.5, the dose from helical scanning is 67% of the dose from conventional scanning, and a collimator pitch of 0.75 corresponds to a helical dose of 133% of the axial dose (i.e., 33% greater), assuming the same mAs was used. The dose changes linearly with the mAs of the study. Because helical scans often use less mAs per 360-degree gantry rotation than axial scans do, the mAs should be factored into the calculation if it differs from the mAs used to measure the CTDI.

C) Current Modulation in Computed Tomography

Several CT manufacturers have introduced scanners that are capable of modulating the mA during the scan. In axial cross section, the typical human body is wider than thick. The mA modulation technique capitalizes on this fact. The rationale behind this technique is fewer x-ray photons (lower mA) penetrate thinner tissue and more x-ray photons (higher mA) are needed to penetrate thicker projections through the body. The SNR in the final image is related to the number of x-rays that pass through the patient and are detected. However, because of the way in which the filtered back-projection technique combines data from all views, the high SNR detected in the thinner angular projections is essentially wasted, because the noise levels from the thicker angular projections dominate in the final image. Therefore, a reduction in patient dose can be achieved with little loss in image quality by reducing the mA during acquisition through the thinner tissue projections. The other benefit of this technique is that because the mA is reduced per gantry rotation, x-ray tube loading is reduced and helical scans can be performed for longer periods and with greater physical converge. The mA modulation technique uses the angular-dependent signal levels (of the detectors) from the first few rotations of the gantry during acquisition (helical and axial) to modulate the mA during subsequent gantry rotations.

2.2 Related Literatures

Lu Z et al [14] evaluated a solid state dosemeter (SD) in direction measurement of CT dose. The studies have been done to compare solid state dosemeter with ion chamber detector for x-ray dosimetry. The responses of such a dosemeter with various technique setting and the limitations implied. A variety of phantoms has been involved, including acrylic cylindrical phantoms with various diameters and anthropomorphic phantoms. The angle and energy dependence of the SD and the effect on dose measurement had been evaluated. The results from SD are compared to the CTDI measurement by a pencil ion chamber(IC). The SD energy response is within ± 10%. It is angle dependent which affects CT dose measurement. It is shown that the IC results are higher than those of SD. The discrepancy increases with kVp, e.g., 20% at 80 kVp, 36% at 100 kVp, 49% at 120 kVp and 61% at 140 kVp using a 16 cm diameter phantom. In addition, the variation appears to be more significant as the phantom size reduces, e.g., 12% at 120 kVp for a 32 cm diameter phantom, 39% for 24 cm, 49% for 16 cm and 77% for 10 cm. Similar trends are observed with anthropomorphic phantoms. This leads to adjust the setting and use the SD sensors in pair with one facing up and the other with facing down. Corrective factors are calculated to compensate for the angle dependence. The angular sensitivity in the solid state dosemeter affects the ultimate dose reading and needs correction factors. Overall, the solid state dosemeter provides a new tool for direct and instantaneous measurement of CT dose. Lu’s paper did not study the effective dose which refers to estimate patient dose during CT examination.

Boonserm N [15] studied the comparison of effective dose in phantom from computed tomography using Monte Carlo simulation and Thermoluminescent dosimetry (TLD) methods. The organ doses and effective doses from calculation by ImPACT spreadsheet of Monte Carlo simulation and measurement by TLD in the Rando phantom had been reported. The organ doses and effective doses for chest and abdominal examinations were estimated from Siemens Sensation 16 computed tomography equipment used at King Chulalongkorn Memorial Hospital. CTDI was measured in air and in body phantom with Scanditronix/Wellhofer DCT 10-RS ionization chamber then the CTDIs and exposed parameters were entered in ImPACT spreadsheet for calculation of the organ dose and effective doses. The TLD-100 chips were calibrated with ^{60}Co beams. The sensitivity, linearity and energy response of TLD-100 chips were determined. The TLD-100 chips inserted in the Rando phantom were irradiated. The organ doses and effective doses were calculated. Finally, the results from two methods were compared in terms of percentage difference. From his study, most of the organ doses for chest and abdominal examinations from TLD were higher than those calculated by Monte Carlo simulation except breast, esophagus, and bone surfaces for chest examination and gonads, lung, and esophagus for abdominal examination. The differences between the organ doses from two methods were within the 11.74% uncertainty of TLD measurement for the organ located in the radiation field except the organs that were difficult to search for the exact location. The effective doses of chest examination were 4.37 mSv from Monte Carlo simulation and 5.42 mSv for TLD, resulted in 19.37% difference. The effective doses of abdominal examination were 7.31 mSv from Monte Carlo simulation and 8.52 mSv for TLD, resulted in 14.20% difference. The results showed the higher measured dose than calculated which agreed with the other published studies. The underestimation of the calculated dose was mainly due to the difference of the design between the Rando phantom and Medical Internal Radiation Dosimetry (MIRD) mathematical phantom in Monte Carlo simulation. For the clinical patient, the organ and effective doses could be estimated by Monte Carlo simulation with the awareness of the under estimation within 20% when compared to TLD.

Lu Z et al [16] studied pediatric patient dose management from a 64 slice VCT. To manage patient dose without compromising image quality, especially in children. A special effort should be made to reduce pediatric patient dose through age- and size-specific protocols. A pediatric 64 slice VCT scanner (GE Lightspeed) was tested with a group of cylindrical acrylic phantom with diameters ranging from 6-32 cm. In addition, anthropomorphic phantoms were employed to correlate the CTDI values with the skin doses measured by a solid state dosimeter (Unfors PSD). The dose affecting factors included: kVp, mAs, beam filtration, beam collimation, pitch, patient size, detector configuration and dose reduction techniques such as mA modulation and post-processing. Various techniques and their combinations were included in this study. The automated CTDI values displayed on the system agreed with our measurements when the standard

phantom sizes were used, i.e., 16 cm in diameter for head, 32 cm for adult body and 16 cm for pediatric body. However, the measured dose differed from the automated CTDI by a factor of 1.72 for a reduced head phantom size of 6 cm in diameter. Patient age also played an important role in estimating effective dose. The changing beam filtration caused a variation of up to 42% in the in-air dose output. The clinical protocols were established based upon the dose level corresponding to the patient size and age as well as the tolerable noise level corresponding to the specific clinical applications.

Dan E Ware et al [17] evaluated radiation effective doses to patients undergoing abdominal CT examinations. The studies have been done to determine the radiation effective dose to adult and pediatric patients undergoing abdominal CT examinations. Technique factors were obtained for three groups of randomly selected patients: 31 children aged 10 years or younger; 32 young adults aged 11-18 years; and 36 adults older than 18 years. The radiographic techniques, together with the measured cross sections of patients, were used to estimate the total energy imparted to each patient. Each value of energy imparted was subsequently converted into the corresponding effective dose to the patient, taking into account the mass of the patient. All abdominal CT examinations were performed at 120 kVp with a section thickness of approximately 7 mm for all sizes of patients. The mean number of CT sections increased from 22.0 for children to 31.5 for adults, and the mean quantity of x-ray in mAs increased from 220 mAs for children to 290 mAs for adults. The mean values (± SD) of energy imparted were 72.1 mJ ± 24.4 for children, 183.5 mJ ± 44.8 for young adults, and 234.7 mJ ±89.4 for adults. The corresponding mean values of patient effective dose were 6.1 mSv ± 1.4 for children, 4.4 mSv ± 1.0 for young adults, and 3.9 mSv ± 1.1 for adults. Values of energy imparted to patients undergoing abdominal CT examinations were a factor of three higher in adults than in children, but the corresponding patient effective dose were 50% higher in children than in adults.

Huda Walter et al [18] studies converting dose-length product to effective dose at CT. The studies have been done to determine effective dose per unit DLP conversion factors for CT dosimetry. A CT dosimetry spreadsheet was used to compute patient E values and corresponding DLP values. The ratio of E to DLP was determined with 16-section CT scanners from four vendors, as well as with five models from one manufacturer that spanned more than 25 years. E-to-DLP ratios were determined for 2 cm scan lengths along the patient axis, as well as for typical scan lengths encountered at head and body CT examinations. The dependence of the ratio of E to DLP on x-ray tube voltage (in kilovolts) was investigated, and the values obtained with the spreadsheet were compared with those obtained by using two other commercially available CT dosimetry software packages. For 2 cm scan lengths, changes in the scan region resulted in differences to E of a factor of 30, but much lower variation was obtained for typical scan lengths at clinical head and body imaging. Inter- and intramanufacturer differences for

E/DLP were generally small. Representative values of E/DLP at 129 kVp were 2.2 μSv/mGy·cm (head scans), 5.4 μSv/mGy·cm (cervical spine scans), and 18 μSv/mGy·cm (body scans). For head scans, E/DLP was approximately independent of x-ray tube voltage, but for body scans, the increase from 80 to 140 kV increased the ratio of E to DLP by approximately 25%. Agreement in E/DLP data for all three software packages was generally very good except for cervical spine examinations which one software package determined an E/DLP ratio approximately double of the other two.

CHAPTER III

RESEARCH METHODOLOGY

3.1 Research Design

This study is an observational descriptive design.

3.2 Research Design Model

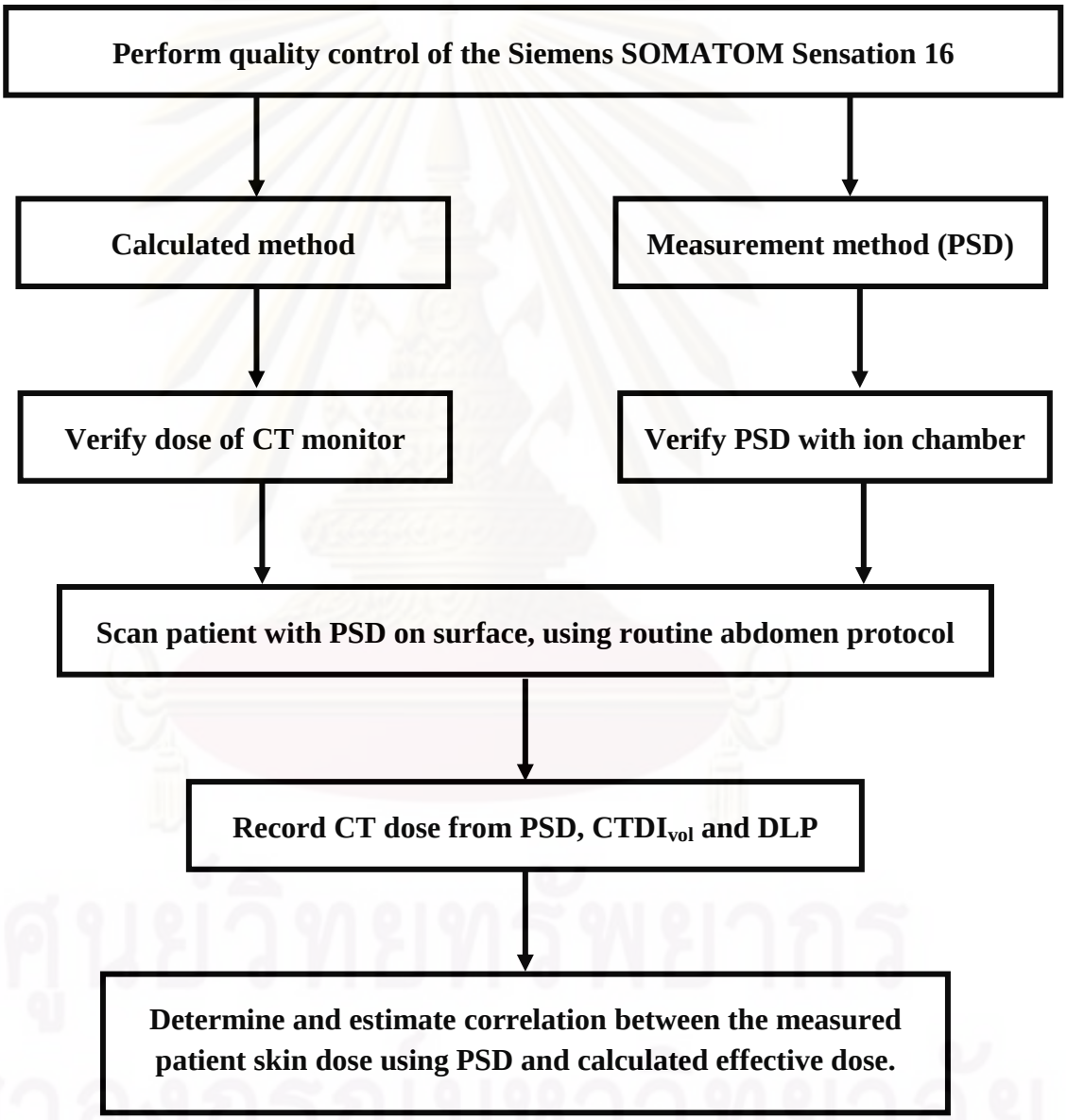

3.3 Conceptual framework

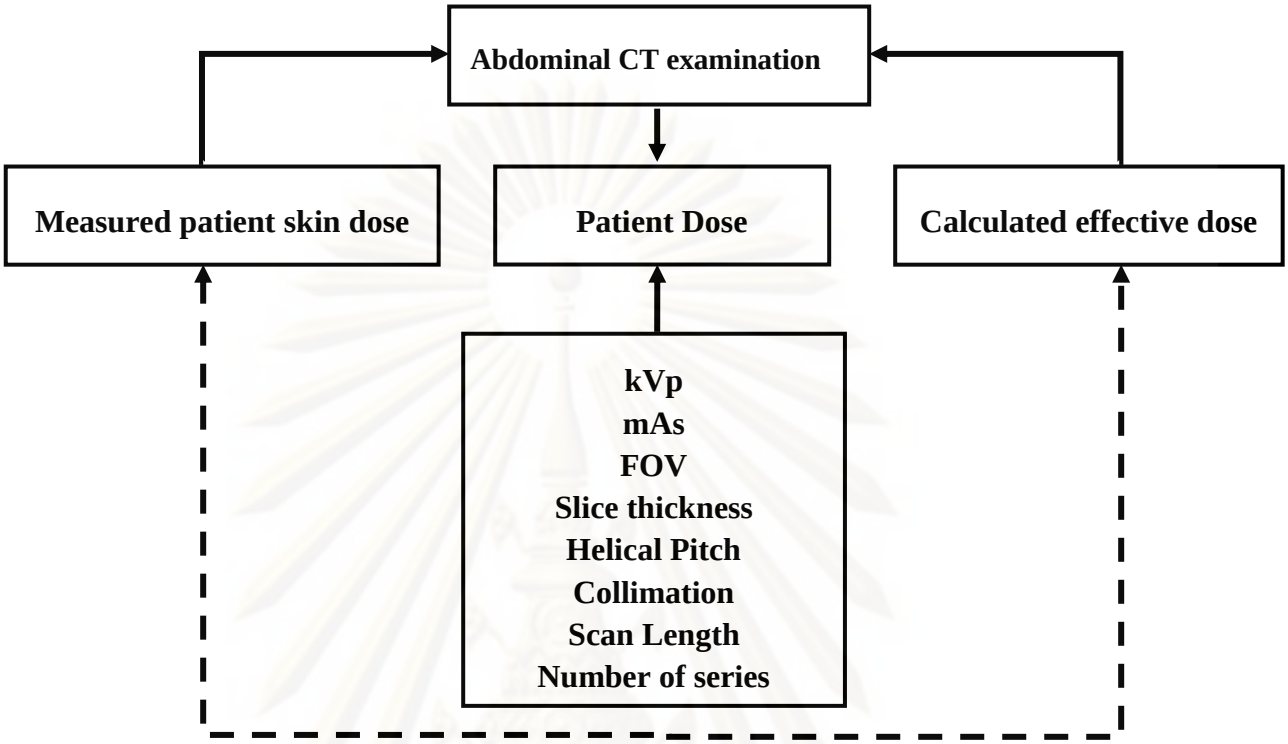

3.4 Key words

- Effective dose
- Solid state dosemeter
- Abdominal CT examination

3.5 Research questions

3.5.1 Primary question

What is the correlation between the measured and the calculated effective dose from abdominal CT examination?

3.5.2 Secondary question

What is the effective dose from abdominal CT examination using solid state patient skin dosemeter?

3.6 Materials

3.6.1 CT scanner: Siemens SOMATOM Sensation 16

Figure 3.1 CT scanner: Siemens SOMATOM Sensation 16.

In this study, we used CT scanner: Siemens Somatom Sensation 16 at Department of Radiology King Chulalongkorn Memorial Hospital, installed in 2003 to acquire the patient information. The Sensation 16 is the third-generation multi-detector CT scanner, featuring a 60 kW generator, 5.3 MHU x-ray tube and fastest gantry rotation time of 0.42 seconds. In helical mode it is capable of imaging 16 slices per rotation, with slice widths of 16 × 1.5 mm and 16 × 0.75 mm, as well as smaller numbers of wider slices. There are 24 parallel rows of solid state detectors, covering 24 mm in the z-direction at the isocenter. The computer software unit uses the operating system Windows NI ® and the application software Syngo. CARE Dose 4D is function of automatic exposure control system in Siemens Sensation 16 and scanner with software version VB10 or higher.

3.6.2 Solid state dosemeter; Unfors Patient skin dosemeter (PSD)

Figure 3.2 The Unfors Patient skin dosemeter with 3 sensors. (http//:www.unfors.com)

The solid state dosemeter is used in CT and fluoroscopy procedures to prevent excessive dose usage and consequential patient lesions. The solid state detector utilized three tiny silicon detector chips 10 mm × 5 mm in size on cables connected to a display unit. The small detectors can be placed on the body and leave a minimal footprint on the x-ray image. The display unit can be placed on the side of the patient table or next to ceiling suspended monitors. When the detectors and display unit have been positioned and the instrument turned on, dose is accumulated and alarms (audible and visual) are triggered when selected dose limits are exceeded. The PSD can be delivered with one, two, three or four sensors depending on the application. The display unit is displayed real-time.

The detectors are calibrated to entrance skin dose (ESD) at 90 kVp in Gy and the energy dependence is < ± 10% for the energy range 60-110 kVp (< 15% for the energy range 40-140 kVp) at a tube filtration 6 mm Al. The entrance skin dose response at 70 kVp, 100 cm focal spot distance and 30 × 30 cm field size. The sensor was mounted on an ISO body phantom which is radially and axially rotated in the radiation field. The cable end of the detector is at 90˚.

The detectors are calibrated on an ISO/ANSI phantom at a field size of 20 × 20 cm. The conversion factor from the dose in free air at the same position is 1.4 (= 1.32 × 1.06), where 1.32 is the scattering factor and 1.06 is the tissue dose to air dose factor. The angular dependence is < 5% for ± 45˚ tilt (< 10% for ± 60˚ tilt).

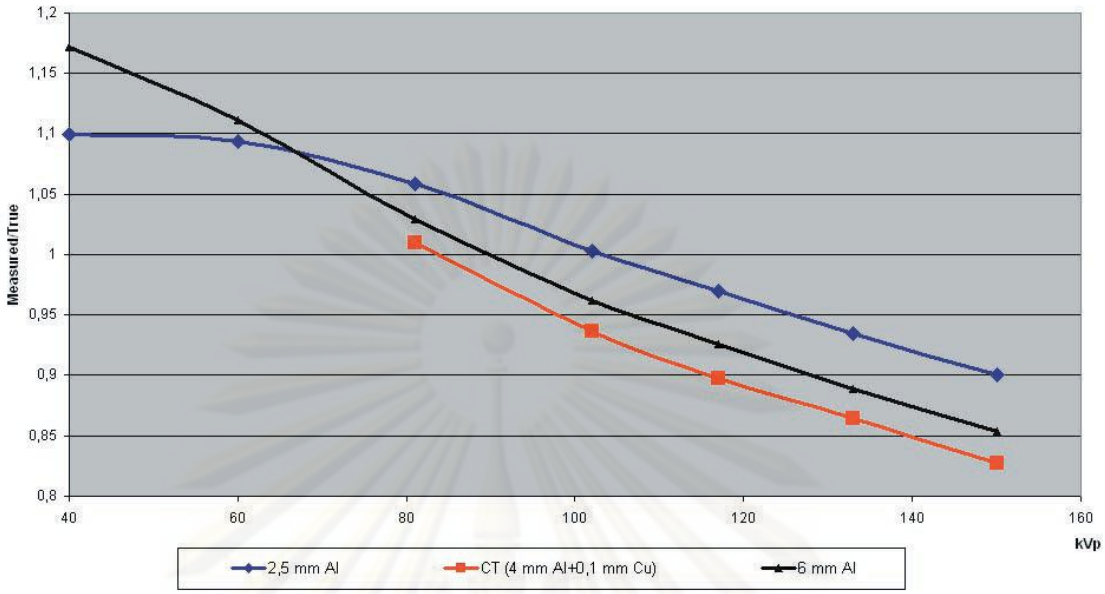

Figure 3.3 The energy dependence for Unfors patient skin dosemeter. (http://www.unfors.com)

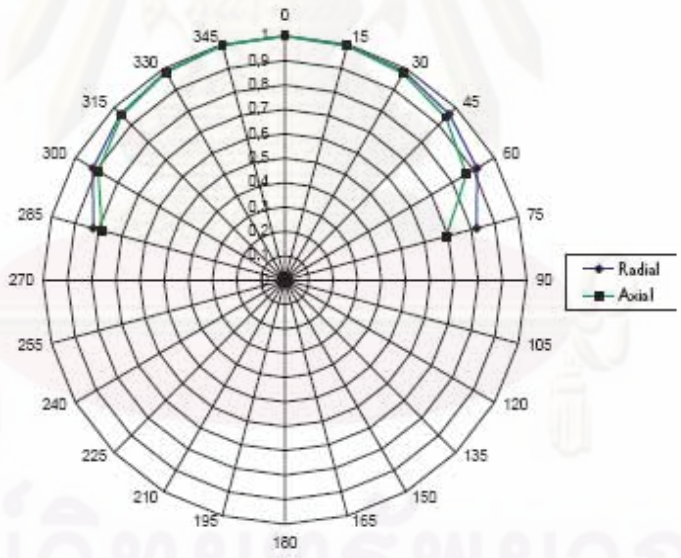

Figure 3.4 Angular dependence for Unfors patient skin dosemeter. (http://www.unfors.com)

Table 3.1 Characteristics of Unfors patient skin dosemeter (PSD)

General	
Dose range	1 µGy – 9999 Gy 100 µR – 9999 R
Start trig level	10 µGy/s, 60 mR/min
Stop trig level	5 µGy/s, 30 mR/min
Maximum dose rate	100 mGy/s, 600 R/min
Reproducibility	1 %
Reset	Manually or automatic
Power off	Manually or automatic after 5, 10, 30 or 240 (default) min of inactivity
Disinfections	Sensor, cable and instrument housing can be wiped off with propyl alcohol
Power source	Two 1.5 V LR06 (AA) alkaline
Battery life time	100 hours
Read out	4 digit LCD display with units and sensor identification
Temperature range	15-35˚C, 59-95 ˚F
Size (H × W × L)	98 × 82 × 21 mm, 3.9 × 3.2 × 0.8 in
Weight	250 gram, 9 oz
Sensor	
Expanded uncertainty	± 6% at calibration point 90 kVp
Angular dependence	± 5% for 45˚ ± 10% for 75˚
Bandwidth	2.4 Hz, 3 dB
Energy dependence	± 10% (60-120 kVp) ± 15% (40-150 kVp) At 6 mm Al
Temperature dependence	Negligible
Pressure dependence	Negligible
Size (H × W × L)	4 × 15 × 15 mm, 0.15 × 0.6 × 0.6 in
Alarms	
Level 1	25% 0f 2 Gy
Level 2	50% of 2 Gy
Level 3	75% of 2 Gy
Level 4	100% 0f 2 Gy
Buzzer	ON or OFF
Flashing diode	ON or OFF

3.6.3 CT Dose Phantom

The CT phantom is used to perform QC for CT system. The CT Dose Phantom is manufactured to comply with the FDA's performance standard for diagnostic x-ray systems. The phantom consists of two 14 cm length made of solid Polymethyl Methacrylate (PMMA) disks measuring 16 cm (head) and 32 cm (body) in diameters as shown in figure 3.3.

There are 9 holes with acrylic rods to plug the holes for both phantoms when not in use. Through holes are 1.31 cm in diameter and 14 cm length to accommodate standard CT probes. One hole is at center and four are around the perimeter, 90˚ apart and 1 cm from hole center to the outside edge of each phantom.

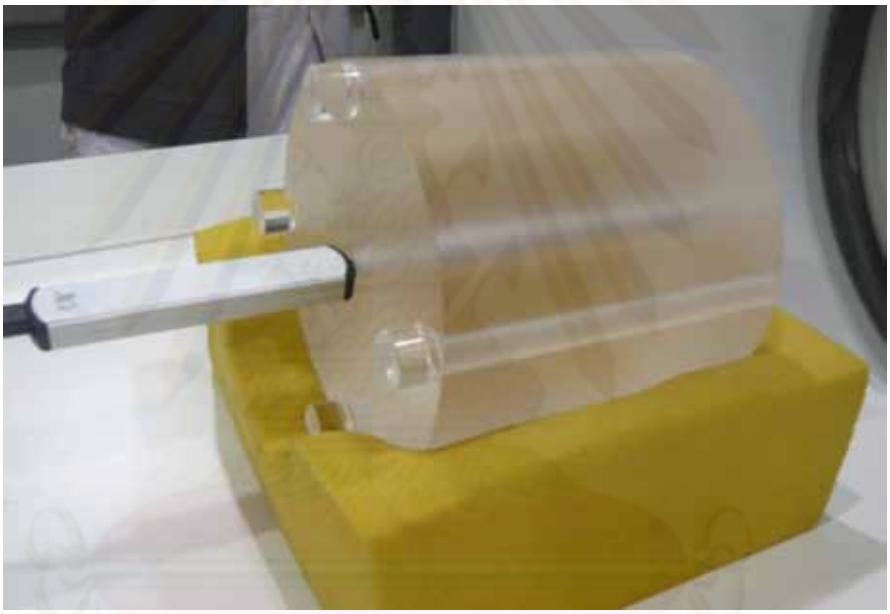

Figure 3.5 CT Dose Phantom with pencil chamber inserted at center.

3.6.4 Catphan® 500 Phantom [19]

The Catphan® phantom is generally used for the CT performance evaluation. The Catphan® phantom is positioned in the CT scanner by mounting on the case which placed directly at the end of the table.

The Catphan® 500 phantom is designed so all test sections can be located by precisely indexing the table from center of section 1 (CTP401) to the center of each subsequence test module. The indexing distances from section 1 are Catphan® 500 test module locations:

Module	Distance from section 1 center
CTP401, slice width, sensitometry and pixel size	
CTP528, 21 line pair high resolution	30 mm
CTP528, Point source	40 mm
CTP515, Sub slice and supra-slice low contrast	70 mm
CTP486, Solid image uniformity module	110 mm

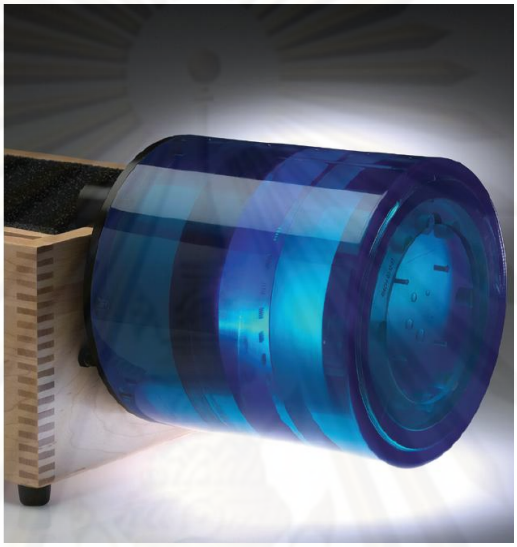

Figure 3.6 Catphan® 500 phantom. (The phantom laboratory, Catphan® 500 and 600 Manual, copyright© 2009)

3.6.5 Unfors model Xi platinum dosemeter

The Unfors Xi platinum prestige is a complete system for multi-parameter measurements on all modalities. This includes R/F, mammography, dental and CT with and added option for luminance and illuminance measurements of medical monitors. The Unfors Xi platinum prestige is the ultimate QA solution fitted into a small and portable aluminum case. All Unfors Xi detectors are interchangeable and function with any base unit. The Unfors Xi platinum prestige will give you the most potential as all capabilities are bundled into one complete system.

Figure 3.7 Unfors model Xi platinum dosemeter (http://www.unfors.com)

Table 3.2 Characteristics of Unfors model Xi platinum dosemeter.

Unfors Xi CT detector	
Unfors Xi base unit firmware	4.0 or higher
Size detector	200 × 20 × 12 mm (7.9 × 0.8 × 0.5 in)
Size diameter detector	7.5 mm (0.30 in)
Size diameter phantom adapter	12.5 mm (0.49 in)
Effective length	100 mm (3.94 in)
Weight	50 g(1.75 oz)
Range	10 µGy – 9999 Gy (1 mR – 9999R) 20 µGy/s – 100 mGy/s (140 mR/min – 680 R/min)
Uncertainty	5% (at reference point RQA9; 120 kV, 42.5 mm Al)
Energy dependence	< 5% (at 80 kV-150 kV; RQR and RQA qualities)
Radial uniformity	± 2%
Axial uniformity	± 3%, within rated length
Influence of relative humidity	< 0.3% (for RH < 80%)
Uncertainty in temp. and pressure correction	2%
Pressure range	80.0 – 106.0 kPa
International standard	Fulfill requirements in IEC 61674

3.7 Methods

3.7.1 Perform the quality control of Siemens SOMATOM Sensation 16

The quality control of Siemens SOMATOM Sensation 16 was performed following the AAPM report No.39 (1993): specification and acceptance testing of CT scanner [20] in the part of performance evaluation and ImPACT information leaflet 1: CT

scanner acceptance testing version 1.02 [21]. The quality control program included the test of performance of electromechanical components, image quality and radiation dose.

3.7.2 Verification of $CTDI_{vol}$.

The $CTDI_{vol}$ is displayed on the monitor of the console of Siemens SOMATOM Sensation 16 before the scan. To make a confidence of using these values, the verification of $CTDI_{vol}$ was performed.

- Pencil ionization chamber was inserted in the 32 cm diameter of PMMA phantom. The positioning of the phantom and chamber were investigated to avoid the alignment errors.
- Computed Tomography Dose Index (CTDI) was recorded where the chamber is inserted at the center and the peripheral positions in phantom. The phantom was scanned three times for each kVp setting.
- The acquisition parameters were 2 × 5.0 mm collimation, 1.0 sec rotation time, helical pitch of 1.0, and effective mAs 100. The $CTDI_{vol}$ that initially displayed on CT console were recorded before running the scan.
- The data shown on dosemeter was recorded for the calculation of $CTDI_{vol}$ and compared to the displayed values on CT monitor and the ImPACT values for each kVp.

3.7.3 Apply PSD at the patient's skin close to the gonad for abdominal CT examination. Using routine abdominal protocol.

In this study, we acquired the data in 144 patients, 58 patients for upper abdominal CT examination and 86 patients for whole abdominal CT examination, respectively by the patient must sign consent form to attend the research before start examination.

Table 3.3 Routine abdominal CT parameters

Scan parameters	
kVp	120
Effective mAs	160
Scanning mode	Helical
Collimation (mm)	16 × 1.5
Rotation time (sec)	0.5
Helical pitch	1

3.7.4 Data recording

Record the patient's information, patient skin dose, $CTDI_{vol}$ and DLP in case record form.

3.7.5 Effective dose calculation

The purpose of this study is to calculate the effective dose from abominal CT examination by separate to upper and whole abdominal CT examination.

3.7.6 Determination of the correlation of the effective dose

The purpose of this study is to determine the correlation between the effective dose from calculation and the patient skin dose from solid state dosemeter

3.8 Sample size

This study aims to define the correlation of the effective dose from calculation method and the patient skin dose measurement using solid state detector for abdominal CT examination. The sample size determination will be calculated by;

Sample size for dependent group: $$\boldsymbol{n} = \left[\frac{Z\alpha_{/2}+Z_{\beta}}{Z(r)}\right]^2 + 3 \quad (3.1)$$

Given confidence interval (CI) 95%, α is 0.05 and $Z_{\alpha/2}$ is 1.96 (two-tail). At power 90%, β is 0.10 and Z_{β} is 1.282. Z(r) can be defined by;

$$\boldsymbol{Z(r)} = \frac{1}{2}\ln\left(\frac{1+r}{1-r}\right) \quad (3.2)$$

When r is the correlation coefficient and will be calculated by;

$$\boldsymbol{r} = \frac{\sum(x-\bar{x})(y-\bar{y})}{\sqrt{\sum(x-\bar{x})^2\,(y-\bar{y})^2}} \quad (3.3)$$

Defined $\bar{x}$ is the average value of patient skin dose for measured method using patient skin dosemeter and $\bar{y}$ is the average value of the effective dose for calculated method.

Due to PSD is new tool, there has been no dose report on this type of dosemeter. Therefore, the pilot study is necessary. After the pilot study for abdominal CT examination in 10 patients, we found that the average value of patient skin dose ($\bar{x}$) is 1.88 mGy and the average value of the effective dose ($\bar{y}$) is 5.78 mSv. The variable in equation 3.3 was added to obtain the correlation coefficient of 1.80, then the correlation coefficient was substituted into equation 3.2 resulting in the Z(r) and add all parameters in the equation 3.1. Finally, the sample size for this study is approximately 29 patients.

3.9 Measurement

Variables

Independent variables: scan length and number of scans

Dependent variables: patient skin dose, $CTDI_{vol}$, DLP and effective dose

3.10 Statistical analysis

3.10.1 Descriptive statistics: mean, standard deviation (SD), minimum, maximum and third-quartile were performed with the statistical program package SPSS statistics 17.0.

3.10.2 Hypothesis testing: correlation between measured patient skin dose from solid state dosemeter and calculated effective dose was evaluated by calculating Pearson rank correlation coefficient to indicate statistically significant differences.

3.11 Data Collection

3.11.1 Patient information: date, age, gender, height, weight, body thickness, kVp, mAs, slice thickness, collimation, FOV, helical pitch, scan length.

3.11.2 The patient skin dose, the real-time read out, $CTDI_{vol}$ and DLP read out from CT monitor.

This data collected at Computed Tomography Unit, Chulachakapong Building, 1^{st} floor, Department of Radiology, King Chulalongkorn Memorial Hospital, Bangkok Thailand, using Siemens SOMATOM Sensation 16.

3.12 Data Analysis

The verification of $CTDI_{vol}$ had been reported as percentage difference between the displayed, the measured and the ImPACT values for each kVp setting. After that the radiation dose data for a specific parameter setting in abdomen CT examination were collected from the values of $CTDI_{vol}$ displayed on the CT console in the unit of mGy and presented in form of table.

Data from patients had been reported as mean, standard deviation and range, then, presented in form of table.

The data from solid state dosemeter as the patient skin dose was calculated to entrance surface dose and were analyzed by determining the mean and standard deviation for each rank. This data presented in form of bar chart.

The data of $CTDI_{vol}$ and DLP displayed on CT console was obtained for the calculation of the effective dose for abdominal examination and presented in form of bar chart.

The determination of the correlation of the effective dose for abdominal CT examination and the patient skin dose was estimated by considering on the results of same patient and presented in form of the scatter plot.

3.13 Outcomes

The patient skin dose at skin over the gonad for routine abdominal CT examination was obtained. The effective dose was calculated by using the $CTDI_{vol}$ and DLP from CT console and other parameters involved.

3.14 Expected Benefits

The total effective dose for gonad from abdominal CT examination and the characteristics of effective dose from abdominal CT examination when the number of scan is increasing, are expected from this study. Furthermore, the correction factor of PSD or CT dose from CT monitor for effective dose determination would be obtained. These would be benefit to the patients and the radiologists in order to justify further investigations. The patient dose saving should be considered.

3.15 Ethical consideration

This study will be performed in patients to investigate the patient skin dose from abdominal CT examination for the calculation of the effective dose and determine the patient dose at the skin nearly the gonad. The ethical consideration had already been approved by Ethics Committee of Faculty of Medicine, Chulalongkorn University.

CHAPTER IV

RESULT

4.1 Quality control of the CT scanner: Siemens SOMATOM Sensation 16

The quality control of CT scanner was performed following the AAPM report No.39 [20] and ImPACT Information Leaflet 1 [21]. Furthermore, the quality control includes the test of performance of electromechanical component, image quality and radiation dose.

The detail of quality control of CT scanner was shown in Appendix B and the summarized report of CT scanner performance test was shown in Table 4.1.

Table 4.1 Report of CT system performance

Location	CT unit, Chulachakapong Building, Floor.G
Date	March 19, 2009
Manufacturer	Siemens
Model	SOMATOM Sensation 16

Pass	Scan Localization Light Accuracy
Pass	Alignment of Table to Gantry
Pass	Table Increment Accuracy
Pass	Slice Increment Accuracy
Pass	Gantry Tilt
Pass	CT No. Position Dependence and SNR
Pass	Beam Alignment
Pass	Reproducibility of CT Number
Pass	mAs Linearity
Pass	Linearity of CT Numbers
Pass	High Contrast Resolution
Pass	Low contrast Resolution
Pass	Radiation Profile Width

4.2 Verification of Computed Tomography Dose Index (CTDI)

4.2.1 $CTDI_{100}$ in air

The $CTDI_{100}$ in air was determined by using head and body protocol and the pencil chamber was set at the isocenter of the CT bore. The scan condition was 100 mA tube current, 1 sec scan time, 1 helical pitch and 2×5.0 mm collimation setting for all measurements at kilovoltage settings of 80, 100, 120 and 140. The measured CTDI was compared with ImPACT scan values for each kVp. The result of CTDI in air was shown

in Table 4.2. From the results, the percentage difference of CTDI in air with the ImPACT scan values was less than ±10 percent in all kVp setting range from -2.37 to -0.38 for head protocol and -0.26 to 2.99 for body protocol.

Table 4.2 The measured $CTDI_{100}$ in air for head and body protocol compared with ImPACT values for each kVp.

kVp	$CTDI_{100}$ in air (head)		% difference	$CTDI_{100}$ in air (body)		% difference
	Measured	ImPACT		Measured	ImPACT	
80	8.88	9.10	-2.37	5.26	5.24	0.34
100	15.83	16.08	-1.55	10.57	10.59	-0.26
120	21.72	21.80	-0.38	15.64	15.26	2.49
140	29.40	-	-	22.28	21.63	2.99

4.2.2 $CTDI_{100}$ in head phantom

The $CTDI_{100}$ in head phantom was determined by using 16 cm diameter PMMA cylindrical phantom placed at the isocenter of the CT bore. The scan conditions were 100 mA, 1 sec scan time, 1 helical pitch, kernel H30s and 2×5.0 mm collimation setting for all measurements at various kVp settings of 80, 100, 120 and 140. The measured CTDI was compared with ImPACT scan values for each kVp. The result of CTDI in head phantom was shown in Table 4.3. From the results, the percentage difference of CTDI in head phantom with the ImPACT scan values were less than ±10 percent in all kVp setting range from -9.63 to -8.61 for center position and -9.63 to -7.95 for periphery position.

Table 4.3 The measured $CTDI_{100}$ at each position of head phantom compared with ImPACT values for each kVp.

kVp	$CTDI_{100}$ in head phantom (mGy)									
	At center		% diff	At periphery						% diff
	Measured	ImPACT		North	East	South	West	Average	ImPACT	
80	5.03	5.50	-8.61	6.40	6.29	5.63	6.04	6.09	6.70	-9.11
100	9.80	10.85	-9.63	11.88	11.75	10.58	11.09	11.32	12.53	-9.63
120	14.03	15.40	-8.92	16.55	16.28	14.92	15.51	15.81	17.18	-7.95
140	19.42	-	-	22.56	22.10	20.44	21.19	21.57	-	-

4.2.3 $CTDI_{100}$ in body phantom

The $CTDI_{100}$ in body phantom was determined by using 32 cm diameter PMMA cylindrical phantom at the isocenter of the CT bore. The scan conditions were 100 mA, 1 sec scan time, 1 helical pitch, kernel B30s and 2×5.0 mm collimation setting for all measurements at various kVp settings of 80, 100, 120 and 140. The measured CTDI was compared with ImPACT scan values for each kVp. The result of CTDI in head phantom was shown in Table 4.4. From the results, the percentage difference of CTDI in body phantom with the ImPACT scan values were less than ±10 percent only at 100 kVp of -9.61 and -8.68 at center and periphery position, respectively. The percentage difference for another kVp were out of acceptable limit range from -14.89 to -14.60for center position and -15.21 to -12.09 for periphery position.

Table 4.4 The measured $CTDI_{100}$ at each position of body phantom compared with ImPACT values for each kVp.

kVp	$CTDI_{100}$ in body phantom (mGy)									
	At center		% diff	At periphery						% diff
	Measured	ImPACT		North	East	South	West	Average	ImPACT	
80	0.95	1.12	-14.89	2.30	2.29	2.07	2.19	2.21	2.61	-15.21
100	2.23	2.47	-9.61	4.98	4.89	4.49	4.70	4.77	5.22	-8.68
120	3.56	4.17	-14.60	7.57	7.36	6.52	7.08	7.13	8.16	-12.59
140	5.29	6.19	-14.61	10.41	10.55	9.75	10.16	10.22	11.62	-12.08

4.2.4 $CTDI_{vol}$ of monitor and calculated CTDIw

The $CTDI_w$ was determined by using 16 and 32 cm diameter PMMA cylindrical phantoms for head and body phantoms, respectively. The scan tecniques were 100 mA, 1 sec scan time, helical pitch 1, 2×5.0 mm collimation, kernel H30s for head protocol, kernel B30s for body protocol for any measurement at various kVp setting. The displayed $CTDI_{vol}$ on CT monitor were recorded to compare percentage difference with the calculated values and the ImPACT values as shown in Table 4.5 for $CTDI_{vol}$ in head phantom and Table 4.6 for $CTDI_{vol}$ in body phantom.

Table 4.5 $CTDI_{vol}$ of monitor and $CTDI_w$ using head techniques mAs 100, collimation 10 mm and pitch 1 and kernel H30s.

kVp	$CTDI_{vol}$ (mGy) in head phantom				
	Calculated	Monitor	%difference (calculated and monitor)	ImPACT	%difference Monitor and ImPACT
80	5.74	6.70	-14.40	6.30	-6.24
100	10.82	11.20	-3.43	11.97	6.42
120	15.22	16.80	-9.41	16.58	-1.35
140	20.86	22.90	-8.93	-	-

Table 4.6 $CTDI_{vol}$ of monitor and $CTDI_w$ using body techniques mAs 100, collimation 10 mm and pitch 1 and kernel B30s.

kVp	$CTDI_{vol}$ (mGy) in body phantom				
	Calculated	Monitor	%difference (calculated and monitor)	ImPACT	%difference (Monitor and ImPACT)
80	1.79	2.10	-14.62	2.11	-0.63
100	3.92	4.00	-1.95	4.30	-7.04
120	5.94	6.30	-5.68	6.83	-7.76
140	8.57	9.10	-5.79	9.81	-7.24

4.3 Patient data and scanning parameter

58 patients for upper abdominal CT examination and 86 patients for whole abdominal examination were requested for abdominal CT examination and completed consent form before examination. The patient data as shown in Table 4.7 was classified into 4 groups by the body weight of patient. The patient data of age, gender, number of series, height, weight and body thickness of 58 patients for upper abdominal CT examination were shown in Table 4.8.

Table 4.7 Patient data and scanning parameters of 58 patients for upper abdominal CT examination and 86 patients for whole abdominal examination.

Parameters	Body weight (kg)			
	26-45	>45-65	>65-85	>85-105
CT upper abdomen				
Number of patient	3	37	16	2
Age (years) Average/range	54.67 (52-57)	58.24 (35-81)	57 (39-80)	48 (30-66)
Weight (kg) Average/range	44 (43-45)	56.19 (46-65)	72.71 (66-82)	87.5 (86-89)
Height (cm) Average/range	160 (152-168)	158.82 (146-175)	167.94 (156-177)	172.5 (170-175)
Body thickness (cm) Average/range	16.63 (16.2-17.2)	19.15 (12.2-25.2)	22.77 (16.8-29)	25.2 (24-26.4)
kVp	120	120	120	120
Effective mAs Average/range	153.33 (140-160)	157.97 (140-170)	165 (140-200)	160
CT whole abdomen				
Number of patient	11	54	19	2
Age (years) Average/range	61.55 (33-83)	57 (19-84)	59.11 (33-86)	66.50 (58-75)
Weight (kg) Average/range	39.77 (32.5-40)	55.64 (46-65)	74.99 (66-85)	88 (86-90)
Height (cm) Average/range	157.73 (148-170)	159.06 (145-175)	170.05 (158-178)	171 (157-185)
Body thickness (cm) Average/range	15.14 (10.3-17.1)	19.34 (13.4-25.4)	22.75 (16.9-29.6)	23.35 (23.2-23.5)
kVp	120	120	120	120
Effective mAs Average/range	152.88 (135-160)	157.98 (133.33-200)	160	163.33 (160-166.67)

Table 4.8 Patient data of 58 patients for CT upper abdominal examination.

Study Number	Age (years)	Gender	Number of series	Height (cm)	Weight (kg)	Body thickness (cm)
U1	54	M	3	165	65	20.4
U2	53	M	4	165	63	20.8
U3	53	M	3	175	75	21.1
U4	71	M	5	164	65	22.0
U5	73	M	3	165	65	20.8
U6	59	M	4	158	55	18.4
U7	52	F	4	173	51	15.0
U8	30	M	4	175	86	24.0
U9	62	F	2	156	70	23.6
U10	73	F	4	160	70.3	24.6
U11	52	F	4	152	46	16.1
U12	54	M	4	162	75	24.3
U13	41	M	4	155	63	21.2
U14	57	F	3	167	74	23.4
U15	55	M	3	162	50	12.2
U16	69	F	4	156	52.5	19.7
U17	63	F	4	153	57	21.2
U18	39	M	5	174	72	16.8
U19	44	M	3	155	52	15.7
U20	60	M	4	170	72	23.2
U21	57	M	3	170	74	22.5
U22	70	M	4	165	63.5	25.2
U23	72	F	3	150	50	20.1
U24	64	F	3	152	46	18.3
U25	53	M	4	160	64	19.4
U26	80	F	4	155	61	22.5
U27	65	M	4	170	60	21.4
U28	52	M	4	165	46	12.8
U29	57	F	3	158	70	21.6
U30	47	F	4	164	66	21.7
U31	62	M	4	162	62	20.8
U32	35	F	4	150	55	19.8
U33	57	M	3	175	78	23.6
U34	60	F	2	160	62.5	20.7
U35	60	F	3	150	51	22.4

**U- Upper abdominal CT examination.*

Table 4.8 Patient data of 58 patients for CT upper abdominal examination (continued).

Study Number	Age (years)	Gender	Number of series	Height (cm)	Weight (kg)	Body thickness (cm)
U36	67	M	2	160	57	16.9
U37	51	M	4	160	58	17.0
U38	75	F	4	160	50	18.0
U39	56	F	3	156	46	17.5
U40	62	M	4	177	70	21.0
U41	47	M	4	163	61	18.7
U42	65	F	5	155	54	22.1
U43	41	F	4	161	64	16.4
U44	81	F	4	150	47	17.7
U45	52	M	3	163	63	25.0
U46	66	F	4	170	89	26.4
U47	55	M	4	168	44	16.5
U48	44	M	4	175	75	23.1
U49	52	M	3	160	45	17.2
U50	43	M	4	175	57	16.9
U51	80	M	3	164	70	24.2
U52	46	F	3	152	54	18.4
U53	61	F	3	158	61.5	21.0
U54	51	F	3	146	49	16.8
U55	60	F	2	155.5	52	19.2
U56	57	F	2	152	43	16.2
U57	50	M	4	172	70	20.6
U58	60	M	4	168	82	29.0

**U- Upper abdominal CT examination.*

Table 4.9 Patient data of 86 patients for CT whole abdominal examination.

Study Number.	Age (years)	Gender	Number of series	Height (cm)	Weight (kg)	Body thickness (cm)
W1	83	M	4	160	41.5	17.1
W2	37	F	5	150	48	17.7
W3	55	M	5	170	71	20.1
W4	77	F	4	150	55	20.3
W5	61	F	3	148	41	15.5
W6	57	F	3	158	58	19.1
W7	83	F	4	162	44	17.0
W8	52	F	4	158	57	17.8
W9	57	F	4	160	78	25.1
W10	58	F	3	148	50	17.4
W11	53	M	3	168	67.8	22.0
W12	56	M	4	169	63	19.3
W13	33	M	1	168	79	21.8
W14	54	F	5	156	56	17.7
W15	71	M	5	170	64	21.9
W16	69	F	4	158	58	22.7
W17	69	M	3	178	82	25.1
W18	53	F	4	153	50	17.1
W19	59	M	3	165	47	16.3
W20	45	F	3	154	56	23.6
W21	63	M	3	160	73	20.9
W22	36	M	3	158	68	22.3
W23	64	F	3	150	48	17.5
W24	19	M	3	165	55	18.5
W25	84	M	3	165	57	20.6
W26	52	F	4	170	43	16.4
W27	72	M	3	162	40	13.9
W28	58	M	4	170	62	19.2
W29	76	M	5	174	79	29.6
W30	86	M	3	170	80	24.7
W31	42	F	4	159	59	24.9
W32	61	M	4	167	67	22.9
W33	50	M	4	173	70	20.1
W34	60	F	4	157	60	25.4
W35	46	M	5	165	65	20.1

**W- whole abdominal CT examination.*

Table 4.9 Patient data of 86 patients for CT whole abdominal examination (continued).

Study Number	Age (years)	Gender	Number of series	Height (cm)	Weight (kg)	Body thickness (cm)
W36	46	F	4	175	53	16.0
W37	61	M	4	158	46	20.2
W38	75	M	2	165	65	16.4
W39	66	F	5	165	61	18.5
W40	71	M	5	162	54	19.0
W41	66	F	3	154	59	20.9
W42	58	M	3	176	85	25.2
W43	36	F	3	152	32.5	15.0
W44	70	M	3	165	65	21.3
W45	56	M	3	162	61.5	20.6
W46	69	M	4	160	55	20.0
W47	66	F	5	145	51	20.0
W48	72	M	4	176	78	24.9
W49	59	F	3	152	50	18.5
W50	75	M	4	157	90	23.2
W51	37	F	4	158	47	16.9
W52	62	F	4	160	55	19.2
W53	53	M	5	165	63	21.9
W54	58	M	4	168	59	20.0
W55	64	F	3	158	51	18.2
W56	47	M	4	174	67	16.9
W57	45	F	4	157	56	17.5
W58	64	M	4	173	69	19.7
W59	52	F	3	152	48	18.7
W60	50	F	1	177	85	26.1
W61	32	F	4	170	63	16.4
W62	83	M	5	178	85	20.4
W63	56	F	3	161	66	22.0
W64	28	F	3	173	58	19.1
W65	33	F	3	150	42.5	16.5
W66	64	F	3	162	42	16.9
W67	74	F	4	150	34	12.8
W68	52	F	4	155.5	51.5	23.7
W69	49	F	3	153	54	18.2
W70	67	F	4	160	52.5	18.5

**W- whole abdominal CT examination.*

Table 4.9 Patient data of 86 patients for CT whole abdominal examination (continued).

Study Number	Age (years)	Gender	Number of series	Height (cm)	Weight (kg)	Body thickness (cm)
W71	82	F	4	165	63	20.2
W72	54	M	4	162	43	15.1
W73	59	F	4	147	58	22.0
W74	54	F	4	158	47	14.0
W75	54	M	4	170	75	22.5
W76	65	M	3	157	34	10.3
W77	73	F	5	157	48	18.2
W78	63	F	3	153	58	19.2
W79	81	F	3	149	57.2	24.0
W80	70	F	5	150	55	20.9
W81	39	F	5	155	47	13.4
W82	39	M	1	175	55	16.2
W83	53	F	4	162	63	22.0
W84	52	F	5	150	60	20.9
W85	48	F	4	156	47	16.3
W86	58	M	3	185	86	23.5

**W- whole abdominal CT examination.*

4.4 Patient dose

The results of the total patient skin dose (PSD), $CTDI_{vol}$, DLP, total scan length and effective dose (E) of 58 patients for CT upper abdominal examination were shown in Table 4.10.

Table 4.10 Patient dose from measurement and CT monitor for 58 patients upper abdominal CT examination.

Study Number	Total PSD (mGy)	Total $CTDI_{vol}$ (mGy)	Total DLP (mGy·cm)	Total scan length (cm)	E (mSv)
U1	0.58	36.16	1170.00	84.50	16.73
U2	0.57	47.36	1628.00	119.50	23.66
U3	0.30	27.40	892.00	83.50	12.76
U4	1.09	58.56	1819.00	132.50	26.24
U5	0.61	36.16	1106.00	79.50	15.74
U6	0.57	47.36	1274.00	90.00	17.82
U7	1.37	47.36	1228.00	85.50	18.60
U8	0.87	47.36	1613.00	120.00	23.76
U9	0.36	19.60	602.00	50.00	9.52
U10	1.71	59.20	1633.00	72.50	18.80
U11	1.06	41.44	1045.00	85.00	16.18
U12	0.65	59.20	1777.00	103.60	25.64
U13	0.36	47.36	1488.00	111.00	21.98
U14	0.96	35.84	1133.00	81.50	17.68
U15	0.36	33.60	987.00	70.50	13.96
U16	2.38	44.80	1148.00	109.00	23.72
U17	5.25	50.48	1397.00	94.00	21.73
U18	4.14	58.56	2429.00	184.50	36.53
U19	0.51	36.16	1028.00	72.50	14.36
U20	1.75	48.64	1401.00	100.50	19.90
U21	0.55	33.60	1078.00	76.00	15.05
U22	1.23	47.36	1315.00	93.00	18.42
U23	0.99	36.16	1050.00	75.00	16.32
U24	0.78	36.16	896.00	62.50	13.60
U25	0.26	47.36	1373.00	99.00	19.60
U26	1.29	47.36	1202.00	83.50	18.17
U27	1.16	47.36	1536.00	112.00	22.18
U28	0.55	47.36	1249.00	89.00	17.62
U29	1.10	36.16	1080.20	79.50	17.30
U30	3.41	44.80	1613.00	120.50	26.22
U31	0.37	47.36	1379.00	98.50	19.50
U32	1.87	47.36	1280.00	90.50	19.69

**U-Upper abdominal CT examination*

Table 4.10 Patient dose from measurement and CT monitor for 58 patients upper abdominal CT examination (continued).

Study Number	Total PSD (mGy)	Total $CTDI_{vol}$ (mGy)	Total DLP (mGy·cm)	Total scan length (cm)	E (mSv)
U33	0.08	36.16	1065.00	76.50	15.15
U34	0.63	19.60	592.00	49.00	9.33
U35	0.95	36.16	933.00	65.00	14.14
U36	0.11	19.60	646.00	55.00	9.53
U37	0.35	47.36	1457.00	106.00	20.99
U38	0.34	47.36	1428.00	103.00	22.41
U39	1.29	36.16	1046.00	75.00	16.32
U40	0.86	53.60	1500.00	90.00	20.15
U41	0.26	47.36	1401.00	100.50	19.90
U42	1.68	58.56	1528.00	112.00	24.37
U43	1.88	43.40	1571.00	121.50	25.62
U44	1.68	47.36	1178.00	82.50	17.95
U45	0.29	36.16	1255.00	91.50	18.12
U46	0.40	47.36	1534.00	112.00	24.37
U47	0.44	47.36	1236.00	86.00	17.03
U48	0.42	56.40	1733.00	106.00	24.93
U49	1.22	36.16	1017.00	72.00	14.26
U50	0.37	47.36	1492.00	108.50	21.48
U51	0.54	36.16	1089.00	78.00	15.45
U52	1.31	36.16	1162.00	84.50	18.39
U53	3.33	36.16	1247.00	91.00	19.80
U54	1.44	36.16	1035.00	73.50	15.99
U55	0.73	19.60	590.00	48.50	9.23
U56	0.79	19.60	612.00	51.00	9.71
U57	0.47	47.36	1516.00	110.50	21.88
U58	0.17	47.36	1368.00	98.00	19.41
Average	**1.05**	**42.12**	**1260.00**	**90.61**	**18.71**

**U-Upper abdominal CT examination*

The results of mean and range of PSD, $CTDI_{vol}$, DLP, scan length and effective dose were classified into 4 groups by the body weight for 58 patients upper abdominal examination as shown in table 4.11.

Table 4.11 PSD, $CTDI_{vol}$, DLP and effective dose for 58 patients CT upper abdominal examination.

Body weight (kg)	Gender	Number of patients	Examination	PSD (mGy)	$CTDI_{vol}$ (mGy)	DLP (mGy·cm)	Effective dose (mSv)
				Mean (Range)	Mean (Range)	Mean (Range)	Mean (Range)
26-45	Female	1	Single phase[a]	0.79	19.6	612	9.71
	Male	2	Dual phase[b]	0.83 (0.43-1.22)	41.76 (36.16-47.36)	1126.5 (1017-1236)	15.64 (14.26-17.03)
>45-65	Male	1	Single phase[a]	0.11	19.6	646	9.53
	Female	2	Single phase[a]	0.68 (0.63-0.74)	19.6	591 (590-592)	9.28 (9.23-9.33)
	Male	17	Dual phase[b]	0.56 (0.26-1.23)	44.57 (33.60-58.56)	1350.41 (987-1819)	19.31 (13.96-26.24)
	Female	17	Dual phase[b]	1.70 (0.34-5.25)	42.86 (36.16-58.56)	1198.47 (896-1571)	19.00 (13.60-25.62)
>65-85	Female	1	Single phase[a]	0.36	19.6	602	9.52
	Male	11	Dual phase[b]	0.90 (0.08-4.14)	45.86 (27.40-59.20)	1440.73 (892-2429)	20.62 (12.76-36.53)
	Female	4	Dual phase[b]	1.79 (0.96-3.47)	44 (35.84-59.20)	1364.75 (1080-1633)	20.00 (17.30-26.22)
>85-105	Male	1	Dual phase[b]	0.87	47.36	1613	23.76
	Female	1	Dual phase[b]	0.40	47.36	1534	24.37

[a] represent 1-2 number of series for abdomen CT examination, such as pre contrast, post contrast.
[b]represent more than 2 number of series for abdomen CT examination, such as post contrast arterial phase, post contrast venous phase, delay phase, delay kidney, delay bladder. * [a] and [b] follow radiologist request protocol for the exam depends on clinical or disease.

The results of the total patients skin dose (PSD), $CTDI_{vol}$, DLP, scan length and effective dose (E) of 86 patients for CT whole abdominal examination were shown in Table 4.13.

Table 4.12 Patient dose from measurement and CT monitor for 86 patients whole abdominal CT examination.

Study Number	Total PSD (mGy)	Total $CTDI_{vol}$ (mGy)	Total DLP (mGy·cm)	Total scan length (cm)	E (mSv)
W1	36.84	38.60	1788.00	162.00	21.91
W2	45.55	58.56	2182.00	147.50	32.10
W3	24.39	56.00	2201.00	168.00	26.32
W4	30.90	47.36	1654.00	121.50	26.44
W5	38.79	33.60	1285.00	98.00	21.32
W6	32.05	29.40	1342.00	122.00	23.23
W7	39.99	47.36	1738.00	131.00	28.51
W8	41.70	47.36	2040.00	155.00	33.73
W9	29.49	47.36	1821.00	136.50	29.70
W10	35.29	30.80	1133.00	100.50	19.14
W11	28.68	30.80	1520.00	131.00	18.85
W12	18.23	47.36	2082.00	159.00	24.91
W13	0.83	11.20	595.00	47.50	7.44
W14	37.91	59.84	2444.00	184.00	40.04
W15	2.00	59.84	2098.00	154.00	24.13
W16	36.16	47.36	1772.00	131.00	28.51
W17	15.22	33.60	1597.00	125.50	19.66
W18	39.14	47.36	2005.00	152.50	33.18
W19	39.51	33.60	1713.00	135.50	21.23
W20	28.08	29.40	1289.00	125.00	23.80
W21	26.66	33.60	1377.00	102.00	15.98
W22	24.96	39.20	1574.00	105.00	18.92
W23	40.19	33.60	1271.00	96.50	21.00
W24	26.73	33.60	1427.00	110.50	17.31
W25	11.80	33.60	1433.00	111.50	17.47
W26	52.16	38.60	1509.00	134.00	24.87
W27	18.92	33.60	1601.00	126.00	19.74
W28	2.45	47.36	2117.00	162.00	25.38

**W- whole abdominal CT examination.*

Table 4.12 Patient dose from measurement and CT monitor for 86 patients whole abdominal CT examination (continued).

Study Number	Total PSD (mGy)	Total $CTDI_{vol}$ (mGy)	Total DLP (mGy·cm)	Total scan length (cm)	E (mSv)
W29	14.96	58.56	1995.00	145.00	22.72
W30	13.62	39.20	1962.00	134.00	24.38
W31	46.81	44.80	1931.00	150.00	32.64
W32	26.20	47.36	1829.00	135.00	21.15
W33	30.87	47.36	2120.00	162.50	25.46
W34	33.22	47.36	2270.00	174.00	37.86
W35	3.78	59.84	2246.00	168.00	26.32
W36	38.58	47.36	1995.00	147.50	32.10
W37	35.56	47.36	1923.00	145.50	22.80
W38	2.78	17.76	931.00	94.50	11.10
W39	16.52	61.12	2347.00	174.50	37.97
W40	28.68	58.56	2363.00	178.50	27.97
W41	30.36	30.80	1491.00	125.80	25.11
W42	1.09	30.80	1637.00	142.00	20.48
W43	32.56	29.40	1396.00	126.00	24.92
W44	1.36	29.40	1405.00	126.50	17.34
W45	25.91	29.40	1190.00	104.50	14.33
W46	28.00	47.36	1974.00	122.50	19.19
W47	41.18	61.12	2418.00	180.00	39.17
W48	27.57	47.36	2150.00	165.00	25.85
W49	30.93	30.80	1343.00	104.00	21.03
W50	6.23	44.80	1923.00	148.00	23.19
W51	40.61	47.36	1922.00	145.50	31.66
W52	35.92	47.36	1986.00	148.50	32.31
W53	4.00	56.00	2525.00	176.50	27.65
W54	11.21	47.36	2012.00	153.00	23.97
W55	33.24	33.60	1535.00	120.00	26.11
W56	24.13	47.36	2169.00	166.50	26.09
W57	36.75	47.36	1879.00	142.00	30.90
W58	38.21	47.36	2049.00	156.00	24.44
W59	33.20	29.40	1415.00	128.00	25.60
W60	1.34	15.60	863.00	52.00	14.14
W61	38.92	47.36	1958.00	148.00	32.20

**W- whole abdominal CT examination.*

Table 4.12 Patient dose from measurement and CT monitor for 86 patients whole abdominal CT examination (continued).

Study Number	Total PSD (mGy)	Total $CTDI_{vol}$ (mGy)	Total DLP (mGy·cm)	Total scan length (cm)	E (mSv)
W62	4.49	64.80	2610.00	189.50	32.53
W63	25.55	29.40	1461.00	132.00	25.13
W64	33.67	29.40	1468.00	133.00	25.32
W65	41.06	33.60	1617.00	128.05	27.86
W66	16.48	33.60	1675.00	133.00	28.94
W67	40.02	47.36	1561.00	113.50	24.70
W68	28.76	47.36	1813.00	135.00	29.38
W69	33.31	33.60	1419.00	110.00	23.94
W70	36.90	47.36	1991.00	150.50	32.75
W71	33.24	47.36	1909.00	143.00	31.12
W72	42.60	47.36	1758.00	130.50	20.45
W73	36.98	47.36	1851.00	138.00	30.03
W74	40.91	47.36	1728.00	127.50	27.74
W75	31.87	47.36	2012.00	168.00	26.32
W76	19.12	33.60	1506.00	117.50	18.41
W77	38.72	58.56	2277.00	171.00	37.21
W78	34.93	33.60	1251.00	95.00	20.67
W79	28.97	33.60	1259.00	95.50	20.78
W80	37.40	58.56	1897.00	138.00	30.03
W81	38.14	58.56	2145.00	160.00	34.82
W82	1.28	11.20	598.00	47.50	7.44
W83	35.59	47.36	2122.00	161.50	35.14
W84	38.42	59.84	2352.00	159.00	34.60
W85	43.09	47.36	1791.00	130.50	28.40
W86	30.87	35.00	1803.00	133.00	22.50
Average	**28.04**	**42.26**	**1763.19**	**135.63**	**25.46**

**W- whole abdominal CT examination.*

The result of mean and range of PSD, $CTDI_{vol}$, DLP, scan length and effective dose were classified into 4 groups by the body weight for 86 patients upper abdominal examination as shown in table 4.13.

Table 4.13 PSD, $CTDI_{vol}$, DLP and effective dose for 86 patients CT whole abdominal examination.

Body weight (kg)	Gender	Number of patients	Examination	PSD (mGy)	CTDIvol(mGy)	DLP(mGy·cm)	Effective dose(mSv)
				Mean (Range)	Mean (Range)	Mean (Range)	Mean (Range)
26-45	Male	4	Dual phase[b]	29.37 (18.92-42.60)	38.29 (33.6-47.36)	1663.25 (1506-1788)	20.13 (18.41-21.91)
	Female	7	Dual phase[b]	37.29 (16.48-52.16)	37.65 (29.4-47.36)	1536.29 (1285-1738)	25.87 (21.32-28.94)
>45-65	Male	2	Single phase[a]	2.03 (1.28-2.78)	14.48 (11.2-17.76)	764.5 (598-931)	9.27 (7.44-11.10)
	Male	14	Dual phase[b]	17.09 (1.36-39.51)	45.05 (29.4-59.84)	1893.43 (1190-2525)	22.14 (14.33-27.97)
	Female	38	Dual phase[b]	35.85 (16.52-46.81)	44.84 (19.40-61.12)	1813.03 (1133-2444)	29.68 (19.14-40.04)
>65-85	Male	1	Single phase[a]	0.83	11.2	595	7.44
	Female	1	Single phase[a]	1.34	15.6	863	14.14
	Male	15	Dual phase[b]	22.19 (1.09-38.21)	44.71 (30.80-64.80)	1920.13 (1377-2610)	23.28 (15.98-32.53)
	Female	2	Dual phase[b]	27.52 (25.55-29.49)	38.38 (19.40-47.36)	1641 (1461-1821)	27.42 (25.13-29.70)
>85-105	Male	2	Dual phase[b]	18.55 (6.23-30.87)	39.9 (35-44.8)	1863 (1803-1923)	22.84 (22.50-23.19)

[a] represent 1-2 number of series for abdomen CT examination, such as pre contrast, post contrast.
[b]represent more than 2 number of series for abdomen CT examination, such as post contrast arterial phase, post contrast venous phase, delay phase, delay kidney, delay bladder.
* [a] and [b] follow radiologist request protocol for the exam depends on clinical or disease.

The result of comparison of male and female for upper and whoel abdominal CT dose values with increasing number of series were shown in Table 4.14 and 4.15, respectively.

Table 4.14 Comparison of male and female for upper abdominal CT dose values with increasing number of series.

Number of series	PSD (mGy)		$CTDI_{vol}$ (mGy)		DLP (mGy·cm)		E (mSv)	
	Male	Female	Male	Female	Male	Female	Male	Female
2	0.11	0.63	19.60	19.60	646	599	9.53	9.45
3	0.50	1.35	34.77	36.12	1068.70	1064.69	15.16	16.62
4	0.61	1.89	48.85	47.36	1459.79	1354.75	20.83	21.12
5	2.61	1.68	58.56	58.56	2124	1528	31.39	24.37

Table 4.15 Comparison of male and female for whole abdominal CT dose values with increasing number of series.

Number of series	PSD (mGy)		$CTDI_{vol}$ (mGy)		DLP (mGy·cm)		E (mSv)	
	Male	Female	Male	Female	Male	Female	Male	Female
1	1.06	1.34	11.2	15.6	596.50	863	7.44	14.14
2	2.78	*	17.76	*	931	*	11.10	*
3	20.32	32.27	33.50	31.62	1553.21	1391.18	19.04	23.76
4	25.71	37.99	46.55	46.85	1993.29	1874.82	23.65	30.63
5	11.76	36.73	59.09	59.52	2291.14	2257.75	26.80	35.74

**No data*

The results of mean, minimum, maximum and third-quartile values of PSD, $CTDI_{vol}$, DLP and effective dose per series for CT upper and whole abdominal examination shown in Table 4.16 and 4.17, respectively. Table 4.18 and Table 4.19 shown the results of mean, minimum, maximum and third-quartile values of PSD, $CTDI_{vol}$, DLP and effective dose per series for CT upper and whole abdominal examination in male and female, respectively.

Table 4.16 Upper abdominal CT dose values per scan series.

	PSD (mGy)	$CTDI_{vol}$ (mGy)	DLP (mGy·cm)	Effective dose (mSv)
Mean	0.27	11.77	352.26	5.24
SD	0.22	1.02	44.35	0.69
Min	0.03	9.13	261.25	4.02
Max	1.17	14.8	485.80	7.31
3rd-Quartile	0.35	12.05	378.67	5.60

Table 4.17 Whole abdominal CT dose values per scan series.

	PSD (mGy)	$CTDI_{vol}$ (mGy)	DLP (mGy·cm)	Effective dose (mSv)
Mean	7.64	11.41	485.59	7.02
SD	3.56	0.94	66.80	1.40
Min	0.36	8.88	377.25	4.54
Max	13.69	15.60	863.00	14.14
3rd-Quartile	10.09	11.84	511.25	7.93

Table 4.18 Upper abdominal CT dose values per scan series for male and female.

	PSD (mGy)	$CTDI_{vol}$ (mGy)	DLP (mGy·cm)	Effective dose (mSv)
Male				
Mean	0.18	11.91	364.65	5.21
SD	0.15	0.97	41.43	0.67
Min	0.03	9.13	297.33	4.25
Max	0.83	14.80	485.80	7.31
3rd-Quartile	0.21	12.05	380.25	5.51
Female				
Mean	0.39	11.59	337	5.27
SD	0.24	1.07	43.80	0.72
Min	0.07	9.80	261.25	4.05
Max	1.17	14.80	415.67	6.60
3rd-Quartile	0.41	12.05	373.27	5.86

Table 4.19 Whole abdominal CT dose values per scan series for male and female.

	PSD (mGy)	$CTDI_{vol}$ (mGy)	DLP (mGy·cm)	Effective dose (mSv)
Male				
Mean	5.39	11.40	501.39	6.04
SD	3.61	0.88	56.14	0.83
Min	0.36	8.88	396.67	4.54
Max	13.17	13.07	654.00	8.13
3rd-Quartile	8.56	11.84	531.75	6.52
Female				
Mean	9.42	11.41	472.30	7.80
SD	2.30	1.00	71.97	1.26
Min	1.34	9.65	377.25	6.01
Max	13.69	15.60	863.00	14.14
3rd-Quartile	10.79	11.84	491.25	8.30

In this study evaluated effective dose values with conversion factors from DLP on CT monitor and calculation with conversion factor for regions of the body and patient group and scanner specific correction for upper and whole abdominal examination were shown in Figure 4.1 and 4.2, respectively.

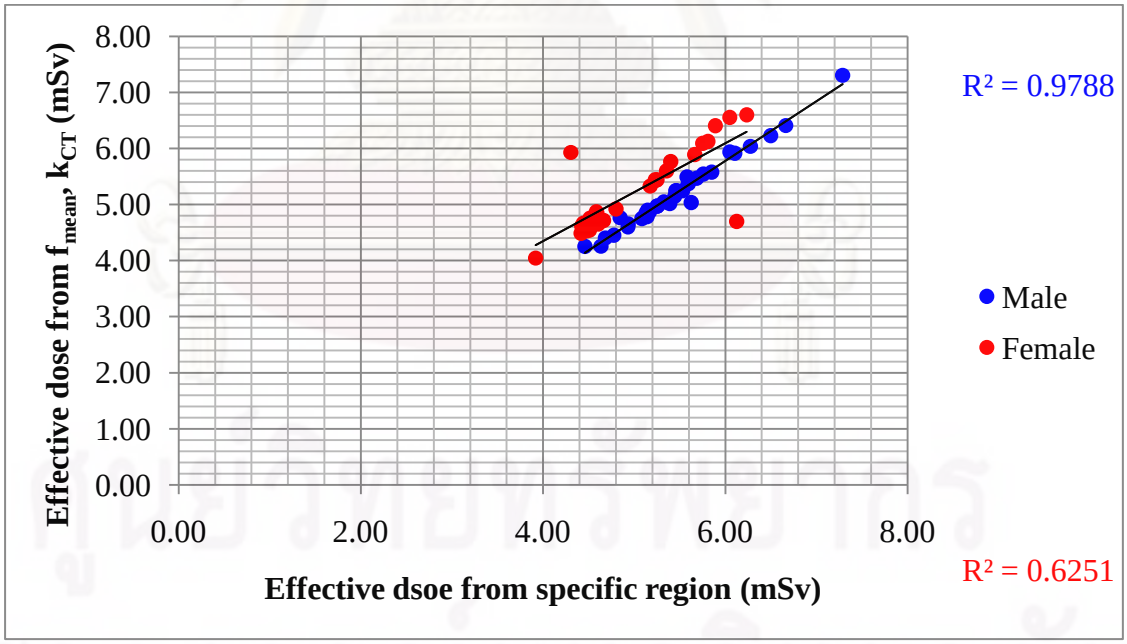

Figure 4.1 Scatterplot of all effective dose values estimated with conversion factors from DLP versus calculation with conversion factor for region of body and patient groups and scanner specific correction based on DLP_{air} calculation for upper abdominal CT examination.

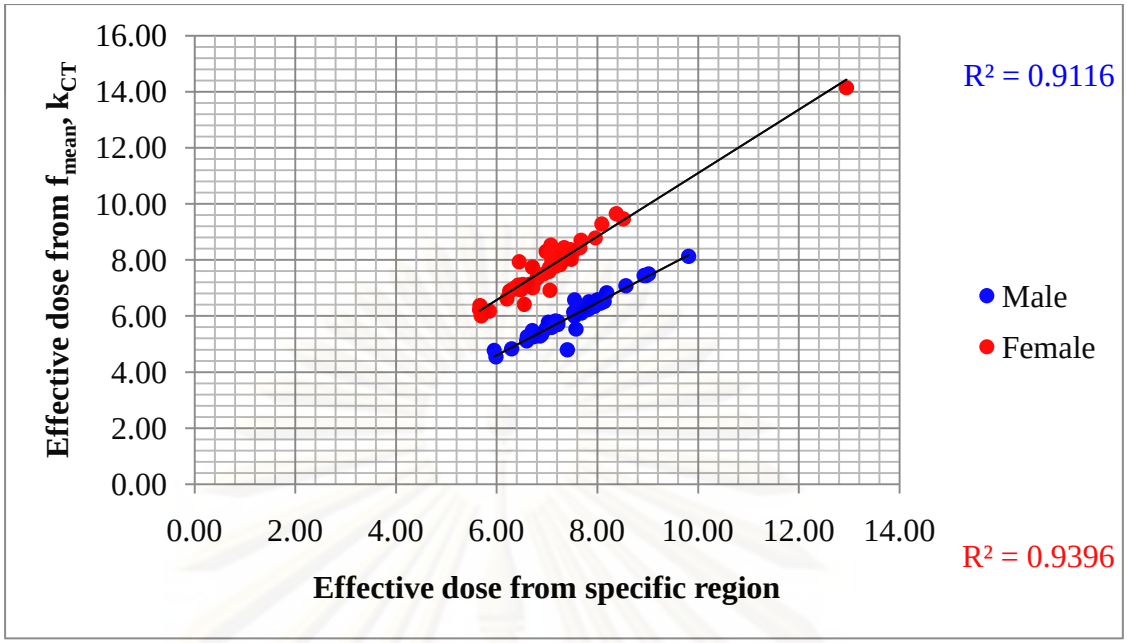

Figure 4.2 Scatterplot of all effective dose values estimated with conversion factors from DLP versus calculation with conversion factor for region of body and patient groups and scanner specific correction based on DLP_{air} calculation for whole abdominal CT examination.

4.5 Correlation between patient skin dose and effective dose

The correlation coefficient (R) between measured patient skin dose and calculated effective dose for upper and whole abdomen per examination were 0.387 and 0.225, respectively.

The correlation coefficient between measured patient skin dose and calculated efffective dose for CT upper abdominal examination in male and female were 0.431 and 0.415, respectively. The correlation coeficient between measured patient skin dose and calculation effective dose for CT whole abdominal examination 0.009 and -0.412, respectively.

Table 4.20 The correlation coefficient (R) between measured patient skin dose and calculated effective dose.

Examination	Number	R	Significant (2-tailed)
Upper abdomen	58	0.387	0.003*
Whole abdomen	86	0.225	0.037**
Male upper abdomen	32	0.437	0.012**
Female upper abdomen	26	0.415	0.035**
Male whole abdomen	38	0.009	0.956
Female whole abdomen	48	-0.412	0.004*

**Correlation is significant at the level 0.01 level (2-tailed).*
***Correlation is significant at the level 0.05 level (2-tailed)*

The correlation (R-square) between measured patient skin dose and calculated effective dose in 32 males and 28 females for CT upper abdominal examination were 0.1934 and 0.172, respectively.

The correlation (R-square) between the average PSD and the effective dose of 38 males and 48 females for whole abdominal CT examination were 0.00009 and 0.0025, respectively.

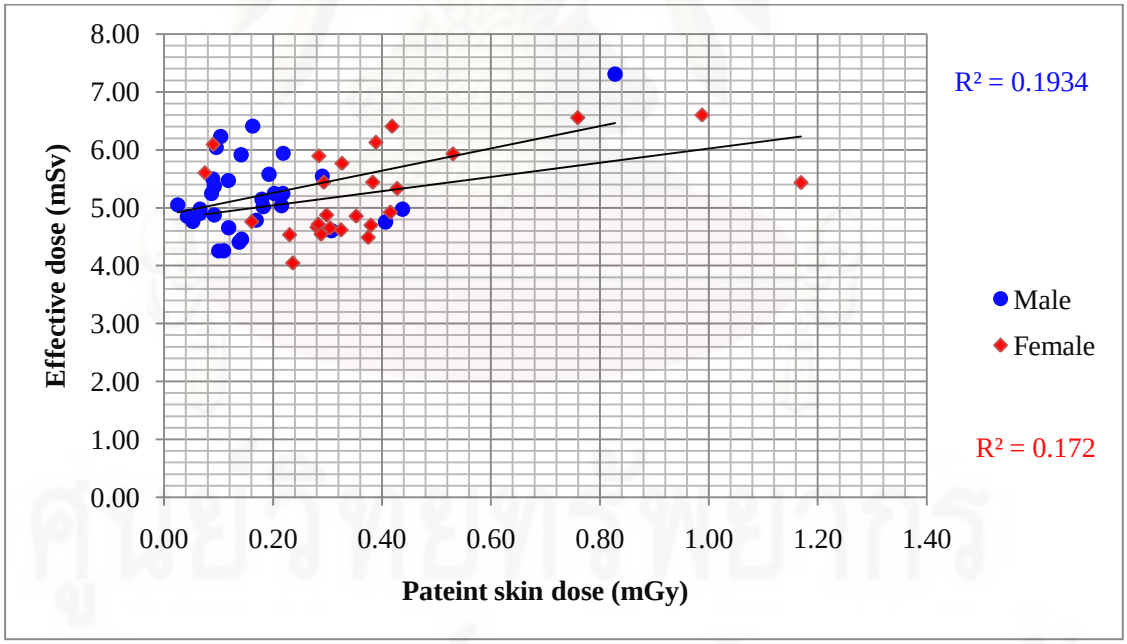

Figure 4.3 The correlation between the PSD and the effective dose for CT upper abdominal examination in male and female patients.

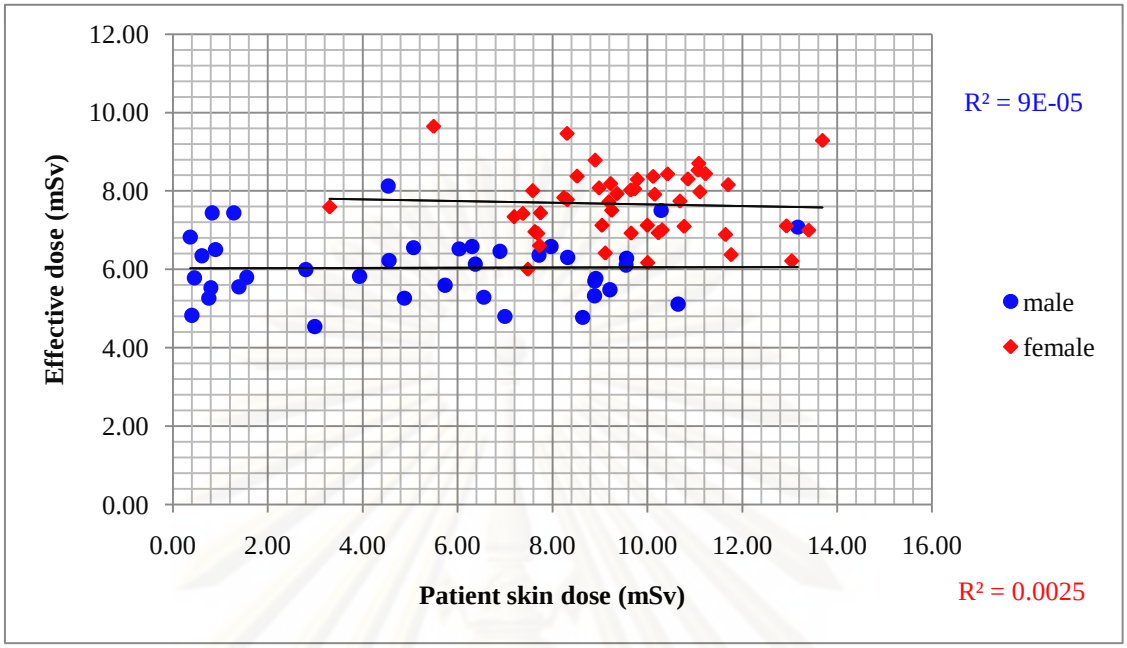

Figure 4.4 The correlation between average PSD and the effective dose for whole abdominal CT examination in male and female patients.

4.6 Conversion factor

The conversion coefficient between the average effective dose and the patient skin dose for CT upper abdomen was 17.82 $mSv \cdot mGy^{-1}$ and 0.92 $mSv \cdot mGy^{-1}$for CT whole abdomen. The conversion coefficient abovementioned can be derived from the average effective dose divided by the average patient skin dose.

CHAPTER V

DISCUSSION AND CONCLUSION

5.1 Discussion

All the measured CT Dose was verified by the ImPACT values. The quality control program of the CT is very important and should be performed prior to the research study. The measured CTDI in air was in acceptable limit when compared to the ImPACT values of less than 10% difference. The measurement in phantom showed the difference of less than 10% for CTDI in head phantom but greater than 10% for CTDI in body phantom. The measured CTDI in body phantom at 120 kVp of at normal setting for routine CT abdominal examination protocol was less than ImPACT value of 12.59 % difference.

The calculated $CTDI_{vol}$ was less than the displayed $CTDI_{vol}$ values in all kVp settings for head phantom. The percentage difference of calculated $CTDI_{vol}$ values were ranged from -14.40 to -3.43. The displayed $CTDI_{vol}$ values were higher than the ImPACT values at 80 and 120 kVp settings except in 100 kVp setting the displayed $CTDI_{vol}$ values was less than ImPACT value. The percentage difference of ImPACT values and displayed $CTDI_{vol}$ were ranged from -6.42 to 6.24 in body phantom, the calculated $CTDI_{vol}$ were less than the displayed $CTDI_{vol}$ values in all kVp setting as the head phantom. The percentage difference of calculated $CTDI_{vol}$ values and the displayed $CTDI_{vol}$ were ranged from -14.62 to -1.95. The percentage difference of displayed $CTDI_{vol}$ values were less than the ImPACT values in all kVp settings. The percentage difference of displayed $CTDI_{vol}$ and ImPACT values was ranged from -7.76 to -0.63.

The main cause of the large difference is the measurement uncertainty as described in IAEA Technical Report Series (TRS) No.457: Dosimetry in Diagnostic Radiology: An International Code of Practice [22]. The factors affecting the measurement uncertainty in the estimation of the CTDI were the characteristics of the ionization chamber/ electro meter, the measurement scenario, the precision of reading, tube loading, chamber and chamber positioning, the phantom construction, the chamber response in phantoms and the inaccuracy on laser beam alignment.

Additional sources of uncertainty arise from the effect of attenuation, scattered radiation inside the phantom, beam hardening and others which may affect the chamber response for measurements in phantom.

Therefore, the conversion factors and the calibration factors of ion chamber and electrometer must be applied.

In addition, the systematic error has to be considered since our x-ray tube has been replaced to a new model which is different from the previous one. As a consequence, it differs from that one used in measurement by ImPACT. This may be

another reason of a large difference of $CTDI_{vol}$ between the measured and the ImPACT values. Furthermore, the CTDI phantom used for ImPACT was different from the phantom in this study.

In calculation of the effective dose, the conversion factor to convert from dose free-in-air on the axis of rotation into effective dose for different regions of the body and patient groups (f_{mean}) and the scanner factor (k_{CT}) was used which were 0.0091 and 0.010 $mSv \cdot mGy^{-1} \cdot cm^{-1}$ for male and female, respectively in CT upper abdominal examination and 0.0072 and 0.010 $mSv \cdot mGy^{-1} \cdot cm^{-1}$ for male and female, respectively in CT whole abdominal examination. Whilst, the study of Van Der Molen A J et al [4] used the EU conversion factor from a European concerted Action on CT (FIGM-CT-2000-20078) which was 0.017 $mSv \cdot mGy^{-1} \cdot cm^{-1}$.and the effective dose was 6.6 mSv for abdomen. Our study showed the effective dose of 7.93 mSv for abdomen CT which was higher than the effective dose from Van Der Molen A J et al study. Both studies were acquired by Siemens SOMOTOM Sensation 16, but the effective dose was less than the study from United Kingdom of 12 mSv [23].

The maximum effective dose in this study 36.53 mSv in male patient with 5 series for CT upper abdomen and 40.04 mSv, male patient with 5 series for CT whole abdomen.

The increasing number of series in CT abdomen result in increasing the patient skin dose, $CTDI_{vol}$, DLP and effective in both genders for CT upper abdomen. Whilst, the $CTDI_{vol}$ and effective dose increased accordingly with the increase of the number of series in both gender for CT whole abdomen. In other hand, the patient skin dose and DLP increased with the increasing of number of series not over more 4 series. If the series was over 4 series, the patient dose decreased.

The correlation between measured patient skin dose and calculated effective dose for all examination were poor correlation. It may be the measured patient skin dose from solid state dosemeter which measured as point dose not volume dose as the CTDI value to calculate the effective in the final. Furthermore calculation effective dose rather depends on the scan length even if the patient were same gender, number of series.

The limitations in this study are, first, no patient in group of the body weight more than 105 kg. Second, the position of the dosemeter on the patient skin may vary during the examination of several series as the patient moved from bed at the end of the series. Lastly as the scan parameter varied from study to study, resulting in the variation of the effective dose in the CT abdomen study.

5.2 Conclusion

Our CTDI measurements provide the CTDI data to verify radiation dose with ImPACT scan and the display on monitor at workstation. The measured and calculated values and the values from ImPACT scan and the monitor values were

acceptable of less than ±10 percent. Therefore, the patient dose readout from monitor of CTDI value could be used according to the results of the verification. The patient skin dose was measured by the patient skin dosimeter (Unfors, PSD) which the detector was attached at the skin close to the gonad during the whole examination, then the dose values were read from the panel and the correction factor for the response at 120 kVp was applied. The effective dose calculation could also be obtained by the DLP multiplication of values with the region specific normalized coefficients from European Commissioning. The patient data included the body weight, number of series, gender, average PSD, $CTDI_{vol}$, DLP and total scan length for CT upper and whole abdomen.

For CT abdomen, the diagnostic reference levels (DRLs), $CTDI_w$ is 35 mGy, DLP is 800 mGy·cm and the effective dose is 12 mSv per examination as recommended by EUR 16262: European Guidelines on Quality Criteria for Computed Tomography [22]. The routine protocol at King Chulalongkorn Memorial Hospital for CT upper abdomen and whole abdomen require 3-5 series. The average patient skin dose per series for male and female were 0.18 and 0.39 mGy for CT upper abdominal examination, $CTDI_{vol}$ per series were 11.91 and 11.59 mGy, DLP per series were 364.65 and 337 mGy·cm and the average effective dose per series were 5.21 and 5.27 mSv. The average patient skin dose per series were 5.39 and 9.42 mGy for CT whole abdominal examination, the average $CTDI_{vol}$ per series for were 11.40 and 11.41 mGy, DLP per series were 502.39 and 472.30 mGy·cm, the average effective dose per series were 6.04 and 7.80 mSv for male and female respectively.

The total dose for CT upper and whole abdomen of 1.05 mGy, 28.04 mGy patient skin dose, 42.12 mGy, 42.66 mGy, $CTDI_{vol}$, 1260 mGy.cm, 1763.19 mGy·cm DLP and 18.71 mSv, 26.46 mSv effective dose.

The consideration of patient's body weight, increasing the body weight not corresponded with increasing the measured patient skin dose straightforward. As $CTDI_{vol}$, DLP and effective dose increased when increasing the patient's body weight.

The patient entrance surface dose (ESD) for the CT abdomen depends on the gender, number of series and the scan length. The average female gonad, obtained higher dose than male as the field of view covered the gonad region while the male gonad was out of the field. The study shows the high risk could be obtained from whole abdomen CT especially in children and female of reproductive age.

5.3 Recommendation

The protocol for data acquisition in all patients should be set up, and the PSD should be attached at the same position of the whole examination. The gonad dose must be determined in all routine abdomen examinations.

REFERENCES

[1] AY M R, Sarkar S, Shahriari M, Ghafarian P. Estimating of patient dose in abdomen-pelvis ct exam as a function of scan techniques in single and multiple slice spiral ct by monte carlo method[online]. Available from: http://rcstim.tums.ac.ir/db/papers/61.pdf. [2009, June 29]

[2] Yates S J, Pike L C, Goldstone K E. Effect of multislice scanners on patient dose from routine ct examinations in East Anglia. The British Journal of Radiology 77(Jun 2004): 472-478.

[3] Crawley M T, Booth A, Wainwright A. A practical approach to the first iteration in the optimization of radiation dose and image quality in CT: estimates of the collective dose savings achieved. The British Journal of Radiology 74 (Jul 2001): 607-614.

[4] Van Der Molen A J, Veldkamp W J H, Geleijins J. 16-slice CT: achievable effective dose of common protocols in comparison with recent ct dose surveys. The British Journal of Radiology 80 (2007): 248-255.

[5] Nickoloff E L, Dutta A K, Lu Z F. Influence of phantom diameter, kvp and scan mode upon computed tomography dose index. Medical Physics. 30 (Mar 2003): 395-402.

[6] Goldman L W. Principles of CT: radiation dose and image quality. Journal of Nuclear Medicine Technology 35(2007): 213-225.

[7] Hidajat N, Mäurer J, Schröder R-J, Nunnemann A, Wolf M, Pauli K et al. Relationships between physical dose quantities and patient dose in CT. The British Journal of Radiology 72(1999): 556-561.

[8] Bauhs J A, Vrieze T J, Primak A N, Bruesewitz M R, McCollough C H. CT dosimetry: comparison of measurement techniques and devices. RadioGraphics 28(2008): 245-253.

[9] Curry S Thomas, Dowdey E James and Murry C Robert, Jr. Christensen's Physics of Diagnostic Radiology. 4th edition. Philadelphia: Lippincott Williams & Wilkins, 1990.

[10] Bushberg J T, Seibert J A, Leidholdt E M and Boone J M. The Essential Physics of Medical Imaging. 2nded. Philadelphia: Lippincott Williams & Wilkins, 2002.

[11] American Association of Physicists in Medicine. The Measurement, Reporting and Management of Radiation dose in CT. Report of AAPM Task group 23 of the Diagnostic Imaging Council CT Committee. Report no.96, 2007.

[12] Rehani M, Kalra M, McCollough C, Nagel H D, Collons L, Kalender W. Managing patient dose in multi-detector computed tomography (MDCT). (Dec 2006).

[13] Galanski M, Hidajat N, Maier W, Nagel H D, Schmidt Th. Radiation exposure in computed tomography: fundamentals, influencing parameters, dose assessment, dose assessment, optimisation, scanner data, terminology. 4th edition. Hamburg: CTB Publications, 2002.

[14] Lu Z F, So J, Nickoloff E, Dutta A. An evaluation of a solid state dosimeter in direct measurement of CT dose. Medical Physics 35(2008): 2644-2645.

[15] Nerysungnoen B.Comparison of Effective Dose in Phantom from Computed Tomography Using Monte Carlo Simulation and Thermoluminescent Dosimetry Methods. Thesis of Master of Science Program in Medical Imaging Faculty of Medicine Chulalongkorn University, 2007.

[16] Lu Z, Nickoloff E, So J, Dutta A. Pediatric patient dose management from a 64 slice VCT. Medical Physics. 34(2007): 2339.

[17] Ware D E, Huda W, Mergo J P, Litwiller L. Anthony. Radiation effective doses to patients undergoing abdominal CT examinations. Radiology 210 (1999): 645-650.

[18] Huda W, Ogden K M, Khorasani M R. Converting dose- length product to effective dose at CT. Radiology 248 (Sep 2008): 995-1003.

[19] The phantom laboratory. Catphan®500 and 600 manual. Copyright© 2009: 1-34.

[20] American Association of Physicist in Medicine. Specification and acceptance testing of computed tomography scanners, report 39 (May 1993).

[21] ImPACT. ImPACT information leaflet 1: CT scanner acceptance testing. version 1.02, (2001): 1-8

[22] International Atomic Energy Agency 2007. Dosimetry in Diagnostic Radiology: An International Code of Practice – Vienna: International Atomic Agency (Technical report series, ISSN 0074-1914; no.457). Vienna, Austria: IAEA.

[23] Olerud M Hilde. CT-dose surveys. Presented at the radiation protection symposium of the North West European RP Societies, Utrecht, the Netherlands, June 2-5, 2003.

[24] European Commission. Quality criteria for computed tomography, Report EUR16262. Luxemburg: Office for Official Publications of the European Communities (1999).

[25] Bouzarjomehri F, Zare H M and Shahbazi-Gahrouei D. Patient Dose Resulting from CT Examinations in Yazd, Iran. Iranian Journal Radiation Research 4(2006): 121-127.

[26] Tsapaki V, Aldrich J E, Sharma R, Staniszewska M A, Krisanachinda A, Rehani M et al. Dose reduction in CT while maintaining diagnostic confidence: diagnostic reference levels at routine head, chest and abdominal CT—IAEA-coordinated research project. Radiology 240 (Sep 2006): 828-834.

[27] Garcia-Ramirez J L, Mutic S, Dempsey J F, Low D A, Purdy J A. Performance evaluation of an 85-cm-bore x-ray computed tomography scanner designed for radiation oncology and comparison with current diagnostic ct Scanners. International Journal of Radiation Oncology. 52 (2002): 1123-1131.

[28] Brix G, Nagel H D, Stamm G, Veit R, Lechel U, Griebel J et al. Radiation exposure in multi-slice versus single-slice spiral CT: results of a nationwide survey. European Radiology 13 (2003): 1979-1991.

[29] Shrimpton P C, Hillier M C, Lewis M A, Dunn M. National survey of doses from CT in the UK: 2003. The British Journal of Radiology 79 (2006): 968-980.

[30] Tsapaki V, Kottou S, Papadimitriou D. Application of European Commission reference dose levels in CT examinations in Crete, Greece. The British Journal of Radiology 74 (Sep 2001): 836-840.

Appendices

Appendix A: Case Record Form

Table 1 Data Collection form of abdominal CT examination

1. Patient information

Study No.: _____ Date: _____

Age: _____ year Gender: _____

Height: _____ cm Weight: _____ kg

Body Thickness: _____ cm

Scout

kVp	mA	Scan length (cm)	Patient skin dose (mGy)

Parameter	Series 1	Series 2	Series 3	Series 4	Series 5
kVp					
mAs_{eff}					
Slice thickness (mm)					
Field of view (mm)					
Helical pitch					
Start position					
End position					
Scan length (cm)					
Patient skin dose (mSv)					
$CTDI_{vol}$ (mGy)					
DLP (mGy ٭ cm)					

Appendix B: Quality Control of CT systems

1. Scan Localization Light Accuracy

Purpose: To test congruency of scan localization light and scan plane.

Method: Tape localization film to the backing plate making sure that the edges of the film are parallel to the plate edge. Place the film vertically along the midline of the couch aligned with its longitudinal axis. Raise the table to the head position. Turn the alignment light. Mark both internal and external light with unique pin pricks along the midline of the light. Expose the internal light localization using the narrowest slice setting at 120 kVp, 50-100 mAs. For external light increment table to light position under software control and expose the film.

Tolerance: The center of the irradiation field from the pin pricks should be less than 2 mm.

Results:

	Measured Deviation	External	0	mm
		Internal	1	mm

Comments: Pass

2. Alignment of Table to Gantry

Purpose: To ensure that long axis of the table is horizontally aligned with a vertical line passing through the rotational axis of the scanner.

Method: Locate the table midline using a ruler and mark it on a tape affixed to the table with the gantry untilted, extend the table top into gantry to tape position. Measure the horizontal deviation between the gantry aperture center and the table midline.

Tolerance: The deviation should not be within 5 mm.

Results:

	Table	Bore
Distance from right to center (mm)	198	349
Distance from center to left (mm)	202	351
Measured Deviation (mm)	**2**	**1**

**Measured deviation = (Distance from right to center – Distance from center to left)/2*

Comments: Pass

3. Table Increment Accuracy

Purpose: To determine accuracy and reproducibility of table longitudinal motion.

Method: Tape a measuring tape at the foot end of the table. Place a paper clip at the center of the tape to function as an indicator. Load the table uniformly with 150 lbs. from the initial position move the table 300, 400 and 500 mm into the gantry under software control (+ve). Record the relative displacement of the pointer on the ruler. Reverse the direction of motion (-ve) and repeat. Repeat the measurements four times.

Tolerance: Positional errors should be less than 3 mm at 300 mm position.

Results:

Indicated (mm)	Measured (mm)	Deviation (mm)
500	500	0
400	400	0
300	300	0
-300	-300	0
-400	-400	0
-500	-500	0

*$Deviation = |Indicated - Measured|$

Comments: Pass

4. Slice Increment Accuracy

Purpose: To determine the accuracy of the slice increment.

Method: Set up as you would for beam profile measurement. Select 120 kVp, 100 mAs and smallest slit width. Perform several scans with different programmed slice separations under auto control. Scan the film with a densitometer and measure the distance between the peaks.

Tolerance: Positional errors should be less than 3 mm at 300 mm position.

Results:

Slice separation in mm	Measured separation in mm	Deviation(mm)
20	20	0
30	30	0
50	50	0

*$Deviation = |Slice\ separation - Measured\ separation|$

Comments: Pass

5. Gantry Angle Tilt

Purpose: To determine the limit of gantry tilt and the accuracy of tilt angle indicator.

Method: Tape a localization film to the backing plate making sure that the edges of the film are parallel to the edges of the backing plate. Place the film vertically along the midline of the couch aligned with its longitudinal axis. Raise the table to the head position. Move the table into gantry. Center plate to alignment light. Expose the film at inner light location using narrowest slit, 120-140 kVp, 50-100 mAs. Tilt the gantry to one extreme from the console. Record the indicated gantry angle. Expose the film using the above technique. Measure the clearance from the closest point of gantry to midline of the table.

Tilt the gantry to its' extreme in the opposite direction. Record clearance and repeat the exposure. Measure the tilt angles from the images on the film.

Tolerance: Deviation between indicated and measured tilt angles $\leq 3^{\circ}$. Gantry clearance should be ≥ 30 cm.

Results:

	Away	**Toward**
Indicated Angle	15°	15°
Measured Angle	15°	15°
Deviation	0	0
Clearance (mm)	455	470

*$Deviation = |Indicated\ angle - Measured\ angle|$

Comments: Pass

6. Position Dependence and SNR of CT Numbers

Method: Position the water phantom centered in the gantry. Using 1 cm slice thickness, obtain one scan using typical head technique. Select a circular region of interest of approximately 400 sq.mm. And record the mean CT number and standard deviation for each of the positions 1 through 5.

Technique: 120 kVp, 250 mA, 1 sec, 300 mm FOV and 10 mm slice thickness

Tolerance: less than 3 HU

Results:

Position	Mean CT number(HU)	SD	CV
1	11.1	3.0	0.270
2	11.1	2.9	0.261
3	11.5	2.8	0.243
4	11.3	3.1	0.274
5	11.1	3.7	0.333

**CV = Standard deviation / mean CT number*

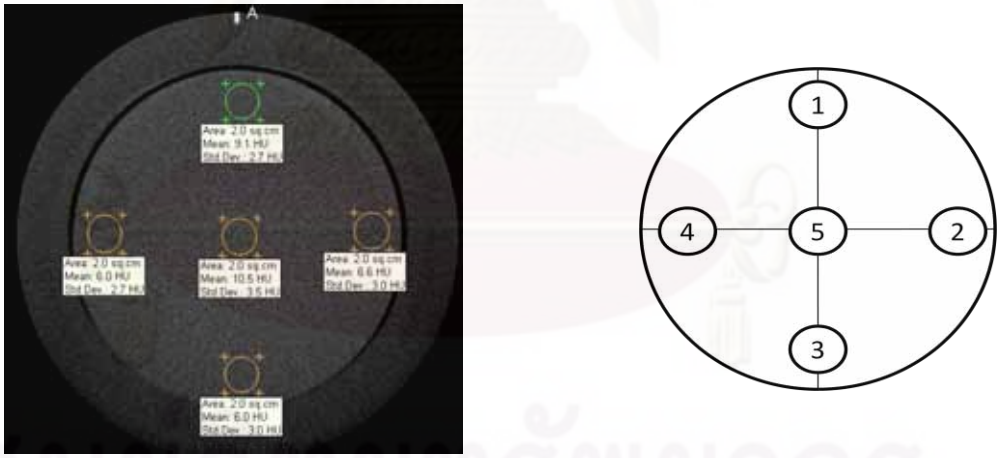

Figure I Position of ROI was measured the CT number.

Comments: Pass

7. Reproducibility of CT Numbers

Method: Using the same set up and technique as position dependence, obtain three scans. Using the same ROI as position dependence in location 5, which is the center of the phantom, obtain mean CT numbers for each of the four scans.

Tolerance: The coefficient of variation of mean CT numbers of the four scans should be less than 0.002

Results:

Run Number	1	2	3	4
Mean CT Number (HU)	10.273	10.279	10.299	10.305

Mean Global CT Number	10.289
Standard Deviation	0.015
Coefficient of Variation	0.001

Comments: Pass

8. mAs Linearity

Method: Set up the same as position dependence and insert 10 cm long pencil chamber in the center slot of the C.T. dose head phantom. Select the same kVp and time as used for head scan. Obtain four scans in each of the mA stations normally used in the clinic. For each mA station record the exposure in mGy for each scan. Scans should be performed in the increasing order of mA. Compute mGy/mAs gor each mA setting.

Technique: 120 kVp, 250 mA, 1 sec, 250 mmSFOV

Results:

mA	Exposure in mGy				mGy/mAs	C.V.
	Run 1	Run 2	Run 3	Run 4		
50	0.762	0.760	0.760	0.763	0.0152	1.000
100	1.456	1.455	1.457	1.455	0.0146	0.022
150	2.178	2.193	2.186	2.187	0.0146	0.001
200	2.916	2.919	2.918	2.917	0.0146	0.000
250	3.646	3.650	3.654	3.656	0.0146	0.001
300	4.392	4.390	4.384	4.394	0.0146	0.001
350	5.158	5.151	5.143	5.152	0.0147	0.003

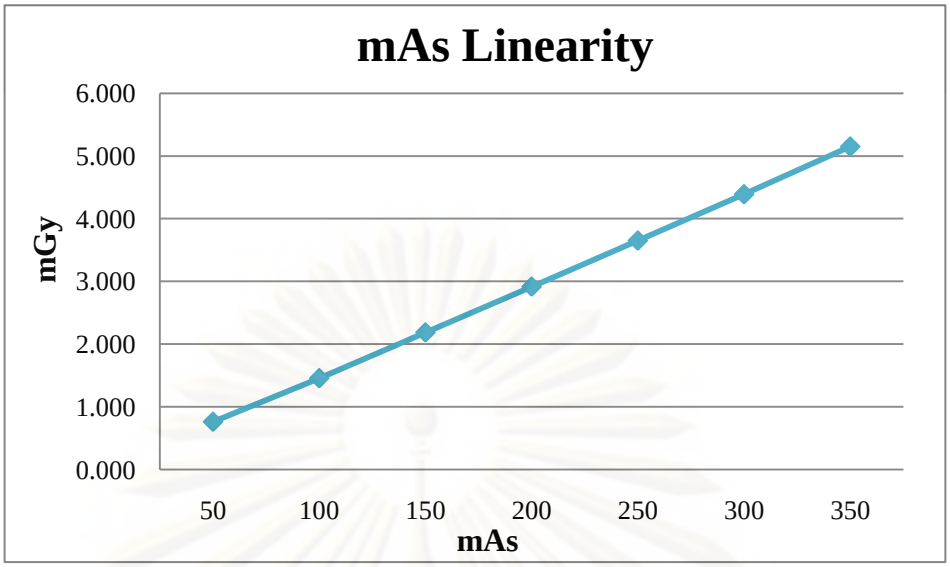

Figure II The relationship of mGy and mAs.

Comments: Pass

9. Linearity of CT Numbers

Method: Set up the Catphan phantom as described in beam alignment. Select the section containing the test objects of difference C.T. numbers. Select the head technique and perform a single transverse scan. Select a region of interest (ROI) of sufficient size to cover the test objects. Place the ROI in middle of each test object and record the mean CT number.

Technique: 120 kVp, 250 mAs, 1 sec, 250 mm SFOV, 10 mm slice thickness

Tolerance: R-square between measured CT number and linear attenuation coefficient (μ) more than 0.9

Results:

Materials	Expected CT number (HU)	Measured CT number (HU)
Air	-1000	-1021.4
Teflon	990	1393.5
Delrin	340	494.3
Acrylic	120	120.7
Polystryline	-35	-43.6
LDPE	-100	-106.2
PMP	-200	-196.3

Note: Expected C.T. numbers are either the predicted ones or the ones obtained during the previous annual measurement.

Comments: Pass

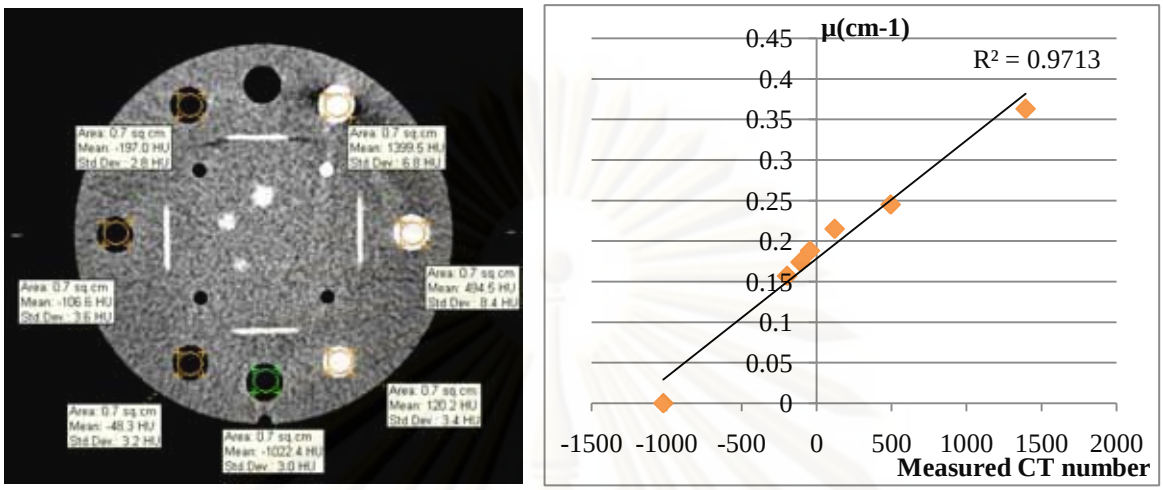

Figure III Linearity of CT number

10. High Contrast Resolution

Method: Set up the Catphan phantom as described in beam alignment. Select the section containing the high test objects. Select the head technique. Perform a single transverse scan. Select the area containing the high resolution test objects and zoom as necessary. Select appropriate window width and level for the best visualization of the test objects. Record the smallest test object visualized on the film.

Technique: 120 kVp, 250 mA, 1 sec, 250 mm SFOV, 10 mm slice thickness
Window width = 150, window level = 200

Figure IV High contrast resolution

Results:

Slice thickness in mm	Resolution
10	4 lp/mm (0.125 cm)

11. Low Contrast Resolution

Method: Select the section containing the low resolution test objects in the Catphan phantom. Perform a single transverse scan utilizing the same technique as high resolution.

Technique: 120 kVp, 250 mA, 1 sec, 250 mmSFOV, 10 mm slice thickness

Window width = 140, window level = 100

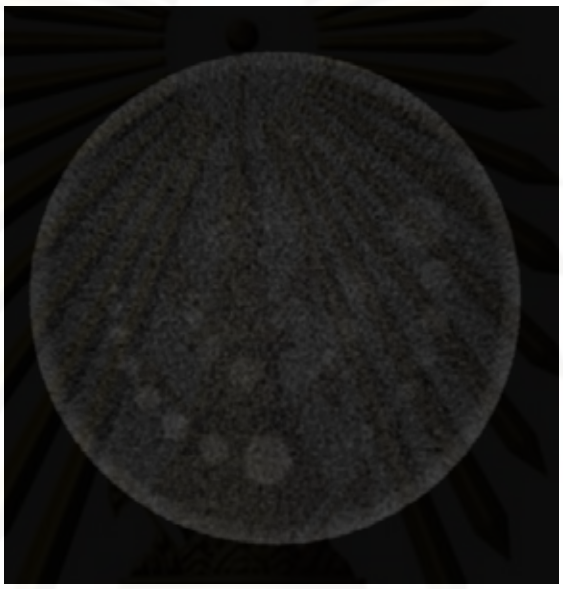

Figure V Low contrast resolution

Slice thickness (mm)	Resolution (mm)
10 mm at supra-slice 1%	4 mm
10 mm at supra-slice 0.5%	4 mm
10 mm at subslice	7 mm

12. CTDI Measurement

Purpose: To verify CTDI of the scanner to ImPACT scan.

Method: The $CTDI_{100}$ measured free in air and in 16 and 32 cm PMMA phantom for head and body were compared the CTDI data spreadsheet of the ImPACT dose survey© 2000-2004. The percent difference were calculated between measured and available ImPACT values

Technique: 120 kVp, 100 mA, 1 sec, 10 mm collimation

Results:

The measured $CTDI_{100}$ free in air and in 16 and 32 cm PMMA phantom for head and body scans were measured and compared to the CTDI data spreadsheet of the ImPACT dose survey © 2000-2004. [(http://impactscan.org/dosesurvey.htm for details of the dose survey)]

Computed tomography dose index in air and the head phantom

kVp	$CTDI_{100}$ (Head, mGy/100 mAs)								
	Air		% diff	Center		% diff	Periphery		% diff
	Measured	ImPACT		Measured	ImPACT		Measured	ImPACT	
80	8.88	9.1	2.37	5.03	5.5	8.61	6.09	6.70	9.11
100	15.83	16.08	1.55	9.80	10.85	9.63	11.32	12.53	9.63
120	21.72	21.8	0.38	14.03	15.4	8.92	15.81	17.18	8.06
140	29.40	-	-	19.42	-	-	21.57	-	-

Computed tomography dose index in air and the body phantom

kVp	$CTDI_{100}$ (Body, mGy/100 mAs)								
	Air		% diff	Center		% diff	Periphery		% diff
	Measured	ImPACT		Measured	ImPACT		Measured	ImPACT	
80	5.26	5.24	-0.34	0.95	1.12	-17.49	2.21	2.61	-17.94
100	10.57	10.59	0.26	2.23	2.47	-10.64	4.77	5.22	-9.50
120	15.64	15.26	-2.49	3.56	4.17	-17.09	7.13	8.16	-14.40
140	22.28	21.63	-2.99	5.29	6.19	-17.12	10.22	11.62	-13.74

13. Radiation Profile Width

Purpose: To determine the accuracy of the slice thickness

Method: Set up as you would for beam profile measurement. Select 120 kVp, 100 mAs, and smallest slit width. Perform several scans with different programmed slice thicknesses under auto control. Scan the film with a densitometer and measure the distance between the peaks. Average measures at least 3 times on each profile.

Result:

Collimation (mm)	Measured (mm)	Deviation
9 mm (12 × 0.75)	11.8	2.8
10 mm (2 × 5)	10.4	0.4
18 mm (12 × 1.5)	20.6	2.6

**Density profiles may also be measured with a scanning microdensitometer or image J*

Appendix C: Patient information sheet

เอกสารข้อมูลคำอธิบายสำหรับผู้ป่วยที่เข้าร่วมการวิจัย (Patient Information Sheet)

การวิจัยเรื่อง สหสัมพันธ์ของปริมาณรังสียังผลที่ผู้ป่วยได้รับจากการตรวจเอกซเรย์คอมพิวเตอร์ส่วนช่องท้องโดยวิธีการคำนวณและการใช้วัดปริมาณรังสีที่ผิวหนังด้วยเครื่องวัดรังสีชนิดโซลิดสเตท

เรียน ผู้ป่วย/บิดา/ มารดา/ ผู้ปกครองทุกท่าน

ท่านเป็นผู้ที่ได้รับเชิญให้เข้าร่วมการศึกษาวิจัย สหสัมพันธ์ของปริมาณรังสียังผลที่ผู้ป่วยได้รับจากการตรวจเอกซเรย์คอมพิวเตอร์ส่วนช่องท้อง โดยวิธีการคำนวณและการใช้วัดปริมาณรังสีที่ผิวหนังด้วยเครื่องวัดรังสีชนิดโซลิดสเตท โดยก่อนที่ท่านตกลงเข้าร่วมการศึกษาดังกล่าว ขอเรียนให้ท่านทราบถึงเหตุผลและรายละเอียดของการศึกษาวิจัยในครั้งนี้

การตรวจเอกซเรย์คอมพิวเตอร์ส่วนช่องท้องนั้นทำให้อวัยวะต่างๆ ที่อยู่ในบริเวณที่ทำการตรวจได้รับรังสี รวมทั้งบริเวณอวัยวะสืบพันธุ์ซึ่งเป็นอวัยวะที่มีความไวต่อรังสีค่อนข้างสูง จึงเป็นเรื่องที่น่าสนใจว่าในการตรวจเอกซเรย์คอมพิวเตอร์ส่วนช่องท้องนั้นอวัยวะสืบพันธุ์ได้รับปริมาณรังสีเกินกว่าค่าปริมาณรังสีสูงสุดที่ยอมรับได้หรือไม่ นอกจากจะเป็นการสำรวจปริมาณรังสีที่ได้รับจากการตรวจเอกซเรย์คอมพิวเตอร์ส่วนช่องท้องแล้ว ยังเป็นการกระตุ้นเตือนในเรื่องการป้องกันอันตรายจากรังสีในส่วนของผลและความเสี่ยงที่เกิดจากการได้รับรังสี

ในการศึกษาครั้งนี้เป็นการใช้เครื่องวัดรังสีชนิดโซลิดสเตท (Patient Skin Dosemeter) ติดที่ผิวหนังใกล้บริเวณอวัยวะสืบพันธุ์เพื่อทำการวัดปริมาณรังสีที่ผู้ป่วยได้รับจากการตรวจเอกซเรย์คอมพิวเตอร์ส่วนช่องท้อง เครื่องวัดรังสีชนิดโซลิดสเตทมีลักษณะของแผ่นตรวจจับรังสีเป็นแผ่นแบน ขนาดประมาณ 1.5 เซนติเมตร มีสายต่อเ ข้าเครื่อง สามารถอ่านค่าได้ทันทีเป็นเครื่องมือที่ไม่รบกวนการทำงานของเครื่องเอกซเรย์คอมพิวเตอร์ขณะทำการตรวจและไม่ก่อให้เกิดอันตรายกับผู้ป่วย

การศึกษาวิจัยในครั้งนี้ มีวัตถุประสงค์เพื่อหาปริมาณรังสียังผลที่ผู้ป่วยได้รับจากการตรวจเอกซเรย์คอมพิวเตอร์ส่วนช่องท้องและหาสหสัมพันธ์ของปริมาณรังสียังผลที่ผู้ป่วยได้รับจากการตรวจเอกซเรย์คอมพิวเตอร์ส่วนช่องท้องโดยวิธีการคำนวณและการวัดปริมาณรังสีที่ผิวหนังด้วยเครื่องวัดชนิดโซลิดสเตท เพื่อเป็นข้อมูลอ้างอิงและ เป็นประโยชน์ต่อผู้ป่วยที่เข้ารับการตรวจในอนาคตข้างหน้า และท่านยังได้รับทราบถึงปริมาณรังสีที่ท่านได้รับจากการตรวจครั้งนี้ ซึ่งเราจะแจ้งให้ท่านทราบภายหลังจากการวิจัยเสร็จสิ้นแล้ว

ดังนั้นเพื่อทำให้สามารถบรรลุวัตถุประสงค์ดังกล่าว นักรังสีการแพทย์จำเป็นต้องได้รับข้อมูลเกี่ยวกับท่านก่อนอันได้แก่ อายุ น้ำหนัก ส่วนสูง และวัดค วามหนาบริเวณกึ่งกลางของส่วน

ของร่างกายที่แพทย์ผู้ทำการตรวจรักษาต้องการให้เข้ารับบริการตรวจด้วยเครื่องเอกซเรย์คอมพิวเตอร์

หากท่านตกลงที่จะเข้าร่วมการศึกษาวิจัยครั้งนี้ จะมีข้อปฏิบัติร่วมดังนี้

ขั้นตอนการตรวจด้วยเครื่องเอกซเรย์คอมพิวเตอร์

1. การเตรียมตัวสำหรับผู้ป่วยก่อนการตรวจ

1.1 งดน้ำ และอาหาร 4-6 ชั่วโมง เพื่อป้องกันการสำลัก การอาเจียนในกรณีที่มีการฉีดสารทึบรังสี

1.2 ผู้ป่วยจะต้องถอดวัตถุทึบรังสีบริเวณที่จะทำการตรวจออกให้หมด

2. การปฏิบัติตัวขณะทำการตรวจ

2.1 นักรังสีการแพทย์จะนำผู้ป่วยไปนอนบนเตียงเอกซเรย์

2.2 นักรังสีการแพทย์จะจัดท่า เพื่อป้องกันการตกเตียงมีอุปกรณ์ช่วยยึดผู้ป่วยกับเตียงเอกซเรย์ และติดเครื่องวัดรังสีที่ผิวหนังบริเวณใกล้กับอวัยวะสืบพันธุ์

2.3 ผู้ป่วยจะต้องนอนนิ่งๆ โดยที่ผู้ป่วยสามารถสื่อสารกับเจ้าหน้าที่ผ่านทางไมโครโฟนแบะอยู่ภายใต้การสังเกตของเจ้าหน้าที่ผ่านทางโทรทัศน์วงจรปิดตลอดเวลาทำการตรวจ (กรณีเด็กญาติหรือผู้ปกครองสามารถเฝ้าในห้องตรวจได้แต่ต้องสวมอุปกรณ์ป้องกันรังสี ถ้าเป็นสตรีต้องไม่อยู่ในระยะตั้งครรภ์)

2.4 นักรังสีการแพทย์จะทำการเอกซเรย์ซึ่งจะสังเกตได้จากเวลาที่เอกซเรย์ออกจะมีสัญญาณไฟสีส้มสว่างขึ้นตรงตำแหน่งหลอดเอกซเรย์เหนือศีรษะของผู้ป่วย โดยขณะที่เอกซเรย์เตียงจะเคลื่อนที่ไปด้วย

2.5 การตรวจเอกซเรย์คอมพิวเตอร์บริเวณลำตัว ต้องให้ผู้ป่วยดื่มสารทึบรังสีในบางกรณีที่ต้องการให้เห็นพยาธิภาพของโรคให้ชัดเจนยิ่งขึ้น อันจะเป็นประโยชน์ต่อผู้ป่วย

3. การปฏิบัติตัวหลังการตรวจ

3.1 กรณีที่ไม่มีการฉีดสารทึบรังสี เมื่อตรวจเสร็จสามารถกลับบ้านหรือหอพักได้เลย

3.2 กรณีที่ฉีดสารทึบรังสี ผู้ป่วยต้องรอสังเกตอาการ 30 นาที เพื่อให้แน่ใจว่า ไม่มีผลข้างเคียงจากสารทึบรังสีที่ฉีดให้ผู้ป่วย รังสีแพทย์จึงจะให้กลับบ้านหรือหอพักได้

3.3 ผู้ป่วยจะได้รับเอกสาร ข้อปฏิบัติตัว เบอร์โทรติดต่อกับแพทย์เมื่อกลับบ้านไปแล้วมีอาการไม่พึงประสงค์ รวมทั้งการนัดหมายมารับผลก็จะแจ้งเอกสารนี้เช่นกัน

ประการสำคัญที่ท่านควรทราบ คือ

- ท่านผู้เข้าร่วมการศึกษาวิจัยนี้ เป็นผู้ป่วยที่ต้องมีคำร้ องขอเข้ารับการวินิจฉัยด้วยเครื่องเอกซเรย์คอมพิวเตอร์ภาพทางรังสีจากแพทย์ผู้ตรวจเท่านั้น เป็นผู้ได้รับเกียรติที่ผ่านเกณฑ์การคัดเลือกกลุ่มตัวอย่างตามแบบฟอร์มโครงร่างงานวิจัยที่ได้รับอนุมัติจากคณะกรรมการพิจารณาจริยธรรมแล้ว
- ท่านจะเสียค่าตรวจวินิจฉัยด้วยเครื่องเอกซเรย์คอมพิวเตอร์เฉพาะในส่วนของภาพรังสีที่แพทย์ส่งตรวจเท่านั้น ไม่มีค่าใช้จ่ายใดๆ เพิ่มเติมจากค่าตรวจปกติทั้งสิ้น
- การเข้าร่วมการศึกษาวิจัยครั้งนี้ ท่านไม่ต้องเสียค่าใช้จ่ายพิ่มเติมนอกจากค่าตรวจปกติเท่านั้น
- ความเสี่ยงที่อาจเกิดขึ้นจากการเข้าร่วมการศึกษาวิจัย ในการวิจัยครั้งนี้ต้องทำการติดเครื่องวัดรังสีขนาดเล็กที่ผิวหนังบริเวณใกล้อวัยวะสืบพันธ์ซึ่งอาจทำให้ผู้เข้าร่วมการการวิจัยเกิดความกระดากอาย แต่ในการติดเครื่องวัดรังสีจะกระทำด้วยเจ้าหน้าที่เพศเดียวกับผู้เข้าร่วมวิจัย
- ประโยชน์ที่ท่านจะได้รับจากการเข้าร่วมการศึกษาวิจัยคือท่านจะได้รับทราบปริมาณรังสีที่ท่านได้รับจากการตรวจเอกซเรย์คอมพิวเตอร์หลังจากที่การศึกษาวิจัยเสร็จสิ้นแล้ว
- การศึกษาวิจัยนี้ไม่มีค่าตอบแทนใดๆ ให้แก่อาสาสมัครผู้เข้าร่วมการวิจัยทั้งสิ้น
- การรักษาความลับ ข้อมูลของท่านจะใช้สำหรับวัตถุประสงค์ทางวิ ชาการและความปลอดภัยของผู้เข้าร่วมวิจัยเท่านั้น โดยข้อมูลต่างๆ จะไม่มีการเปิดเผยชื่อของท่านตามกฎหมาย
- การศึกษาวิจัยนี้ต้องการผู้เข้าร่วมการวิจัยประมาณ 50 คน โดยแบ่งกลุ่มตามน้ำหนักตัวเป็น 5 กลุ่ม กลุ่มละประมาณ 10 คน
- การศึกษาวิจัยนี้เป็นการเก็บข้อมูลที่จำเป็นในการกำหนดปริมาณรังสีแก่ผู้ป่วยที่เข้ารับการวินิจฉัยด้วยเครื่องเอกซเรย์คอมพิวเตอร์ที่พึงปฏิบัติตามปกติวิสัยของการตรวจเอกซเรย์คอมพิวเตอร์
- การศึกษาวิจัยนี้เป็นการเก็บข้อมูลปริมาณรังสีที่ผู้ป่วยได้รับจากการตรวจเอกซเรย์คอมพิวเตอร์ มิได้เป็นการให้หรือเว้นการให้สิ่งใดแก่ผู้เข้าร่วมการศึกษาวิจัย
- ก่อนการตรวจทุกครั้ง ท่านจะได้รับทราบข้อมูลของการตรวจด้วยเครื่องเอกซเรย์คอมพิวเตอร์จากนักรังสีการแพทย์ที่ทำการเก็บข้อมูลตามความเป็นจริง อันได้แก่ส่วนของร่างกายที่จะทำการตรวจ การฉีดสารทึบรังสี และการปฏิบัติตัวระหว่างการรับบริก ารการตรวจเอกซเรย์คอมพิวเตอร์
- ในระหว่างการตรวจด้วยเครื่องเอกซเรย์คอมพิวเตอร์ ท่ านต้องปฏิบัติตามคำแนะนำของนักรังสีการแพทย์ผู้ปฏิบัติงาน
- หากเกิดอันตรายกับผู้เข้าร่วมการวิจัย ฝ่ายรังสีวิทยา โรงพยาบาลจุฬาลงกรณ์ สภากาชาดไทย จะเป็นผู้ดูแลรักษาและออกค่าใช้จ่ายด้านการตรวจวินิจฉัย

- หากท่านไม่ได้รับการชดเชยอันควรต่อการบาดเจ็บหรือเจ็บป่วยที่เกิดขึ้นโดยตรงจากการวินิจฉัยหรือท่านไม่ได้รับการปฏิบัติตามที่ปรากฏในเอกสารข้อมูลคำอธิบายสำหรับผู้เข้าร่วมในการวิจัย ท่านสามารถร้องเรียนได้ที่ คณะกรรมการจริยธรรมการวิจัย คณะแพทยศาสตร์ จุฬาลงกรณ์มหาวิทยาลัย ตึกอานันทมหิดลชั้น 3 โรงพยาบาลจุฬาลงกรณ์ ถนนพระราม 4 ปทุมวัน กรุงเทพฯ 10330 โทร 0-2256-4455 ต่อ 14,15 ในเวลาราชการ
- การเข้าร่วมการศึกษาครั้งนี้เป็นไปโดยมัครใจ และไม่มีค่าตอบแทนใดๆ ท่านอาจปฏิเสธที่อาจจะเข้าร่วมหรือถอนตัวจากการวิจัยนี้ได้ทุกเมื่อโดยไม่กระทบต่อการให้บริการการตรวจวินิจฉัยของท่านที่จะได้รับจากนักรังสีการแพทย์, นักฟิสิกส์การแพทย์และรังสีแพทย์ หรือผู้ให้บริการท่านอื่นๆ

หากท่านมีปัญหาหรือข้อสงสัยประการใด กรุณาติดต่อ ร .ท.หญิง เพียงตะวัน กาญจนะ สาขาวิชาฉายาเวชศาสตร์ ภาควิชารังสีวิทยา คณะแพทยศาสตร์ จุฬาลงกรณ์มหาวิทยาลัย โทร . 08-9414-3050 ซึ่งยินดีให้คำตอบแก่ท่านทุกเมื่อ

หากท่านต้องการร้องเรียน กรุณาติดต่อ ภาควิชารังสีวิทยา โทร. 0-2256-4418

ขอขอบพระคุณในความร่วมมือของท่านมา ณ โอกาสนี้

Study No…… **ใบยินยอมเข้าร่วมการวิจัย (Consent Form)**

การวิจัยเรื่อง สหสัมพันธ์ของปริมาณรังสียังผลที่ผู้ป่วยได้รับจากการตรวจเอกซเรย์คอมพิวเตอร์ส่วนช่องท้องโดยวิธีการคำนวณและการใช้วัดปริมาณรังสีที่ผิวหนังด้วยเครื่องวัดรังสีชนิดโซลิดสเตท

เลขที่ผู้ป่วย.....ชื่อและนามสกุล .....

ก่อนที่จะลงนามในใบยินยอมให้ทำการวิจัยนี้ ข้าพเจ้าได้รับการอธิบายจากผู้วิจัยถึงวัตถุประสงค์ของการทำวิจัย วิธีการวิจัย อันตรายหรืออาการที่อาจจะเกิดขึ้นจากการทำวิจัยอ ย่างละเอียดและมีความเข้าใจดีแล้ว

ผู้วิจัยรับรองว่าจะตอบคำถามต่างๆ ที่ข้าพเจ้าสงสัยด้วยความเต็มใจไม่ปิดบังซ่อนเร้นจนข้าพเจ้าพอใจ

ข้าพเจ้ามีสิทธิ์ที่จะบอกเลิกการเข้าร่วมในโครงการวิจัยนี้เมื่อใดก็ได้และเข้าร่วมโครงการนี้โดยสมัครใจ และการบอกเลิกการเข้าร่วมการวิจัยนี้จะไม่มีผลใดๆ ต่อข้าพเจ้า

ผู้วิจัยรับรองว่าจะเก็บข้อมูลเกี่ยวกับตัวข้าพเจ้าไว้เป็นความลับ และจะเปิดเผยได้เฉพาะในรูปที่เป็นสรุปผลการวิจัย และการเปิดเผยข้อมูลเกี่ยวกับตัวข้าพเจ้าต่อหน่วยงานต่างๆ ที่เกี่ยวข้องจะทำได้ในเฉพาะกรณีที่จำเป็นด้วยเหตุผลทางวิชาการเท่านั้น

ข้าพเจ้าได้อ่านข้อความข้างต้นแล้ว และมีความเข้าใจดีทุกประการ และได้ลงนามในใบยินยอมนี้ด้วยความเต็มใจ

ลงนาม.....ผู้ยินยอม
(.....)
วันที่.....เดือน.....พ.ศ.....

ลงนาม.....พยาน
(.....)
วันที่.....เดือน.....พ.ศ.....

ลงนาม.....
(.....)
นักรังสีการแพทย์ผู้ให้บริการถ่ายภาพรังสี

ลงนาม.....
(.....)
นักรังสีการแพทย์ผู้ทำการเก็บข้อมูล

ลงนาม.....ผู้วิจัยหลัก
(ร.ท.หญิง เพียงตะวัน กาญจนะ)
วันที่.....เดือน.....พ.ศ.....

เอกสารข้อมูลสำหรับอาสาสมัครโครงการวิจัย สำหรับเด็กอายุ10-17 ปี (Assent Form)

การวิจัยเรื่อง สหสัมพันธ์ของปริมาณรังสียังผลที่ผู้ป่วยได้รับจากการตรวจเอกซเรย์คอมพิวเตอร์ส่วนช่องท้องโดยวิธีการคำนวณและการใช้วัดปริมาณรังสีที่ผิวหนังด้วยเครื่องวัดรังสีชนิดโซลิดสเตท

ผู้วิจัย เรืออากาศโทหญิง เพียงตะวัน กาญจนะ

ที่อยู่ สาขาวิชาฉายาเวชศาสตร์ ภาควิชารังสีวิทยา คณะแพทยศาสตร์ จุฬาลงกรณ์-มหาวิทยาลัย

ชื่อผู้เข้าร่วมการวิจัย.....อายุ.....ปี

แบบขอความยินยอมในการเข้าร่วมการวิจัยฉบับนี้สำหรับ: เด็กที่มีอายุระหว่าง 10-17 ปี

ข้อความต่อไปนี้เป็นการอธิบายถึงข้อสงสัยที่อาจเกิดขึ้นได้ ถ้ามีข้อสงสัยใดๆ ในคำอธิบายด้านล่างหรือข้อสงสัยอื่นที่เกี่ยวกับการวิจัยนี้สามารถถามได้ และหนูจะได้รับสำเนาหนังสือฉบับนี้เพื่อเก็บไว้เป็นหลักฐาน

ผู้วิจัยจะทำการวิจัยครั้งนี้เพราะว่าเมื่อต้องได้รับการตรวจเอกซเรย์คอมพิวเตอร์ส่วนช่องท้องทำให้อวัยวะสืบพันธุ์ได้รับรังสีจากการตรวจ ซึ่งอวัยวะสืบพันธุ์เป็นอวัยวะที่มีความไวต่อรังสีค่อนข้างสูง ผู้วิจัยจึงอยากรู้ว่าปริมาณรังสียังผลที่อวัยวะสืบพันธ์ได้รับเป็นเท่าไหร่และจะก่อให้เกิดอันตรายต่อผู้รับการตรวจเอกซเรย์คอมพิวเตอร์ส่วนช่องท้องหรือไม่

ถ้าหนูเข้าร่วมการวิจัยนี้ ผู้วิจัยจะต้องทำการติดเครื่องวัดรังสีที่ผิวหนังใกล้กับอวัยวะสืบพันธุ์ก่อนเริ่มการตรวจและเอาแผ่นวัดรังสีนี้ออกเมื่อตรวจเสร็จเรียบร้อย ซึ่งแผ่นวัดรังสีของเครื่องวัดรรังสีนั้นเป็นแผ่นแบน ขนาดเล็ก ไม่รบกวนการทำงานของเครื่องเอกซเรย์และไม่เป็นอันตรายต่อตัวหนู

ก่อนทำการตรวจผู้วิจัยจำเป็นต้องซักถามน้ำหนัก ส่วนสุง และวัดความหนาของส่วนช่องท้องของหนูเพื่อใช้ประกอบการวิจัย หนูจะต้องเตรียมตัวและปฏิบัติตามคำแนะนำของเจ้าหน้าที่เหมือนกับผู้รับการตรวจเอกซเรย์คอมพิวเตอร์ช่องท้องทั่วไป ในขณะที่ทำการตรวจผู้วิจัยและเจ้าหน้าที่จะทำการดูแลหนูอย่างใกล้ชิด หนูจะได้รับการตรวจเหมือนกับการตรวจเอกซเรย์คอมพิวเตอร์ช่องท้องตามปกติ

ผู้วิจัยขอย้ำว่า ถ้าหนูไม่อยากเข้าร่วมการวิจัยครั้งนี้ก็ไม่เป็นไร และจะไม่มีใครโกรธหนูเลย นอกจากนี้ถ้าหนูเข้าร่วมการวิจัยไปแล้วและอยากหยุดในภายหลังก็สามารถทำได้ด้วยเช่นกัน

ผู้วิจัยคิดว่าการติดเครื่องมือวัดรังสีในการวิจัยนี้จะไม่ทำให้หนูมีอันตรายใดๆ แต่ หนูอาจจะรู้สึกรำคาญบ้างตอนที่ติดเครื่องมือวัดรังสีที่ผิวหนัง

ผู้วิจัยขอย้ำว่าจะไม่มีใครรู้ว่าหนูเข้าร่วมการวิจัย นอกจากคุณพ่อ คุณแม่ ผู้วิจัยและเจ้าหน้าที่ที่เกี่ยวข้องเท่านั้น ถ้าหนูมีคำถามใดๆ สามารถโทรหา ผู้วิจัยที่เบอร์ 08-9414-3050 ผู้วิจัยยินดีจะพูดคุยและอธิบายรายละเอียดให้หนูเข้าใจด้วยความเต็มใจ

ผู้ดำเนินการขอความยินยอม (ตัวบรรจง).....

วันที่.....เดือน.....พ.ศ.....

ชื่อเด็กผู้เข้าร่วมการวิจัย (ตัวบรรจง).....

วันที่.....เดือน.....พ.ศ.....

ชื่อผู้ปกครองหรือผู้ปกครองโดยชอบด้วยกฎหมาย.....

วันที่.....เดือน.....พ.ศ.....

VITAE

Name	Flying Officer Piangtawan Kanjana
Date of birth	January 25, 1981
Place of birth	Nakhonsawan,Thailand
Education	Bachelor of Science in Radiological Technology, Faculty of Allied Health Science, Naresuan University, 2006.
Work Experience	2003-2004: Radiological Technologist of Thanyarak Breast Center at Siriraj Hospital 2004-Present: Radiological Technologist of Radiological Department at Chandrubeksa Hospital
Address	47/3 M.3 T.Thatako A.Thatako ,Nakhonsawan, 60160 Thailand